Radboud Repository

Radboud University Nijmegen

PDF hosted at the Radboud Repository of the Radboud University Nijmegen

The following full text is a publisher's version.

For additional information about this publication click this link.
http://hdl.handle.net/2066/135292

Please be advised that this information was generated on 2017-12-05 and may be subject to change.

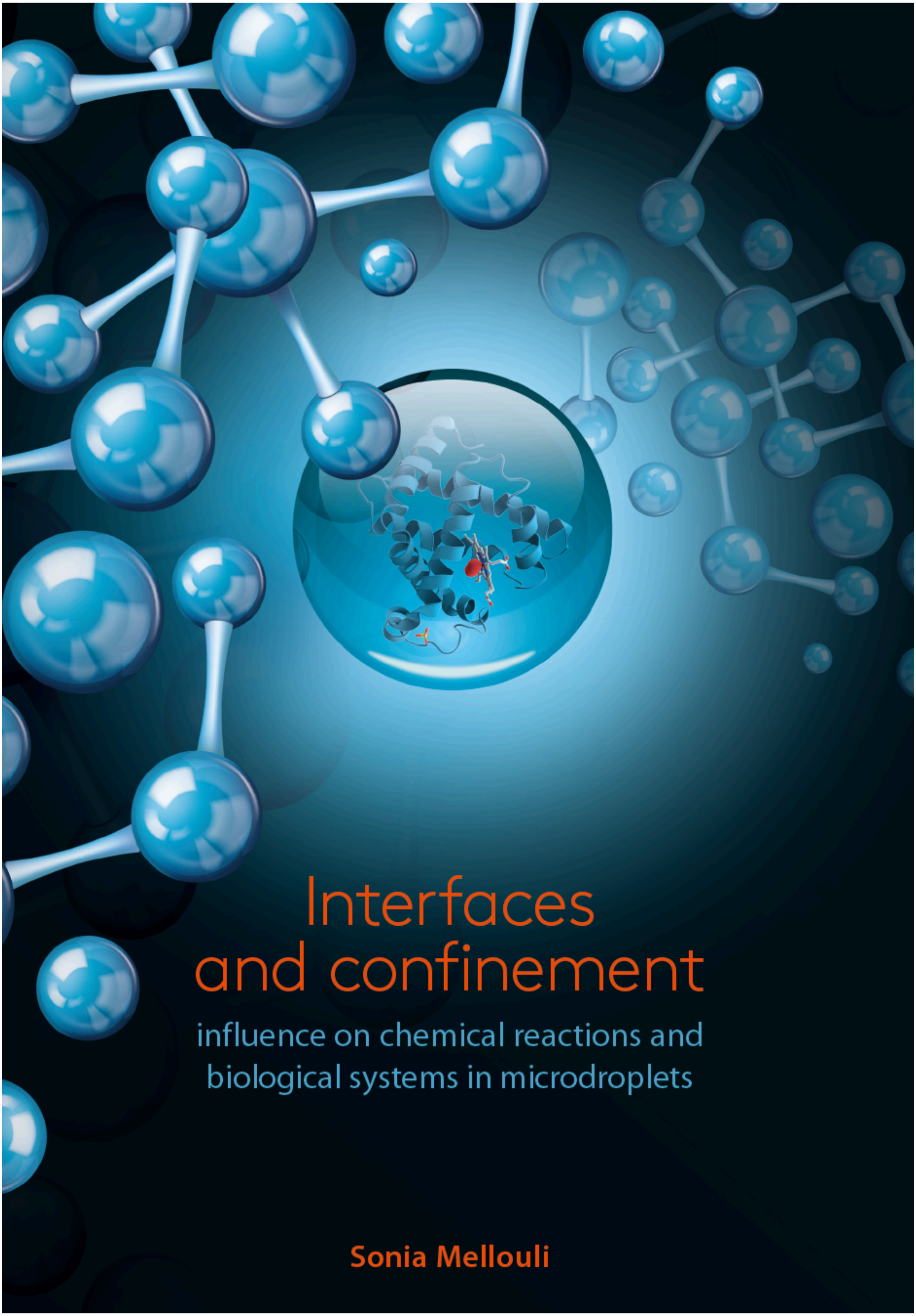

Interfaces and confinement

influence on chemical reactions and biological systems in microdroplets

Sonia Mellouli

Interfaces and confinement: influence on chemical reactions and biological systems in microdroplets

Proefschrift

ter verkrijging van de graad van doctor
aan de Radboud Universiteit Nijmegen
op gezag van de rector magnificus prof. dr. Th.L.M. Engelen,
volgens besluit van het college van decanen
in het openbaar te verdedigen op vrijdag 23 januari 2015
om 16.30 uur precies

door

Sonia Mellouli
geboren op 31 Mei 1985
te La Ciotat (Frankrijk)

Promotor

Prof. dr. Wilhelm Huck

Manuscriptcommissie

Prof. dr. R.J.M. Nolte

Prof. dr. S. Otto (RuG)

Dr. G. Rivas Caballero (CIB Madrid, Spanje)

Paraninfem

Marlies Nijemeisland

Sjoerd Postma

ISBN: 978-90-9028653-2

Omslag illustratie: Harald Pieper

Gedrukt door: Ipskamp Drukkers, Nijmegen, Nederland

Interfaces and confinement: influence on chemical reactions and biological systems in microdroplets

Doctoral Thesis

to obtain the degree of doctor
from Radboud University Nijmegen
on the authority of the Rector Magnificus prof. dr. Th.L.M. Engelen,
according to the decision of the Council of Deans
to be defended in public on Friday, January 23, 2015
at 16.30 hours

by

Sonia Mellouli
Born on May 31, 1985
in La Ciotat (France)

Supervisor

Prof. dr. Wilhelm Huck

Doctoral Thesis Committee

Prof. dr. R.J.M. Nolte

Prof. dr. S. Otto (University of Groningen)

Dr. G. Rivas Caballero (CIB Madrid, Spain)

Paranymphs

Marlies Nijemeisland

Sjoerd Postma

The work presented in this thesis was conducted in the physical-organic chemistry group, Institute for Molecules and Materials at the Radboud University Nijmegen, the Netherlands.

ISBN: 978-90-9028653-2
Cover design: Harald Pieper
Printed by: Ipskamp Drukkers, Nijmegen, The Netherlands

Table of contents

Chapter 1 General introduction and thesis outline 11

1.1 Cell versus biochemical reactions in test tubes 12
1.2 Water interfaces 13
1.3 Crowding 15
1.4 Compartmentalization and confinement in microdroplets 18
1.5 References 22

Chapter 2 Investigation of 'on water' conditions using a biphasic microfluidic platform 27

2.1 Introduction 28
2.2 Results and discussion 31
  2.2.1 Model reactions 31
  2.2.2 Influence of the water contact area 34
  2.2.3 Influence of the temperature 37
  2.2.4 Blocking the reactive water surface 40
  2.2.5 Influence of the reactants nature 41
2.3 Conclusions 42
2.4 Experimental section 43
2.5 References 45

Chapter 3 Self-organization of the bacterial cell-division protein FtsZ in confined environments 49

3.1 Introduction 50
3.2 Results and discussion 51
  3.2.1 Microdroplets in microfluidics 51
  3.2.2 Dynamics of FtsZ bundles 54
  3.2.3 Effect of crowder concentration on FtsZ bundle distribution 57
  3.2.4 Effect of FtsZ concentration on bundle distribution 58
  3.2.5 Discussion 61

3.3 Conclusions 62
3.4 Experimental section 63
3.5 References 66

Chapter 4 Reconstitution of the divisome system in E. coli: from droplets to liposomes 71

4.1 Introduction 72
4.2 Results and discussion 74
  4.2.1 Emulsion droplets containing proteins of the divisome 74
    4.2.1.1 FtsZ and FtsA in lipid coated droplets 74
    4.2.1.2 FtsZ and sZipA in lipid coated droplets 76
  4.2.2 Liposomes formation for divisome encapsulation 81
    4.2.2.1 Liposomes production in chip 82
    4.2.2.2 Liposomes production by combining on and off chip methods 84
  4.2.3 Mimicking the nucleoid occlusion 87
4.3 Conclusions 90
4.4 Experimental section 91
4.5 References 94

Chapter 5 Microtubules dynamics in crowded and confined environment 97

5.1 Introduction 98
5.2 Results and discussion 101
  5.2.1 Preparation of stabilized microtubules 101
  5.2.2 Stabilized microtubule in bulk emulsions 102
  5.2.3 Stabilized microtubules in droplet microfluidics 103
  5.2.4 Dynamics of microtubules in crowded environment: bulk versus bulk emulsion 106
  5.2.5 Microtubules dynamics in temperature controlled microfluidic devices 110
  5.2.6 Microtubules dynamics in droplet microfluidics 113
5.3 Conclusions 117
5.4 Experimental section 118
5.5 References 121

Chapter 6 Conclusions and future perspectives **125**

Summary **130**

Samenvatting **132**

Acknowledgements **136**

About the author **138**

Chapter 1

General introduction and thesis outline

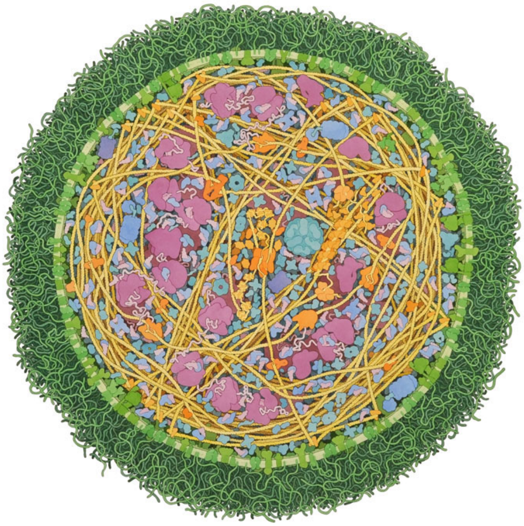

Crowding in Mycoplasma mycoides cell (by David S. Goodsell, 2011).

1.1 Cell versus biochemical reactions in test tubes

The interior of a living cell is an extremely crowded environment, composed of macromolecules, organelles and cytoskeletal filaments enclosed in a lipid bilayer membrane (Figure 1. 1). The concentration of proteins and RNA inside a cell of *Escherichia coli* is in the range of 300-400 g/L.[1] In order to understand the complexity of the cell, single elements like proteins are typically studied *in vitro* with low concentrations of 1-10 g/L. However, it has been long known that molecular crowding has both thermodynamic and kinetics effects and overlooking this difference between reactions in cells or in a test tube should matter.[2] Other elements to take into account while studying components of the cell are interfaces and compartmentalization. The cell membrane contains membrane proteins which allow the cell to transport small molecules in and out or act as catalysts/enzymes for some specific reactions. Compartmentalization, present in the cell with regions separated by a physical barrier (organelles), as well as differences in local composition, are thought to have profound implications for cell function.[3]

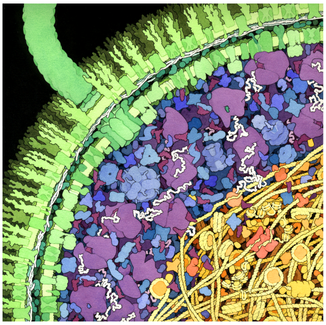

Figure 1. 1 Crowding in a cross-section of a small portion of an *E. coli* cell. The cell wall is constituted of a lipid bilayer with transmembrane proteins and a large flagellar (green). The blue and purple regions correspond to the cytoplasmic area with ribosomes, RNAs and enzymes. The nucleoid region is shown in yellow and orange, with DNA and DNA polymerase. (© David S. Goodsell 1999)

Although we do not aim to discover in detail how the physical environment impacts on all aspects of cellular processes, we would like to study, from a physico-chemical point of view, cell components *in vitro* under conditions as close as possible to that of the cell. For instance, while studying the stability of a protein or the activity of an enzyme, crowding and compartmentalization should be taken into account. In this thesis, we used microdroplets in microfluidics as a tool for mimicking the cell, and we studied the effect of crowding and the shape of the container on the behaviour of cytoskeleton proteins (FtsZ and tubulin). In parallel, we studied enhanced chemical reactions at water interfaces, of particular relevance for prebiotic chemistry.[4]

1.2 Water interfaces

In organic chemistry, water is not commonly used as a solvent mainly because of the insolubility or the incompatibility of the organic compounds. This situation changed when Breslow and Rideout showed the rate enhancement of Diels-Alder reactions in the presence of water.[5] The authors explained the increase of reaction rates of two apolar molecules in water with the hydrophobic effect, leading to a very high local concentration of reactants. The interest in water as a solvent was further invigorated in the 1990's with the introduction of the Green Chemistry concept.[6] Being cheap, safe and harmless, water is the perfect candidate as the ultimate 'green' solvent. Examples of green chemistry using the potential of water interface have been reported for a wide range of chemical reactions.[7-10]

A new approach for the use of water as a solvent was described in 2005 by Sharpless and co-workers, who found that reactions can be accelerated by water despite the non-solubility of the reactants.[11] This phenomenon was called 'on water' chemistry and a striking example from their study is the cycloaddition reaction between quadricyclane and dimethyl azodicarboxylate (Figure 1. 2). This transformation took prolonged reaction times and heating when carried out in organic solvent (18h in methanol, 2 days in neat, 5 days in toluene). In contrast, the reaction went to completion in 10 min 'on water' at room temperature. Since this initial report, the surprising rate-enhancing effect of water as a solvent has been widely reported for numerous organic reactions.[12]

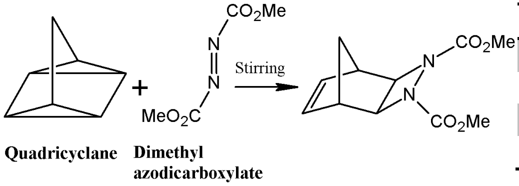

Solvent	Conc.[a]	Time to completion
Neat	4.53 M	48 h
Toluene	2 M	> 120 h
Methanol	2 M	18 h
On H_2O	4.53 M	10 min

Figure 1. 2 Cycloaddition reaction between quadricyclane and dimethyl azodicarboxilate using different solvents. The reaction performed 'on water' had the smallest time to completion, being around 290 times faster than that of the neat reaction.[11] [a]Concentrations of the neat and heterogeneous reactions are calculated from the measured density of a 1:1 mixture of the reactants.

Marcus and Jung proposed a model which suggests that interactions of hydrophobic organic molecules with the water interface may be responsible for the rate enhancement observed 'on water'.[13] The authors described kinetic models for the neat (reactants only) and surface ('on water') Diels-Alder reactions to compare with experimental systems. It was concluded that the rate enhancement observed in 'on water' reactions is due to the unbounded hydroxyl groups of interfacial water molecules which form hydrogen bonds with organic reactants and with the transition state (Figure 1. 3). Some years later, this theory was further confirmed by experimental and theoretical studies using vibrational sum frequency spectroscopy. Stiopkin *et al.* reported evidence that the water surface is only one layer of molecules thick interacting with the subsurface layer in a similar way as the molecules in bulk water.[14] Interestingly, most water molecules at the interface form hydrogen bonds with each other, but 23 % of water molecules at the air/water interface have free hydroxyl groups. These hydroxyl dangling bonds are believed to have a surprising effect on the kinetics of some chemical reactions.

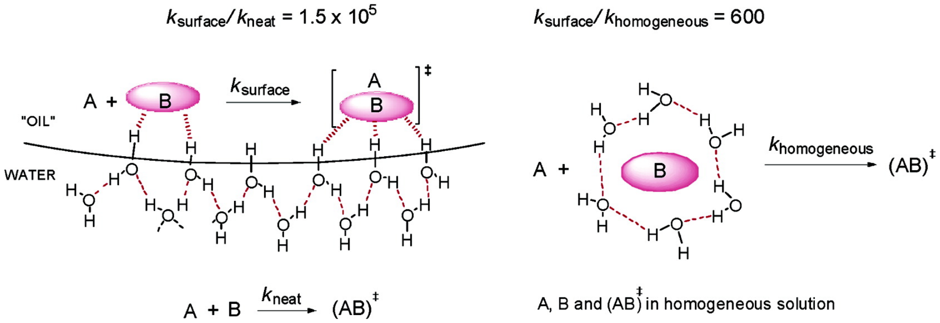
$k_{surface}/k_{neat}$ = 1.5 x 10^5
$k_{surface}/k_{homogeneous}$ = 600
A + B
$k_{surface}$
A
B
‡
"OIL"
WATER
A + B $\xrightarrow{k_{neat}}$ $(AB)^‡$
A + B
$k_{homogeneous}$
$(AB)^‡$
A, B and $(AB)^‡$ in homogeneous solution

Figure 1. 3 Cartoon on the 'on water' catalysis with hydrogen bonds forming with the reactant and the intermediate (left) in comparison to the neat (reactants only) and aqueous homogeneous reactions with water molecules tangentially oriented around the hydrophobic solute (right). Using the reaction between quadricyclane and dimethyl azodicarboxylate as a model, the ratio of the reaction rate constants between the surface reaction and neat or homogenous reactions showed an increase of 1.5 x 10^5 and 600, respectively.[13]

Studying the reactivity and the behaviour of molecules at the interface between water and a second interface is important to understand from a fundamental molecular-level point of view, how the interfacial region differs in dynamics, structure, and reactivity from the behaviour in bulk liquid or in the gas phase. Up to now, a number of hypotheses have been proposed in order to address the exact role of water as a solvent but no uniform answer has emerged. **In Chapter 2**, the ‘on water’ reaction is studied using two model reactions and droplet microfluidics to have a control on the interfacial contact between the oil (reactants) and water droplets. Changing parameters like the temperature and the surface contact, we tried to discriminate between the two most probable origins of the ‘on water’ reactivity: the hydrophobic effect from Rideout and Breslow, or the hydrogen bonds with the reactant/intermediate state postulated by Jung and Marcus.

1.3 Crowding

Biochemical reactions in living systems usually take place in media containing a very high concentration of macromolecules (50-400 mg/ml).[1] Rather than ‘concentrated’, such a solution is referred to as ‘crowded’ or ‘confined’. Macromolecular crowding is defined by the effects of volume excluded by one soluble macromolecule to another whereas molecular confinement represents the effect of a fixed boundary to a soluble macromolecule.[15]

The most fundamental interaction between macromolecules in solution is the steric repulsion, which is always present and independent of the presence of electrostatic or hydrophobic interactions. The volume inaccessible to other molecules in the system is defined as excluded volume. Figure 1. 4 shows schematically the importance of size in volume exclusion.[16] The squares represent an area containing macromolecules that occupy ~ 30% of the total volume. If a very small molecule compared to the macromolecules in that region is added to the system, the volume available is approximately 70 % (Figure 1. 4. A). However, if the molecule added to the system has a similar size (or larger) to the macromolecules is that region, the available volume is highly reduced since the centre of that molecule can approach the centre of any other macromolecules to no less than the distance at which the surface of two macromolecules meet. This restriction is depicted by a circular shell with a radius that corresponds to the radius of the macromolecules. Then the volume available, depicted in blue in Figure 1. 4. B, is relatively small, pointing out the importance of the relative size of the molecules present in a solution and those added to the solution as well as the density of the macromolecules in the solution.

Crowding and confinement in the cell have great effects on macromolecular reaction rates and equilibria.[16-19] *In vitro* experiments are usually conducted on solutions containing low concentrations of proteins (around 1 mg/ml), but in order to mimic the crowding of the cell, high concentrations of natural or synthetic macromolecules can be added to the system. It is important to mention that the choice of the crowder is crucial when studying its effect on protein reactivity.

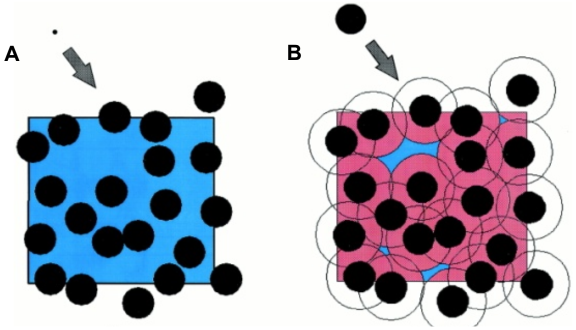

Figure 1. 4 Excluded (pink and black) and available (blue) volume in a solution of spherical background macromolecules. **A**. volume available to a test molecule of infinitesimal size; **B**. volume available to a test molecule of size comparable with background molecules.[16]

To be described as pure excluded-volume models, the interactions between proteins and crowder should predominantly be repulsive. The synthetic polymer polyethylene glycol (PEG) is one of the most popular crowders although attractive interactions with the hydrophobic parts of some proteins have been reported.[20-23] As a general caution, we stress that the contribution of the attractive or repulsive interactions is unknown for most systems, and the effect can vary between different proteins. As an alternative to PEG, there is a large variety of inert polysaccharides and proteins which can be used as crowding agents for use in quantitative studies (ficoll, dextran, hemoglobin, BSA…).[24]

An illustrative example of the effect of crowding is capsid formation. A capsid, the protein shell of a virus enclosing its genetic material, is believed to assemble *in vitro* only at very high ionic strength. The effect of molecular crowding agents on the assembly of the capsid protein of the Human Immunodeficiency Virus (HIV) was studied *in vitro*.[25] The authors showed that in the presence of 100 g/L ficoll and low ionic strength (close to physiological), the half-time for protein assembly was 10 fold lower than in the absence of crowder. The protein assembled into a hollow cylinder shaped capsid identical to that formed in diluted and high ionic strength solutions. Thus, the use of crowder may lead to a better *in vitro* system to study capsids assembly. Recently, the important role of crowding in capsid assembly was further characterized using computational simulations which showed that the sequences of reaction steps needed for nucleation and growth are more complicated than simple nucleation-growth models.[26]

Molecular crowding can also greatly influence enzyme activity. The effect of two types of crowding agents (globular proteins or polymers) on the reaction rates of three different decarboxylating enzymes (urease, pyruvate and glutamate) was studied *in vitro*.[27] The enzyme activity dramatically increased at globular protein concentrations up to 30%, decreasing with higher crowder concentrations. However, polymeric crowding agents caused a concentration dependent decrease in enzyme activity that might be explained by a decrease in the diffusion rate.

To mimic conditions close to *in vivo* systems, the rate of amyloid fibrillation by α-synuclein, a presynaptic protein abundant in the brain[28], was studied in the presence of crowders (Figure 1. 5).[29] With 150 g/L ficoll or Dextran (neutral sugar polymers) the rate of fibril formation increased significantly (3 times faster than the control). However, with the same PEG concentration the reaction was 10-fold faster. The differences in effects may be due to the relatively high viscosities of the polysaccharide solutions compared to that of PEG, which may affect the rates of macromolecular diffusion and consequently the rates of α-synuclein fibrillation. Molecular crowding also modulates the efficiency of direct interaction of this protein with metal ions, a possible factor in the pathogenesis of disorders related to this protein as Parkinson’s disease.

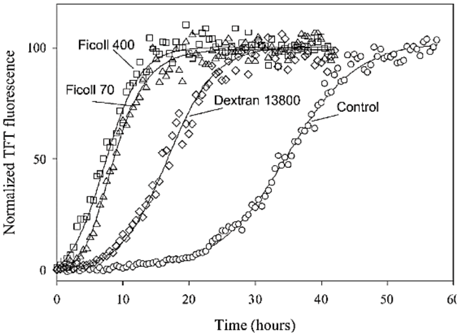

Figure 1. 5 Effect of high concentrations of polysaccharides on the fibrillation of α-synuclein.[29] With 150 g/L ficoll or dextran, the rate of fibrillation is significantly increased compared to that of the control and was 3 times faster.

From Chapter 3 to Chapter 5, we studied crowding effects on cytoskeletal proteins (FtsZ and microtubules bundles formation) using droplet microfluidics, investigating its effect on the bundles arrangement and organization.

1.4 Compartmentalization and confinement in microdroplets

The first droplet experiment was reported in the 1950s when Joshua Lederberg performed single cell analysis by spraying water droplets containing cells into mineral oil.[30] Around 10 years later, Rotman published a study of single enzyme kinetics in droplets dispersed on a cover slip covered with oil, measuring the conversion by fluorescence microscopy (Figure 1. 6. a).[31] Despite these ground-breaking findings, it took almost 50 years for microdroplets to become popular in the scientific world, which was probably due to the low throughput and lack of powerful microfluidic tools. With the creation of digital cameras, more sensitive fluorescent detection and advances in microfluidics, the field of droplet microfluidics has grown considerably in the last 5-10 years.

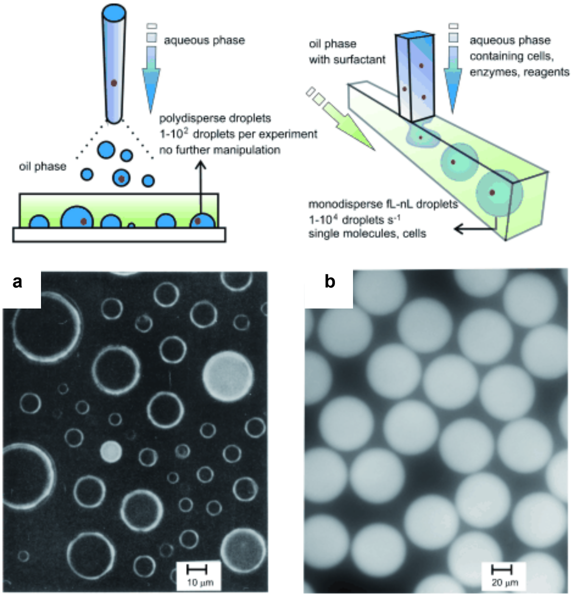
aqueous phase
polydisperse droplets
1-10² droplets per experiment
no further manipulation
oil phase
oil phase
with surfactant
aqueous phase
containing cells,
enzymes, reagents
monodisperse fL-nL droplets
1-10⁴ droplets s⁻¹
single molecules, cells
a
b
10 µm
20 µm

Figure 1. 6 Top: Schematic of droplet formation with conventional techniques (left) or a microfluidic platform (right). Micrographs **(a)** and **(b)** show the outcome of each technique. a) Rotman's classic experiment on single-enzyme kinetics using microdroplets dispersed in oil.[31] b) Monodisperse droplets from a microfluidics platform for biological and chemical experiments.[32]

Droplet microfluidics offers possibility for compartmentalizing reactions in extremely small volumes (nanolitre to femtolitre droplets), with every droplet acting as a reactor of the same volume and composition (Figure 1. 6. b).[32] Single cell or single molecule encapsulation is possible and by varying the conditions within each droplet multiple reactions can be performed, making droplet microfluidics suitable for high-throughput experiments.

Microfluidic channels can be used to produce highly monodisperse emulsions by shearing of two immiscible phases. Droplet generation is typically carried using a T-junction or flow-focusing geometry. In the T-junction configuration (Figure 1. 7. A), the tip of the aqueous phase entering the main channel elongates, due to the shear forces generated by the continuous phase, until the neck of the dispersed phase thins out and eventually breaks the stream into a droplet. In the flow-focusing configuration (Figure 1. 7. B), the continuous phase intersects the disperse phase in a narrow region of the microfluidic device, perpendicularly on both sides applying symmetric shearing onto it. This configuration enables faster, more controlled and more stable generation of droplets. In both cases, droplets size depends on the channel dimensions, the relative flow rates and viscosities of both phases. For high viscosity ratio of both phases, the dispersed thread experiences a linear thinning procedure called the jetting regime (Figure 1. 8. b). Droplet stability is often regulated by addition of surfactant in the continuous phase[33] but the surface properties of the channels also plays a critical role in droplet formation. The channels must be hydrophobic to produce water droplets in oil and hydrophilic to form the inverted emulsion.[34]

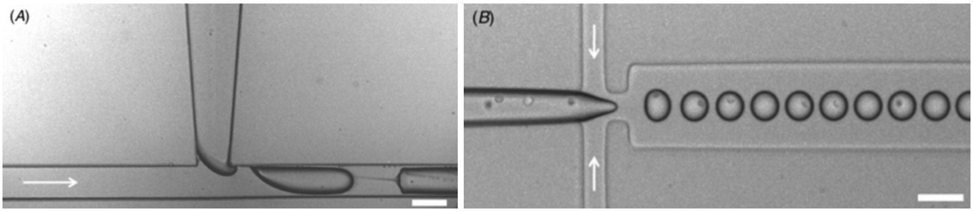

Figure 1. 7 Characteristic images of the two types of microfluidic device for droplet production, namely (A) T-junction and (B) flow-focusing. White arrows indicate the oil phase flows.[35] Scale bar: 100 µm.

The increasing research activity in the field of microdroplets in microfluidics resulted in a range of methods to manipulate droplets (Figure 1. 8)[32]. Microdroplets can be seen as chemical or biochemical reactors of well-defined shape and reagent concentrations. Unlike bulk experiments, it is possible to add reagents in droplets at a specific point in time and space in two different ways. The first method is to use different streams of reagents before the intersection with the continuous phase, as nicely demonstrated by Ismagilov and co-workers.[36, 37] The other method is to encapsulate the reagents in separate droplets and induce droplet fusion using an electric field (active way, Figure 1. 8. d)[38] or using a specific channel geometry (passive way, Figure 1. 8. e)[39]. Opposite to fusing, droplet division can be beneficial to increase throughput and carry out multiple reactions in parallel. Via control of the flow rate of continuous phase and the relative fluidic resistance of the channels, droplets can be divided symmetrically or asymmetrically (Figure 1. 8. g). [40]

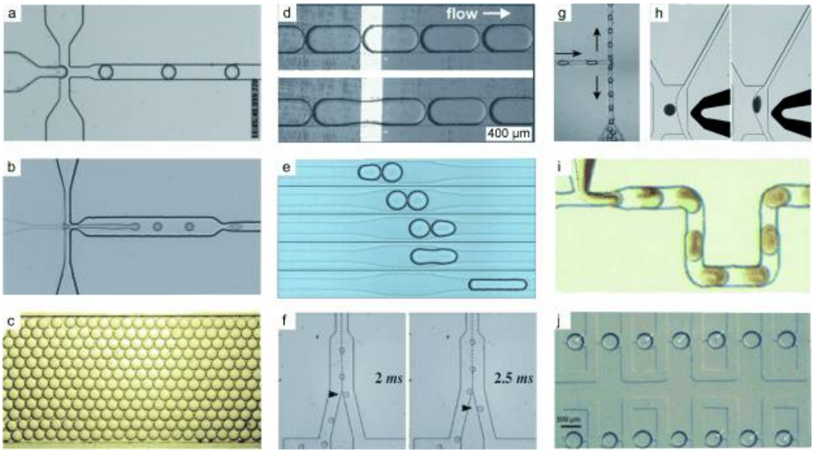

Figure 1. 8 An overview of commonly used droplet-manipulation modules. a) Droplet formation in a flow-focusing device. b) Droplet formation from jetting in a flow-focusing device. c) Delay line/storage area[44] d) Droplet fusion by electrocoalescence[38] e) Passive, channel-geometry-mediated droplet fusion[39] f) Electrosorting of droplets[43] g) Channel-geometry-mediated droplet splitting[40] h) Electric-field-induced emulsion separation[45] i) Mixing the contents of droplets in a winding channel[41] j) Droplet storage.[46] Remaining figures were reproduced from Theberge *et al.*[32]

When carrying out a chemical reaction, a good mixing of the reagent is very important to obtain a uniform solution and improve the reaction yield. Mixing in droplet microfluidics can be induced by narrow and winding channels (Figure 1. 8. i). These microscale features cause ‘chaotic advection’ that relies on repeated folding and stretching of the fluid layers in the droplet becoming exponentially thinner and allowing rapid mixing by diffusion.[41] One of the key advantages of droplet microfluidics is the ability to select the droplets of interest using droplet sorting. In order to sort droplets, passive microfluidic channel geometries using a bifurcating flow design and controlling the widths of the daughter channels result in droplets to be separated according to their sizes.[42] Active droplet sorting is achieved by electric pulses generated by microfabricated electrodes which deflect the droplets via dielectrophoresis into a separate channel (Figure 1. 8. f).[43]

This technology can also be used to sort droplets according to their fluorescent content, which can be detected and used to trigger an electric signal. Fidalgo *et al.* demonstrated the efficiency of this method by selecting 30 nM fluorescein droplets from a mixture of 10 and 30 nM fluorescein in droplets with less than 1% false positives (Figure 1. 8. h).[45] Chemical reactions as well as some biological experiments require long reaction times with processes occurring on a timescale of hours. Large-scale devices can be used for purpose of maintaining the droplets inside the device and monitoring them over time (Figure 1. 8. c).[44] Long-term droplet storage can also be achieved by integrating a droplet trap array as shown in Figure 1. 8. j.[46] Aside from the advantages of miniaturization mentioned previously, microfluidic devices are easier to handle, safer, cheaper (the consumption of reagent is reduced), and could allow higher reaction and analysis rates (via online monitoring) than conventional chemical reactions performed in a flask.[47] Shear forces at the channel walls can induce internal flow circulation in droplet microfluidics, which can enhance mass transfer at the liquid-liquid interface. The droplet-microfluidics technology enables fast and sensitive screening which facilitate high throughput biological assays.[48] Numerous examples of single cell experiment in droplet microfluidics were reported during recent years, with applications ranging from the assessment of single cell behaviour under various conditions to monitoring heterogeneity of drug action over time.[49-54]

Microdroplets can also be used to investigate the mechanical properties of gels. Fibrin networks were encapsulated in nanoliter volumes to study their behaviour in droplets travelling within microfluidic channels of different geometries (Figure 1. 9).[55] The device presented alternated narrow channels and wide channels where the droplets were first squeezed (acquiring an elongated shape) and then relaxed back to the initial spherical shape. Figure 1. 9. A shows that when the same droplet travels through the channels and deforms repeatedly from spherical to squeezed, the fibrin network presented negligible structural differences. The remarkable ability of the fibrin network to compress and extend indicates that the system is flexible. However, when the flow rates were almost double, the fibrin network is concentrated toward the rear of the droplet with respect to the direction of the droplet movement in the microchannel due to hydrodynamic forces (Figure 1. 9. B).

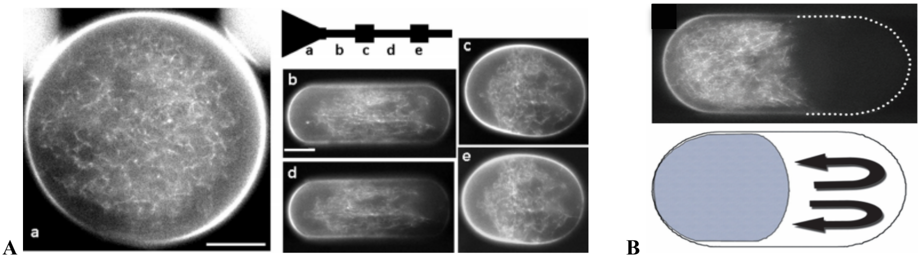

Figure 1. 9 Fluorescent images of the fibrin network in droplet microfluidics. **A**. Structural arrangement of a fibrin network in the same droplet at the positions a–e, indicated in the sketch of the device. Scale bar: 40 mm. **B**. Modification of the network arrangement due to hydrodynamic forces generated at higher flow rates, pushing the fibrin network towards the back of the droplet.

In Chapter 3 to 5, we used the microfluidic technology to study the behaviour of cytoskeleton proteins in confined and crowded environments. Typically, water droplets in oil are stabilized by surfactants. To provide a closer mimic to cellular conditions, we tried to produce water-in-water droplets (or better: liposomes) using microfluidics. In **Chapter 4**, the three main proteins involved in the division in *E. coli* were encapsulated in droplets and liposomes in order to reproduce and understand the mechanics of this process. In **Chapter 5**, dynamic microtubules were encapsulated in microdroplets under crowded environment to investigate changes in behaviours depending on protein/crowder concentrations or container properties. The thesis ends with a brief summary of results and an outlook of future research in **Chapter 6.**

1.5 References

1. S. B. Zimmerman and S. O. Trach, *J Mol Biol*, **1991**, *222*, 599-620.
2. T. C. Laurent, *Biochem J*, **1963**, *89*, 253-261.
3. H. Walter and D. E. Brooks, *FEBS Lett*, **1995**, *361*, 135-139.
4. A. Fallah-Araghi, K. Meguellati, J. C. Baret, A. E. Harrak, T. Mangeat, M. Karplus, S. Ladame, C. M. Marques and A. D. Griffiths, *Physical Review Letters*, **2014**, *112*, 028301.
5. D. C. Rideout and R. Breslow, *J Am Chem Soc*, **1980**, *102*, 7816-7817.
6. J. Clark, R. Sheldon, C. Raston, M. Poliakoff and W. Leitner, *Green Chem*, **2014**, *16*, 18-23.
7. C. Santi, B. Battistelli, L. Testaferri and M. Tiecco, *Green Chem*, **2012**, *14*, 1277-1280.

8. P. Saiprathima, K. Srinivas, B. Sridhar and M. M. Rao, *Rsc Adv*, **2013**, *3*, 7708-7712.
9. S. Paladhi, M. Bhati, D. Panda and J. Dash, *Journal of Organic Chemistry*, **2014**.
10. M. Mamaghani, N. O. Mahmoodi, F. Shirini, A. Azimi-Roshan and A. Monfared, *J Chem-Ny*, **2013**.
11. S. Narayan, J. Muldoon, M. G. Finn, V. V. Fokin, H. C. Kolb and K. B. Sharpless, *Angew Chem Int Edit*, **2005**, *44*, 3275-3279.
12. A. Chanda and V. V. Fokin, *Chemical Reviews*, **2009**, *109*, 725-748.
13. Y. S. Jung and R. A. Marcus, *J Am Chem Soc*, **2007**, *129*, 5492-5502.
14. I. V. Stiopkin, C. Weeraman, P. A. Pieniazek, F. Y. Shalhout, J. L. Skinner and A. V. Benderskii, *Nature*, **2011**, *474*, 192-195.
15. H. X. Zhou, G. N. Rivas and A. P. Minton, *Annu Rev Biophys*, **2008**, *37*, 375-397.
16. A. P. Minton, *Journal of Biological Chemistry*, **2001**, *276*, 10577-10580.
17. O. Bounedjah, L. Hamon, P. Savarin, B. Desforges, P. A. Curmi and D. Pastre, *Journal of Biological Chemistry*, **2012**, *287*, 2446-2458.
18. A. Miermont, F. Waharte, S. Q. Hu, M. N. McClean, S. Bottani, S. Leon and P. Hersen, *P Natl Acad Sci USA*, **2013**, *110*, 5725-5730.
19. C. A. Strulson, J. A. Boyer, E. E. Whitman and P. C. Bevilacqua, *RNA*, **2014**, *20*, 331-347.
20. G. Tubio, B. Nerli and G. Pico, *J Chromatogr B*, **2004**, *799*, 293-301.
21. J. Bloustine, T. Virmani, G. M. Thurston and S. Fraden, *Physical Review Letters*, **2006**, *96*.
22. D. J. Winzor and P. R. Wills, *Biophys Chem*, **2006**, *119*, 186-195.
23. P. Chanphai, L. Bekale, S. Sanyakamdhorn, D. Agudelo and H.-A. Tajmir-Riahi, *Polymer*, **2014**, *55*, 572-582.
24. N. A. Chebotareva, B. I. Kurganov and N. B. Livanova, *Biochemistry-Moscow+*, **2004**, *69*, 1239-+.
25. M. del Alamo, G. Rivas and M. G. Mateu, *J Virol*, **2005**, *79*, 14271-14281.
26. Gregory R. Smith, L. Xie, B. Lee and R. Schwartz, *Biophysical Journal*, **2014**, *106*, 310-320.
27. B. K. Derham and J. J. Harding, *Bba-Proteins Proteom*, **2006**, *1764*, 1000-1006.
28. R. Jakes, M. G. Spillantini and M. Goedert, *Federation of European Biochemical Societies Letters*, **1994**, *345*, 27-32.
29. L. A. Munishkina, E. M. Cooper, V. N. Uversky and A. L. Fink, *J Mol Recognit*, **2004**, *17*, 456-464.
30. J. Lederberg, *J Bacteriol*, **1954**, *68*, 258-259.
31. B. Rotman, *P Natl Acad Sci USA*, **1961**, *47*, 1981-&.
32. A. B. Theberge, F. Courtois, Y. Schaerli, M. Fischlechner, C. Abell, F. Hollfelder and W. T. S. Huck, *Angew Chem Int Edit*, **2010**, *49*, 5846-5868.
33. J. C. Baret, *Lab Chip*, **2012**, *12*, 422-433.
34. W. Li, Z. H. Nie, H. Zhang, C. Paquet, M. Seo, P. Garstecki and E. Kumacheva, *Langmuir*, **2007**, *23*, 8010-8014.
35. J. Hong, A. J. deMello and S. N. Jayasinghe, *Biomed Mater*, **2010**, *5*.
36. B. Zheng, J. D. Tice and R. F. Ismagilov, *Anal Chem*, **2004**, *76*, 4977-4982.

37. J. D. Tice, H. Song, A. D. Lyon and R. F. Ismagilov, *Langmuir*, **2003**, *19*, 9127-9133.
38. C. Priest, S. Herminghaus and R. Seemann, *Appl Phys Lett*, **2006**, *89*.
39. N. Bremond, A. R. Thiam and J. Bibette, *Physical Review Letters*, **2008**, *100*.
40. D. R. Link, S. L. Anna, D. A. Weitz and H. A. Stone, *Physical Review Letters*, **2004**, *92*.
41. M. R. Bringer, C. J. Gerdts, H. Song, J. D. Tice and R. F. Ismagilov, *Philos T Roy Soc A*, **2004**, *362*, 1087-1104.
42. Y. C. Tan, J. S. Fisher, A. I. Lee, V. Cristini and A. P. Lee, *Lab Chip*, **2004**, *4*, 292-298.
43. K. Ahn, C. Kerbage, T. P. Hunt, R. M. Westervelt, D. R. Link and D. A. Weitz, *Appl Phys Lett*, **2006**, *88*.
44. C. Holtze, A. C. Rowat, J. J. Agresti, J. B. Hutchison, F. E. Angile, C. H. J. Schmitz, S. Koster, H. Duan, K. J. Humphry, R. A. Scanga, J. S. Johnson, D. Pisignano and D. A. Weitz, *Lab Chip*, **2008**, *8*, 1632-1639.
45. L. M. Fidalgo, G. Whyte, D. Bratton, C. F. Kaminski, C. Abell and W. T. S. Huck, *Angew Chem Int Edit*, **2008**, *47*, 2042-2045.
46. W. W. Shi, J. H. Qin, N. N. Ye and B. C. Lin, *Lab Chip*, **2008**, *8*, 1432-1435.
47. W. P. Bula, W. Verboom, D. N. Reinhoudt and H. J. G. E. Gardeniers, *Lab Chip*, **2007**, *7*, 1717-1722.
48. M. T. Guo, A. Rotem, J. A. Heyman and D. A. Weitz, *Lab Chip*, **2012**, *12*, 2146-2155.
49. M. Y. He, J. S. Edgar, G. D. M. Jeffries, R. M. Lorenz, J. P. Shelby and D. T. Chiu, *Anal Chem*, **2005**, *77*, 1539-1544.
50. L. Mazutis, J. Gilbert, W. L. Ung, D. A. Weitz, A. D. Griffiths and J. A. Heyman, *Nat Protoc*, **2013**, *8*, 870-891.
51. M. A. Khorshidi, P. K. Rajeswari, C. Wahlby, H. N. Joensson and H. Andersson Svahn, *Lab Chip*, **2014**, *14*, 931-937.
52. M. Junkin and S. Tay, *Lab Chip*, **2014**.
53. H. N. Joensson and H. Andersson Svahn, *Angew Chem Int Ed Engl*, **2012**, *51*, 12176-12192.
54. T. Geng, R. Novak and R. A. Mathies, *Anal Chem*, **2014**, *86*, 703-712.
55. H. M. Evans, E. Surenjav, C. Priest, S. Herminghaus, R. Seemann and T. Pfohl, *Lab Chip*, **2009**, *9*, 1933-1941.

Chapter 2

Investigation of ‘on water’ conditions using a biphasic fluidic platform

---

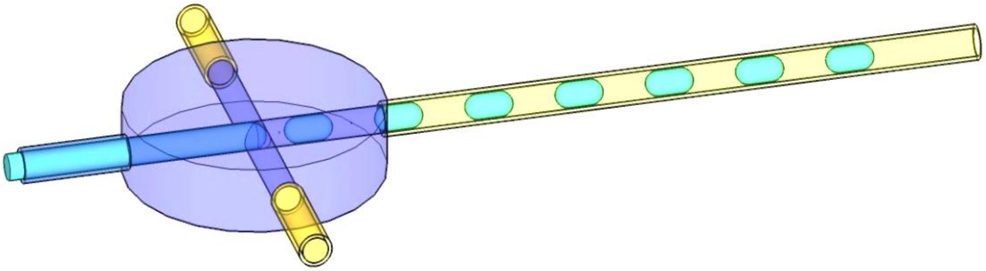

Parts of this chapter have been published:
S. Mellouli, L. Bousekkine, A. B. Theberge, W. T. S. Huck, *Angew. Chem. Int. Ed.* **2012**, *51*, 7981 – 7984.

2.1 Introduction

An important goal in modern organic chemistry is the development of new, efficient, and environmentally benign synthetic methodologies.[1] Progress toward this goal requires the use of safer solvents and the design of safer chemicals. There have been considerable advances in this area, especially in the development of aqueous organic reactions, over the last two decades. The use of water as a solvent offers many advantages: it is cheap, non-toxic and more interestingly, a strong rate enhancement has been observed for some reactions with insoluble reactants in the presence of water.[2]

Water is the most abundant liquid on the planet and is a unique solvent due to the internal structure arising from the hydrogen bond network.[3-5] It is well known that water has a strong effect on the reactivity of dissolved hydrophobic organic molecules.[6-11] Breslow and co-workers reported surprisingly high rate enhancements (up to 200-fold) for Diels-Alder reactions in water compared to aprotic non-polar organic solvents.[6] The authors explained this observation by the hydrophobic effect: when two hydrophobic molecules are mixed together in aqueous solution, they have a tendency to aggregate in order to minimize unfavourable interactions with water. In other words, the reaction of two apolar molecules could be accelerated in water because the hydrophobic effect leads to a very high local concentration of reactants. The rate enhancements in water have been attributed to many other factors including 'enforced hydrophobic interactions',[6-12] enhanced hydrogen bonding of the transition state,[13-16] the unusually high 'cohesive energy density' of water,[17-20] and in more general terms to the decrease of the hydrophobic surface area of the reactants during the activation process combined with hydrogen-bond stabilization of the polarized activated complex.[21, 22]

In a landmark paper, Sharpless and co-workers studied a range of reactions accelerated by water despite the non-solubility of the reactants under so-called 'on water' conditions.[23] Insoluble reactants were stirred in aqueous emulsions or suspensions and the surface of water is thought to catalyse the reaction. Although a large number of studies have exploited these 'on water' conditions and have reported rate enhancements,[2] there is no conclusive agreement on the molecular origin of the effect. A major reason for our limited understanding of 'on water' reactions, lies in the very nature of the experiment. Typically, 'on water' reactions are carried out by vigorously stirring two immiscible phases. On a laboratory scale, the water surface area and the surface-to-volume ratio cannot be controlled reproducibly as they are strongly dependent on stirring rates, volumes, ratio of water to organic phase, and the size of both stirrer bar and reaction flask. Figure 2. 1 shows an example of 'on water' reaction with the reactants in the upper phase and water in the lower phase. When the mixture is vigorously stirred, an emulsion of unknown droplet sizes is formed during the reaction, making any estimate of the effect of the water surface on the reaction rate an educated guess. The droplets formed are polydisperse, and this could lead to different reaction rates. As a result, there have been no systematic studies exploring the 'on water' effect and it is still unclear how much the water surface really contributes to the observed reaction rates.

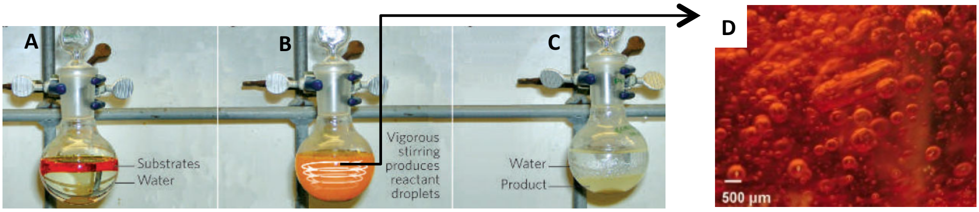

Figure 2. 1 'On water' reaction in bulk. A. The top red layer corresponds to the reactants (quadricyclane and DMAD) and the transparent one to the water phase. B. The stirring of two insoluble solutions produce polydisperse droplets (D), which could lead to different reactions rate. C. The product of the reaction is a solid and can by collected at the bottom of the flask.[24]

Examples in the literature already demonstrated that the kinetics of chemical reactions in droplet microfluidics were faster compared to those in bulk solution.

Segmented flow conditions have been used in order to accelerate the rate of Heck reaction of aryl halides with diazonium.[25] The solution of reactants was mixed in a so-called T-inlet, and upon the introduction of an inert immiscible solvent using a 'cross inlet' a segmented flow was obtained, with small plugs of reagents separated by an inert carrier fluid. Those inlets were connected to PTFE microtubing (500 µm inner diameters) immersed in an oil bath for temperature control. Due to the large surface-to-volume ratio as well as internal mixing provided by segmented flow, the Heck reaction was found to be more efficient than in laminar flow or in bulk with reaction yields in segmented flow significantly higher than in laminar flow even with low amounts of catalyst.

It should be noted here that mixing of reagents is slow in typical microfluidic reactors due to the presence of a laminar flow profile, where turbulent mixing cannot occur and all mixing results from diffusion. The internal flow circulation in droplet microfluidics has been used by several groups for rapid mixing of reagents, leading to significant enhancement of the reaction rates. This was demonstrated by Ahmed *et al.* with the hydrolysis of p-nitrophenyl acetate in toluene with aqueous sodium hydroxide as a biphasic reaction.[26] The rapid mixing within the different fluid segments caused by the internal vortex fluid flow induces a mass transfer between contiguous fluids segments enhanced by the continuously refreshed interface. A similar trend was observed in the biphasic alkaline hydrolysis reaction, with the aqueous phase containing sodium hydroxide and the organic phase containing saturated n-butyl acetate.[27]

Using microfluidics to produce monodisperse compartments, Griffiths and co-workers demonstrated that both the kinetics and thermodynamics of the reversible reaction of an amine with an aldehyde to form a fluorescent imine was enhanced in water microdroplets.[28] The concentration of the fluorescent product as a function of time was measured in droplets of different sizes and compared to bulk values. The reaction rate in droplets is higher compared to those in bulk, increasing when the droplet size is decreased. For example, in 2.5 pL droplets, the reaction rate was 45-fold higher than in bulk. The authors explained those results by a simple reaction-adsorption mechanism, in which the reactants adsorbed at the droplets interface react and diffuse back to the bulk. From these studies it is unclear however what the chemical nature of this rate enhancement is.

The aim of the present study is to quantify the 'on water' effect per unit area of interface for the first time. We present a fluidic approach to generate precisely defined oil-water interfaces, which allows us to systematically probe the influence of the water surface on chemical reactions. Monodisperse water and organic phase plugs (typical frequencies around 0.06 Hz) are generated in PTFE (polytetrafluoroethylene) tubing by connecting an aqueous flow with an oil flow via a CTFE (chlorotrifluoroethylene) cross-junction (Figure 2. 2 a).[29, 30] This approach gives excellent control over the water surface area by changing the relative flow rates of the water and organic phase or the internal diameter of the tubing (Figure 2. 2 b).[31, 32]

The question then arises: what is the real cause of the increase in reaction rate for the 'on water' reaction? Out of the hypothesis previously listed, the hydrophobic effect and the formation of hydrogen bonds between water and the reactant and/or intermediate state are the most probable. In the course of this study, we will try to elucidate this question.

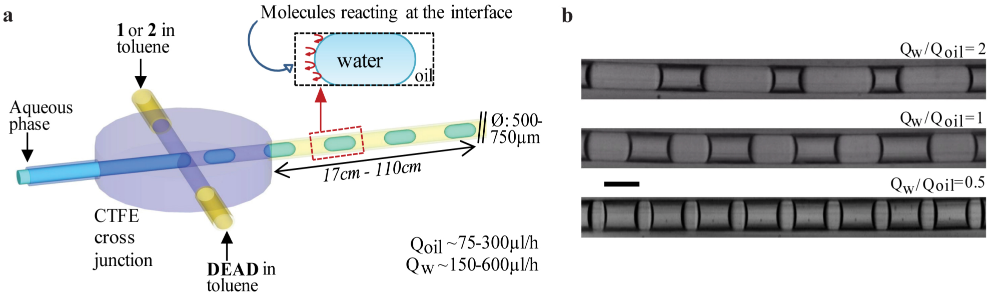
a
1 or 2 in toluene
Molecules reacting at the interface
water
oil
Aqueous phase
Ø: 500-750µm
17cm - 110cm
CTFE cross junction
DEAD in toluene
Qoil ~75-300µl/h
Qw ~150-600µl/h
b
Qw/Qoil=2
Qw/Qoil=1
Qw/Qoil=0.5

Figure 2. 2 Experimental set up. a) Plugs form at junction between toluene solutions containing reagents (‘oil phase’) and aqueous phase, and travel down PTFE tubing to allow reaction to occur. 1 is quadricyclane, 2 is β-pinene and DEAD is diethyl azodicarboxylate b) Plug size and water surface area are controlled by varying the relative flow rates of the two phases. Images taken from fast camera were analyzed with Matlab software to calculate plug lengths, volumes and surface areas. Scale bar = 250 µm.

2.2 Results and discussions

2.2.1 Model reactions

The present study focuses on two model reactions: the cycloaddition of quadricyclane (**1**) and diethyl azodicarboxylate (DEAD)[23] (Scheme 2. 1a), and the Ene reaction between β-pinene (**2**) and DEAD[2] (Scheme 2. 1b). These reactions were shown by Sharpless et al. to be significantly accelerated under ‘on water’ conditions.[2, 33]

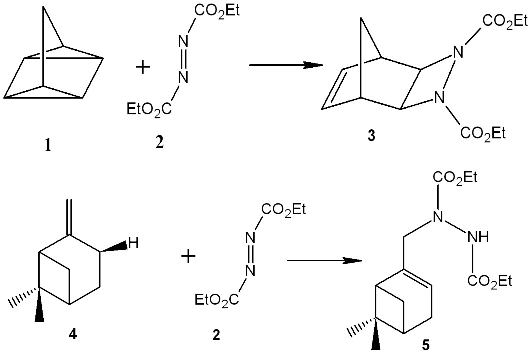
CO2Et
N
N
EtO2C
1
2
3
H
NH
4
5

Scheme 2. 1 Model reactions selected in this study: a) the cycloaddition of quadricyclane (**1**) with DEAD (**2**) ; b) the Ene reaction between β-pinene (**4**) and DEAD (**2**).

DEAD (**2**) is shock and light sensitive and commercially available as a 40 wt% solution in toluene; therefore we performed all reactions in toluene and in toluene ‘on water’, with concentrations in the 1M to 3M range. Furthermore, bulk experiments (Figure 2. 3) show that the reaction rate is linear for the reaction with quadricyclane but slightly plateauing with β-pinene and therefore we concentrate our studies on conversions under 10% where the conversion is linear with time.

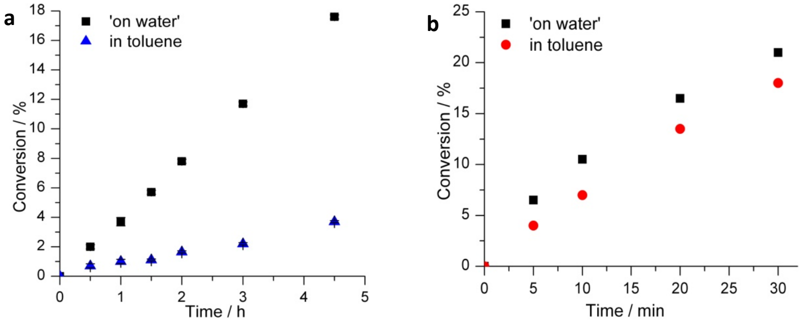

Figure 2. 3 Model reactions performed in bulk for the reactions between a) DEAD and quadricyclane b) DEAD and β-pinene. The ‘on water’ reactions show higher conversions compared to that of the same reactions in toluene, with a moderate effect for the reaction with β-pinene.

The model reactions were then performed in microfluidics. As shown in Figure 2. 4a**,** the ‘on water’ reaction between **1** and DEAD is indeed accelerated to 4.3 ± 0.2 % and 6 ± 0.2 % conversion after 60 min ‘on water’ for water-oil (Q_w/Q_{oil}) flow ratios of 1 (Q1) and 2 (Q2), respectively, compared to only 1.1 ± 0.2 % conversion in toluene.

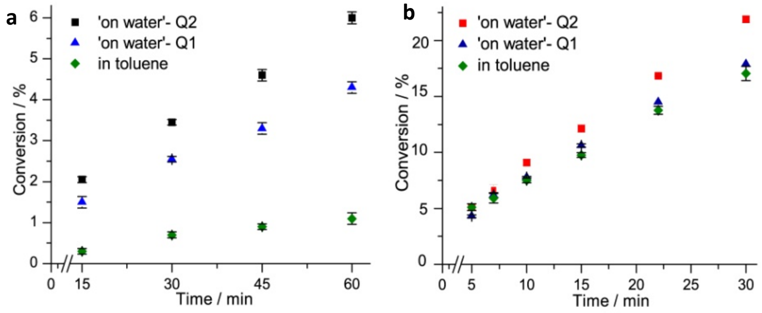

Figure 2. 4 Influence of water on the percent conversion for model reactions in toluene and “on water”. a) The reaction between **1** and DEAD under different water–organic flow ratios (Q_w/Q_o=1=Q1, Q_w/Q_o=2=Q2). b) The reaction between **4** and DEAD under the same water–organic

flow ratios. Note: fits of these data do not pass through the origin because there is a lag between sampling and 1H NMR acquisition.

This indicates that the reaction essentially takes place as a result of the introduction of water. In contrast, we found that the ‘on water’ effect for the reaction of **4** with DEAD is much smaller (Figure 2. 4b). However, the reaction is sensitive to changes in the water surface area as demonstrated by the 5 ± 0.3 % increase in conversion after doubling the water-oil (Q_w/Q_{oil}) flow ratio which resulted in a concomitant increase in water-oil surface area.

We then determined the order of the reaction by systematically varying the concentration of each reactant between 0.5 M and 3 M. The reaction between DEAD and **1** was performed with a flow ratio $Q_w/Q_{oil}=1$ and the reaction between DEAD and **4** with a flow ratio of two. The conversions were not corrected for conversions in toluene phase due to the low conversion in toluene for the reaction between DEAD and **1**. The slopes of the product concentration versus time give access to the initial reaction rate r_0 (Table 2. 1). The partial order was obtained by comparing the reaction with initial concentrations of 2 M for both reagents and a reaction with a lower or higher concentration of one reagent. For both reactions, the observed total reaction order is close to two, strongly indicating that the reaction under these conditions is a simple bimolecular reaction, presumably occurring at the water interface.

Table 2. 1 Partial order for the reaction between DEAD and **1** or **2**. Using different combinations of reactant initial concentrations, the partial reactions order for both reactions was found to be around 1, corresponding to a total reaction order of 2.

$[1]_0$ [mol L^{-1}]	$[DEAD]_0$ [mol L^{-1}]	$[4]_0$ [mol L^{-1}]	r_0 [mol L^{-1} min^{-1}]	Partial order
2	2	-	$5.83 \pm 0.2x10^{-4}$	1.3
2	1.5	-	$3.75 \pm 0.3x10^{-4}$	1.5
2	1	-	$2.67 \pm 0.3x10^{-4}$	1.1
1	2	-	$2.33 \pm 0.3x10^{-4}$	1.3
3	2	-	$7.67 \pm 0.3x10^{-4}$	0.7
-	2	**2**	$5.83 \pm 0.1x10^{-3}$	1
-	1	**2**	$3.08 \pm 0.1x10^{-3}$	0.9
-	2	**1**	$2.58 \pm 0.1x10^{-3}$	1.2

The kinetic isotope effect (KIE) is described as the ratio of reaction rates of two isotopes in a chemical reaction. The substitution of an isotope by another one can highly modify the kinetics when the replacement involves a chemical bond forming or breaking in the rate limiting step: this situation is termed primary isotope effect. When no bond forming or breaking are involved, a secondary isotope effect is observed. Since the largest KIE are observed when a hydrogen atom is exchanged for deuterium, we measured the rate constant ratio of the model reactions in the presence on water H_2O and deuterium oxide D_2O (k_H/k_D). Using the same final concentrations of reactant (1 M) in droplet and knowing that the partial reaction order is one, the reaction rate is equal to the reaction rate constant ($r = k[1]^1[1]^1$). Therefore, the measure of the initial slopes representing the conversion over time gives us access to the reaction rate constant. As expected for a non-acid/base catalysed reaction, we measured small kinetic solvent isotope effects (Figure 2. 5). For both reactions, there is a higher conversion 'on water' than 'on D_2O' and this difference stays the same when the water/oil flow ratio is increased (Q_w/Q_{oil}=1=Q1, Q_w/Q_{oil}=2=Q2) with k_H/k_D in the range of ~ 1.1 to 1.2 and independent of the flow rate ratios. Since no bond forming or breaking are involved, these results indicate that water could be involved in the stabilization of the transition state by formation of hydrogen bonds.

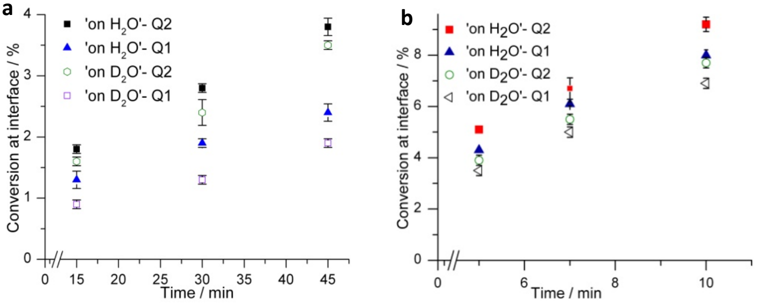

Figure 2. 5 Isotope effect measured 'on water' and 'on D_2O' performed in tubing for the reaction between a) **1** and DEAD and b) between **4** and DEAD. Note: the axis label 'conversion at interface' indicates that the 'on water' conversions have been corrected for conversion in toluene phase.

2.2.2 Influence of the water contact area

The fluidics platform allows systematic variation of the surface area available to the reacting molecules while keeping all other parameters constant. In order to establish that the reaction between water and the reactants is only happening at the hemispherical cap of the water plug, a series of experiments were performed using the reaction between DEAD and **1**. The first experiment was done in 750 µm inner diameter (ID) tubing; the initial concentration was 2 M for both reagents, and the total flow rate was 300 µL h^{-1}. By increasing the water/oil flow ratio from 1 (Q1) to a flow ratio of 2 (Q2), the initial rate constant went from 6.2 x 10^{-6} L mol^{-1} s^{-1} to 1.1 x 10^{-5} L mol^{-1} s^{-1} respectively (values obtained from Figure 2. 4). The increased factor is around 1.8 and represents a good illustration of the water effect. When the flow ratio is doubled, the water plug length is doubled and we did not observe films between water plug and tubing wall under the microscope at the flow rates and plug volumes used (Figure 2. 6). Considering that the reaction is occurring only at the plug caps, the surface cap to volume ratio goes from 1.65 x 10^{-3} μm^{-1} to 2.8 x $10^{-3}\mu m^{-1}$ for a flow ratio of 1 and 2 respectively. As the increase in rate constant (1.8) correlates to the increase of surface contact (1.7), we can conclude that the reaction is occurring mainly at the interface between the water caps and the oil phase.

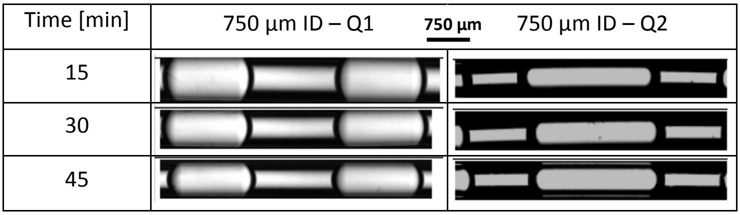

Figure 2. 6 Images of water droplets in time in 750 µm PTFE tubing and different flow ratios. Q1 and Q2 correspond to water/oil flow ratios of 1 and 2, respectively. No apparent oil films were visible between the water plugs and the tubing walls.

The absence of a toluene film between the water droplet and the tubing walls was further demonstrated using fluorescence microscopy. With a fluorescent dye diluted in toluene (1 mg mL^{-1}, Nile red), we formed water plugs in tubing as described in Figure 2. 2 (total flow rate 300 µl/h, flow ratio Q_{water}/Q_{oil}=1).

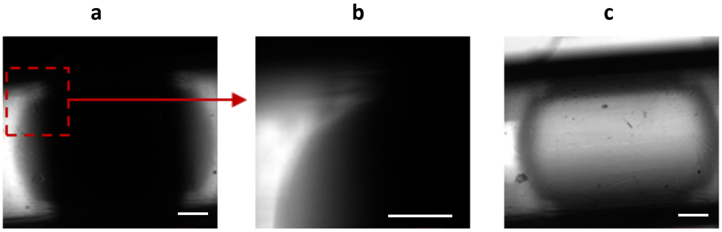

Figure 2. 7 Fluorescent images of water plugs in died toluene with Nile red, flowing in PTFE tubing. a. No fluorescent signal was detected between the water plugs and tubing wall, confirmed by the 10 X magnify image represented in b. The bright field image of the same droplet is depicted in c. Scale bar = 200 µm.

Using a fluorescence microscope and specific excitation and emission wavelengths (λ_{exc}= 488nm, λ_{em}=617nm), fluorescence images (Figure 2. 7a 4x objective, b;

10x objective) clearly show the absence of any toluene film between the water droplet and the tubing walls as there is no fluorescence. Picture c shows the plug in bright field mode. Therefore, the water surface area is taken as the hemispherical cap of water meniscus. [34-38]

To probe directly the effect of the water surface, we measured conversions at three different reaction times while varying the surface-to-volume ratio by changing the water and organic phase flow rates and by using 750 and 500 µm internal diameter tubing. As shown in Figure 2. 8, there is a linear relationship between the surface area and conversion which implies that the contact between the oil and the water phase is directly involved in the observed rate enhancements.

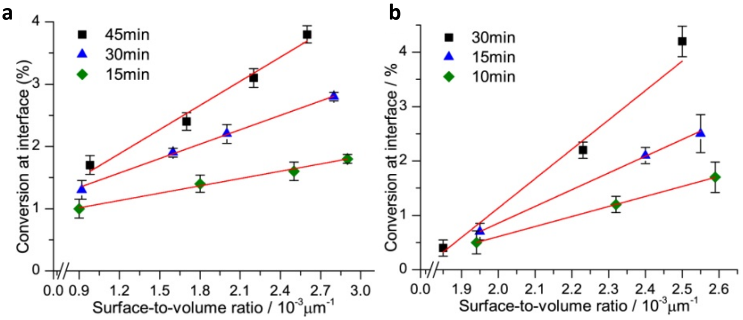

Figure 2. 8 Influence of the surface-to-volume ratio on the percent conversion of DEAD with a) 1 or b) 2. Note: "Conversion at interface" indicates that the "on water" percent conversions have been corrected for the conversion that takes place in the toluene phase.

For a constant initial concentration of DEAD (2 M), we increased the concentration of **1** and **4** from 2 M to 10.5 M and 6.4 M, respectively (close to neat conditions). As expected, the increase of concentration leads to an increase of reaction rate for the reactions in toluene (Figure 2. 9). Unexpectedly, the 'on water' reaction does not show a similar dependence of rate enhancement on starting material concentration. The 'on water' reaction of DEAD with **1** (10.5 M) is accelerated almost 3-fold, whereas the reaction of DEAD with **4** (6.4 M) is slowed down 3-fold compared to the reaction rates at 2M starting concentration (as estimated from initial reaction rates). These results strongly suggest that the reaction with quadricyclane is limited by diffusion of reagent molecules to the surface. For the reaction with β-pinene, we hypothesized that the reaction products remain pinned at the interface and prevent the water surface from catalysing further reactions. This results in a decreased reaction rate at higher concentration of reactants or prolonged reaction times.

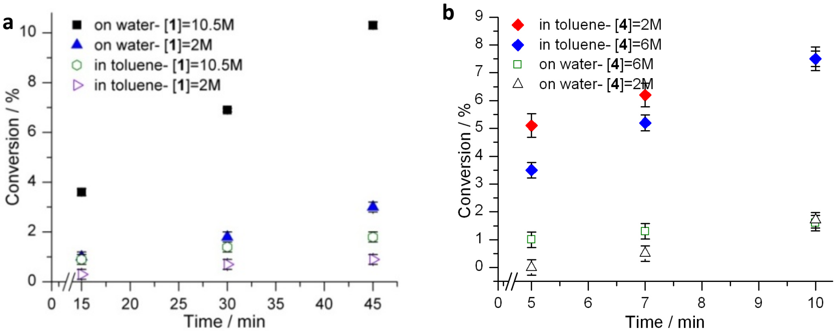

Figure 2. 9 a), b) effect of the starting material concentrations on the kinetics for in toluene and ‘on water’ reactions between DEAD and **1** or **4**, respectively. When the reactions were performed in toluene, an increase of reactant concentrations led to an increase of the reaction rate. For the ‘on water’ reaction, the same effect was observed with **1** whereas with **4**, it showed the opposite effect. The diffusion of the product from the water/oil interface could be the limiting step of the reaction with DEAD and **4**. Note: the ‘on water’ conversions have been corrected for conversion in toluene phase at water/oil flow ratios $Q_w/Q_{oil}=2$.

2.2.3 Influence of the temperature

As we know the conversion at a certain reaction time and the total amount of interface associated with this conversion, we can calculate the number of molecules reacted per unit surface area per unit time (i.e. a turnover number, Table 2. 2). We collected 100 µL reaction volume at three different time points (15, 22 and 30 min) and measured the conversion (corrected for background reaction in toluene). Surprisingly, for both reactions the turnover number decreases of 11-14% over the course of 15 minutes.

Table 2. 2 Turnover for the reactions between DEAD and **1** or **2**. The number of molecules reacting per surface area and per second is decreasing for both reactions implying that limiting steps can involve the diffusion of the reactant and/or of the product from and to the oil/water interface.

Reaction	**1 + DEAD**			**4 + DEAD**		
Time [min]	**15**	**22**	**30**	**15**	**22**	**30**
Conversion at interface [%]	1.8	2.4	3.1	2.5	3.3	4.2
Molecules reacted (x 10^{18})	1.1	1.4	1.9	1.5	2.0	2.5
Surface contact [10^{-3} x μm^{-1}]^{a}	2.87	2.86	2.79	2.55	2.57	2.50
Molecule/μm^2/s	4.2 x 10^6	3.8 x 10^6	3.7 x 10^6	6.6 x 10^6	5.9 x 10^6	5.6 x 10^6

[a] Surface contact error ± 0.05 x 10-3

This suggests that the interfacial activity decreases over time, perhaps due to product molecules remaining at the interface. This form of ‘product inhibition’ could explain why it is sometimes difficult to reproduce 'on water' conditions in stirred bulk emulsions, where fresh oil-water interface is continuously generated.

Arrhenius plots were used to determine the temperature dependence of the reaction rates for both reactions 'on water' and in toluene. Equation 1, where k is the rate constant, A the pre-exponential factor and R the gas constant, is used to determine the activation energy E_a.

$$\ln k = \ln A - \frac{Ea}{R}\left(\frac{1}{T}\right) \tag{1}$$

For the reaction between **1** and DEAD, the conversion was measured at 5° C, 20 °C and 35 °C and for the reaction between **4** and DEAD, at 20 °C, 40 °C and 60 °C(Figure 2. 10). The increase or decrease of temperature was achieved by placing the tubing in a warm bath or cold bath, respectively. An advantage of our tubing-based microfluidic system is the ease with which the reaction temperature can be modulated using standard laboratory equipment, as opposed to traditional chip-based microfluidic systems that require sophisticated apparatus for heating and cooling.

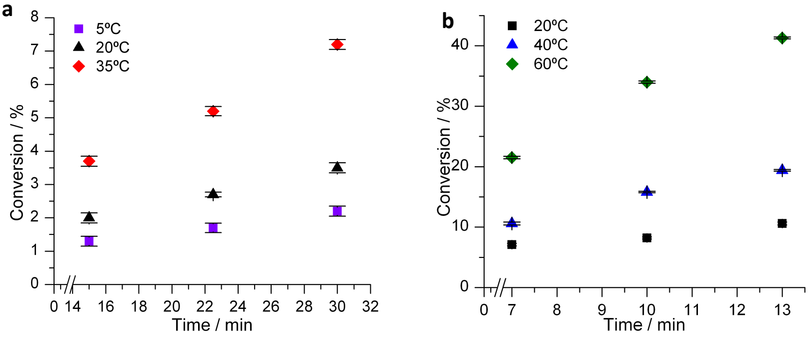

Figure 2. 10 Activation energy determination a), b) Show the conversion versus time at different temperature for the reaction 'on water' between DEAD and **1** or **4**, respectively. These plots give us access to the initial rate constants which allowed the calculation on the activation energy.

As previously explained, the initial slope of the conversion versus time gives us access to the reaction rate constant. Therefore, by plotting the natural logarithm of the rate constant (ln k) versus one over the temperature (1/T), we can determine the value of the activations energy. Both reactions show a considerable drop in activation energy (ΔE_a = 5.4 and 2.4 kcal mol^{-1} for reaction of DEAD with **1** and **4**, respectively) upon introduction of water plugs as summarized in Table 2. 3. A drop in the energy barrier by 5.4 kcal mol^{-1} is in rather good agreement with a theoretically predicted value of around 7.5 kcal mol^{-1} for a hydrogen bond-stabilized transition state the reaction of **1** with DMAD (instead of DEAD) reported by Jung and Marcus[22] . Their mechanistic hypothesis is based on free hydroxyl groups at the water surface, reacting with the intermediates, lowering the energetic barrier and therefore accelerating the reaction (Figure 2. 11.a) Using the Eyring equation, we determined the values for $\Delta H^{\ddagger}$ and $\Delta S^{\ddagger}$ for both ‘on water’ and toluene reactions. For both reaction, the large change in $\Delta H^{\ddagger}$ (23 and 10 kJ mol^{-1}) is accompanied by a more negative value for $\Delta S^{\ddagger}$ for both reactions (-59 and -38 J mol^{-1} K^{-1}, respectively), which indicates that the interfacial nature of the ‘on water’ reaction may put constraints on the reactivity of molecules at the interfaces (Figure 2. 11.b).

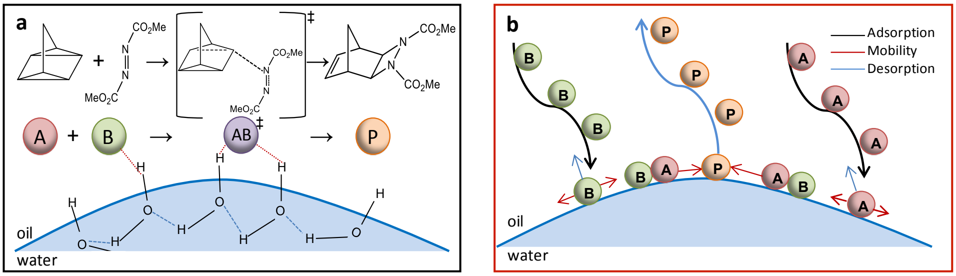

Figure 2. 11 Cartoon of ‘on water’ catalysis. a) Mechanistic hypothesis proposed by Yung and Marcus. The free hydroxyl group at the interface stabilize the reactants and the transition state. b) The reactivity of molecules at the interface is affected by adsorption and desorption processes as well as by their mobility on the surface.

We calculated the rate constants $k_{s,cal}$ (obtained from the activation energy plots) and compare these with $k_{s,obs}$ experimentally determined values from Figure 2. 4 at the same flow rate (Table 2. 3). The striking agreement between the calculated and observed values for the rate constants demonstrate that the biphasic flow approach has provided us with a detailed insight into ‘on water’ reactions

Table 2. 3 Activation energies and rate constants for the reaction between DEAD and **1** or **2.** The calculated surface rate constant k_s from the activation energy correspond well with the observed rate constant k_{obs} obtained from experimental value in Figure 2.4.

Reaction	E_{aS} [a] [kcal mol^{-1}]	E_{aT} [kcal mol^{-1}]	ΔE_a [kcal mol^{-1}]	$k_{s,cal}$ [L mol^{-1} s^{-1}]	$k_{T,cal}$ [L mol^{-1} s^{-1}]	$\mathbf{k_{s,obs}}$ [L mol^{-1} s^{-1}]
1 + DEAD	3.9 ± 0.4	9.3 ± 1.3	5.4	1.3×10^{-5}	1.6×10^{-6}	$\mathbf{1.1 \pm 0.9 \times 10^{-6}}$
4 + DEAD	5.4 ± 1.0	7.8 ± 0.3	2.4	5.2×10^{-5}	7.5×10^{-5}	$\mathbf{5.8 \pm 0.5 \times 10^{-5}}$

[a] the experiments were performed at a flow rate ratio of $Q_w/Q_{oil} = 2$

2.2.4 Blocking the reactive water surface

In order to determine whether the increase in reaction rate is due to interactions with water and not only due to the hydrophobic effect or compartmentalization of the reactants, we added a surfactant to the water phase to create a barrier at the water-oil interface, minimizing interaction of the reactants with the water interface. The hydrophobic effect was proposed by Breslow and Rideout[6] to explain the increase of reaction rate for hydrophobic molecules in water. The authors stipulate that when hydrophobic molecules are dissolved in water, they have a tendency to aggregate to minimise the interaction with water molecules.

The addition of the anionic surfactant SDS (sodium dodecyl sulfate) to the aqueous phase at a concentration above the critical micelle concentration leads to a water surface covered with SDS molecules, making the free hydroxyl groups of water not accessible to the reactants. Figure 2. 12 shows the effect of the addition of SDS in the water phase on the conversion over time for both model reactions. The reactions were performed in tubing, at room temperature and the initial concentrations for both starting materials was 2 M. Four different experimental conditions were compared: reaction in toluene, reaction 'on water' with water/oil flow ratios equal to 1 (Q1), 2 (Q2) and reaction 'on water' with 2% of SDS in the water phase. When SDS is added to the aqueous phase, the reactions essentially came to a halt, with conversions below 'on water-Q1' and similar to the reaction in toluene only. By covering the water interface with surfactant, the reaction is inhibited which demonstrated that the reaction is happening at the interface.

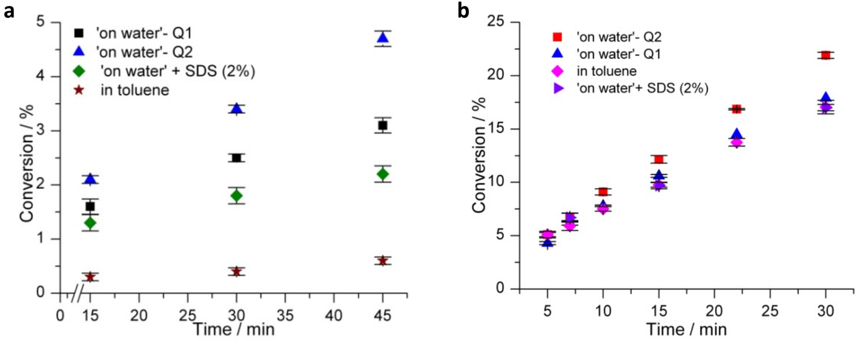

Figure 2. 12 Modification of the water phase in flow, performing reactions in toluene, 'on water' and 'on water + SDS'. a) Reaction between DEAD and **1**. b) Reaction between DEAD and **4**. The initial concentration for both starting materials is 2M. The addition as SDS in water led to a decrease in conversions for both reactions showing that the contact between the reactant and water is a more important factor than compartmentalization.

2.2.5 Influence of the nature of the reactants

In the model proposed by Jung and Marcus[22], the free hydroxyl groups at the water interface are believed to interact with the starting material as well as the intermediate state, lowering the energetic barrier and therefore facilitating the conversion to the final product. Considering the reaction between **1** and DEAD, this will mean the hydrogen bonds would be formed with the nitrogen of DEAD, increasing its electrophilicity and therefore improving the nucleophile attack of **1**. This leads us to ask if there is 'on water' effect with reactant not able to form H-bonds? This question can be addressed by preforming a reaction between **1** and a molecule similar to DEAD that is not able or is less able to form hydrogen bonds. As a substitute, we chose dimetyl acetylenedicarboxylate (DMAcD, **6**), which has an alkynyl group instead of an azo group as depicted in Scheme 2. 2. The lone pair left on the N atom in DEAD attracts the slight positive charge on the H atoms of water molecules: this is the hydrogen bond. However, in DMAcD, the fully saturated carbons of the alkynyl group are not able to form hydrogen bonds.

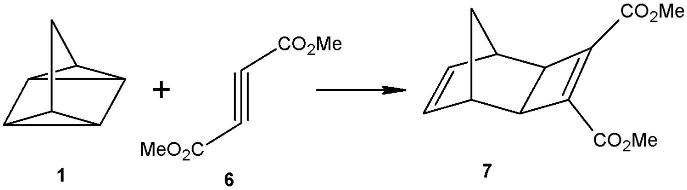

Scheme 2. 2 Cycloaddition of quadricyclane (**1**) and DMAcD (**6**)

Figure 2. 13 shows the conversion over time for the reaction between **1** and DMAcD at two different temperatures (35 °C and 60 °C), 'on water' and neat at the initial concentration of 2 M. At both temperatures, the conversion over time of the reaction performed on water was below that of the reaction performed neat. We propose that the reaction between **1** and DMAcD is not accelerated 'on water' because the carbon atoms in DMAcD do not form hydrogen bonds with water (in contrast to the nitrogen atom in DEAD). This experiment provides further evidence to support the mechanism proposed in Figure 2. 11 in explaining the 'on water' effect observed for the reaction of **1** and DEAD.

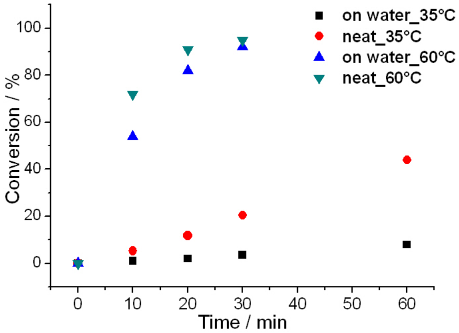

Figure 2. 13 Conversion in time of the reaction between **1** and DMAcD. The neat reactions show higher conversions than the 'on water' reactions, independently of the temperature.

2.3 Conclusions

To conclude, we have demonstrated how biphasic flow can be used to study interfacial reactions on a macroscopic scale. Total flow rate, residence times and most importantly, the interfacial area between the water and the oil phase can be precisely known and controlled in a (micro)fluidic system, which is not possible in bulk emulsions. We have used this technique to quantify the 'on water' effect for the first time. Capitalizing on the versatility of our microfluidic system, we have conducted a series of experiments to further elucidate the molecular mechanism underlying the on water effect. Our data correspond well with the model proposed by Jung and Marcus in which hydrogen bonds stabilize the transition state of the reaction thereby accelerating it. But it is also quite apparent that the magnitude of the 'on water' effect can be rather modest (as seen in the reaction with **4**), and even if the reaction is accelerated initially, the effect becomes less pronounced with longer reaction times. As shown in Figure 2. 11 b, the interfacial nature of the reaction can greatly influence the overall reaction rates as product molecules might become pinned at the interface. These factors strongly counteract the favourable reduction in activation energy. In bulk emulsion studies, where the emphasis has been on high conversions, these effects are not observable because droplets are formed and merged continuously, thereby exposing 'fresh' water/oil interfaces. Our method provides a robust platform for rapidly establishing the key features of 'on water' conditions, improving their potential for reducing the use of organic solvents towards a green chemistry.

2.4 Experimental section

Chemicals and reagents

Quadricyclane was purchased from Mercachem, diethyl azodicarboxylate (40 wt % in toluene) and beta-pinene were purchased from Sigma-Aldrich. All reagents were used as received. Deionized (DI) water from a Milli-Q purifier was used throughout this study.

Kinetics analysis

1H NMR spectra were recorded on a Brüker Avance 500 Cryo Ultrashield (500 MHz) and on a Varian Inova400 (400 MHz) spectrometers using toluene-d8 or benzene-d6 as internal standards. Reactions were quenched by diluting the samples in a vial containing benzene-d6 or toluene-d8 (with stirring) placed on ice. For every data point and regardless of the overall reaction time, the same volume (100 µL) of reaction mixture was collected from the outlet tubing, which takes 20 min using flow rates of 300 µl/h. The conversions of the quenched reaction mixtures were determined using NMR spectra by comparing product peak integration to reactant peak integration. Conversions reported are average values from at least two experiments.

Fluidic methods

The oil and aqueous phases were loaded into Hamilton glass syringes with 21G disposable needles attached. PTFE tubing (500 or 750 µm ID) was fitted over the needles and used to transport the liquid to the droplet formation cross. To form droplets a 500 µm or a 750 µm bore CTFE cross (VICI) was connected such that the oil and aqueous phases entered the cross at right angles to each other with the fourth exit connected to an additional length of PTFE tubing (500 or 750 µm ID) for the reaction tube. Flow rates were maintained using Harvard PHD 2000 infusion syringe pumps. For all reactions, the droplet frequency was estimated to be around 0.06 Hz (calculated from videos of 40 droplets). The reaction time could be controlled either by varying the total flow rate of the solutions or by changing the length of the reaction tube. Outlet channels were imaged in real time using an inverted Olympus IX71 microscope connected to a Phantom fast camera (Miro eX4). Images were then analyzed with Matlab software to estimate surface-to-volume ratios with high precision.

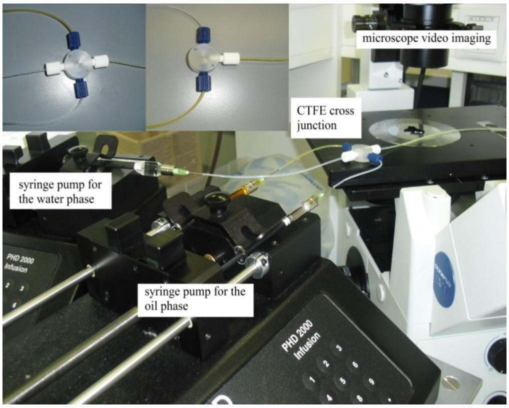
microscope video imaging
CTFE cross junction
syringe pump for the water phase
syringe pump for the oil phase
PHD 2000 Infusion

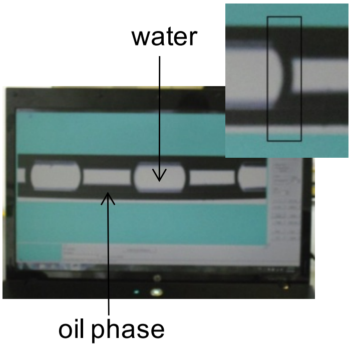
water
oil phase

Cycloaddition of quadricyclane (1) with diethyl azodicarboxylate (2) in microfluidics

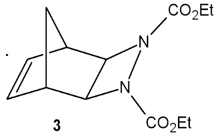
CO2Et
N
N
CO2Et
3

The flow of “40%” DEAD in toluene solution (2 M) meets the flow of quadricyclane solution (2 M) leading to the initial concentration of 1 M for both starting material. The conversion in time was monitored by NMR. Data for **3**: ^{1}H NMR (400 MHz, benzene-d6) δ 5.56 (s, 2H), 4.15 (q, 4H), 4.1 (s, 2 H), 3.1 (s, 2 H), 1.9 and 1.50 (AB system, 2H), 0.9 (t, 6H);

The ene reaction between β-pinene (4) and diethyl azodicarboxylate (2) in microfluidics

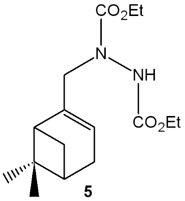
CO2Et
N
NH
CO2Et
5

The flow of “40%” DEAD in toluene solution (2 M) meets the flow of β-pinene solution (2 M) leading to the initial concentration of 1 M for both starting material. The conversion in time was monitored by NMR. Data for **5**: ^{1}H NMR (400 MHz, Toluene-d8) δ 6.25 (m,1H), 5.4 (s, 1H), 4.2 (m, 4H), 4.03 (bs, 2H), 2.37 (m, 1H), 2.26 (m, 2H), 2.09 (m, 2H), 1.28 (s, 3H), 1.25 (t, 6H), 1.13 (d, 1H), 0.78 (s, 3H).

Cycloaddition of quadricyclane (1) and DMAcD (6) in microfluidics

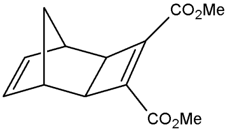
CO2Me
CO2Me
7

The flow of quadricyclane solution (2 M) meets the flow of DMAcD solution (2 M) leading to the initial concentration of 1 M for both starting material. The conversion in time was monitored by NMR. Data for **7:** ^{1}H NMR (400 MHz, CDC13) δ 6.05 (s, 2H), 3.96 (s, 2H), 3.52 (s, 6H), 2.95 (s, 2H), 1.62 and 1.08(AB system, 2H)

Statistics on droplets uniformity (300 µl/h total flow rate)

Flow ratio Q_{water}/Q_{oil}	**Mean droplet size [µm]**	**Mean Surface-to-volume ratio [μm^{-1}]**	**Number of droplets**
1	1801 ± 39	$1.7 \pm 0.07 \times 10^{-3}$	40
2	2441 ± 60	$2.7 \pm 0.09 \times 10^{-3}$	30

Flow ratio Q_{water}/Q_{oil}	**Mean droplet size [µm]**	**Mean Surface-to-volume ratio [μm^{-1}]**	**Number of droplets**
1	1512 ± 36	$1.9 \pm 0.04 \times 10^{-3}$	80
2	2269 ± 50	$2.8 \pm 0.04 \times 10^{-3}$	60

2.5 References

1. P. T. Anastas and M. M. Kirchhoff, *Accounts Chem Res*, **2002**, *35*, 686-694.
2. A. Chanda and V. V. Fokin, *Chem Rev*, **2009**, *109*, 725-748.
3. K. M. Lange, K. F. Hodeck, U. Schade and E. F. Aziz, *Journal of Physical Chemistry B*, **2010**, *114*, 16997-17001.
4. K. J. Tielrooij, R. L. Timmer, H. J. Bakker and M. Bonn, *Physical Review Letters*, **2009**, *102*, 198303.
5. R. Ludwig, *Angew Chem Int Ed Engl*, **2001**, *40*, 1808-1827.
6. D. C. Rideout and R. Breslow, *J Am Chem Soc*, **1980**, *102*, 7816-7817.
7. P. A. Grieco, P. Garner and Z. He, *Tetrahedron Lett*, **1983**, *24*, 1897-1900.
8. R. Breslow, *Accounts Chem Res*, **1991**, *24*, 159-164.
9. M. C. Pirrung, K. D. Sarma and J. M. Wang, *J Org Chem*, **2008**, *73*, 8723-8730.
10. W. Blokzijl, M. J. Blandamer and J. B. F. N. Engberts, *J Am Chem Soc*, **1991**, *113*, 4241-4246.
11. A. Meijer, S. Otto and J. B. F. N. Engberts, *J Org Chem*, **1998**, *63*, 8989-8994.
12. S. Otto and J. B. Engberts, *Org Biomol Chem*, **2003**, *1*, 2809-2820.
13. R. Breslow, U. Maitra and D. Rideout, *Tetrahedron Lett*, **1983**, *24*, 1901-1904.
14. S. Otto, W. Blokzijl and J. B. F. N. Engberts, *J Org Chem*, **1994**, *59*, 5372-5376.
15. G. K. vanderWel, J. W. Wijnen and J. B. F. N. Engberts, *J Org Chem*, **1996**, *61*, 9001-9005.
16. J. Chandrasekhar, S. Shariffskul and W. L. Jorgensen, *Journal of Physical Chemistry B*, **2002**, *106*, 8078-8085.
17. A. Lubineau, J. Auge and Y. Queneau, *Synthesis-Stuttgart*, **1994**, 741-760.
18. A. Lubineau and J. Auge, *Top Curr Chem*, **1999**, *206*, 1-39.

19. A. Lubineau and E. Meyer, *Tetrahedron*, **1988**, *44*, 6065-6070.
20. J. J. Gajewski, *J Org Chem*, **1992**, *57*, 5500-5506.
21. W. Blokzijl and J. B. F. N. Engberts, *Angew Chem Int Edit*, **1993**, *32*, 1545-1579.
22. Y. Jung and R. A. Marcus, *J Am Chem Soc*, **2007**, *129*, 5492-5502.
23. S. Narayan, J. Muldoon, M. G. Finn, V. V. Fokin, H. C. Kolb and K. B. Sharpless, *Angew Chem Int Ed Engl*, **2005**, *44*, 3275-3279.
24. J. E. Klijn and J. B. F. N. Engberts, *Nature*, **2005**, *435*, 900-900.
25. B. Ahmed-Omer, D. A. Barrow and T. Wirth, *Tetrahedron Lett*, **2009**, *50*, 3352-3355.
26. B. Ahmed, D. Barrow and T. Wirth, *Adv Synth Catal*, **2006**, *348*, 1043-1048.
27. B. J. Xu, W. F. Cai, X. L. Liu and X. B. Zhang, *Chem Eng Res Des*, **2013**, *91*, 1203-1211.
28. A. Fallah-Araghi, K. Meguellati, J. C. Baret, A. E. Harrak, T. Mangeat, M. Karplus, S. Ladame, C. M. Marques and A. D. Griffiths, *Physical Review Letters*, **2014**, *112*, 028301.
29. S. L. Anna, N. Bontoux and H. A. Stone, *Appl Phys Lett*, **2003**, *82*, 364-366.
30. V. Trivedi, A. Doshi, G. K. Kurup, E. Ereifej, P. J. Vandevord and A. S. Basu, *Lab Chip*, **2010**, *10*, 2433-2442.
31. T. Hatakeyama, D. L. Chen and R. F. Ismagilov, *J Am Chem Soc*, **2006**, *128*, 2518-2519.
32. A. B. Theberge, F. Courtois, Y. Schaerli, M. Fischlechner, C. Abell, F. Hollfelder and W. T. Huck, *Angew Chem Int Ed Engl*, **2010**, *49*, 5846-5868.
33. An even faster reaction was reported using dimethyl azodicarboxylate (DMAD) instead of DEAD. However, the DMAD ester is not stable in the presence of water and in our hands hydrolyzed rapidly forming gas bubbles in the tubing within minutes.
34. G. Bercic and A. Pintar, *Chem Eng Sci*, **1997**, *52*, 3709-3719.
35. M. T. Kreutzer, P. Du, J. J. Heiszwolf, F. Kapteijn and J. A. Moulijn, *Chem Eng Sci*, **2001**, *56*, 6015-6023.
36. N. Harries, J. R. Burns, D. A. Barrow and C. Ramshaw, *Int J Heat Mass Tran*, **2003**, *46*, 3313-3322.
37. J. R. Burns and C. Ramshaw, *Lab on a Chip*, **2001**, *1*, 10-15.
38. J. Jovanovic, E. V. Rebrov, T. A. Nijhuis, V. Hessel and J. C. Schouten, *Ind Eng Chem Res*, **2010**, *49*, 2681-2687.

Chapter 3

Self-organization of the bacterial cell-division protein FtsZ in confined environments

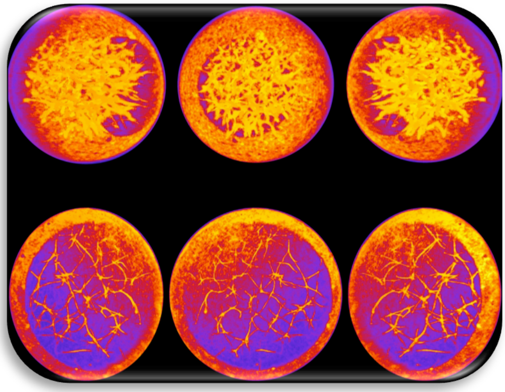

Parts of this chapter have been published:
S. Mellouli, B. Monterroso*, H. R Vutukuri, E. te Brinke, V. Chokkalingam, G. Rivas and W. T. S. Huck, *Soft Matter*, **2013**, *9*, 10493-10500.

3.1 Introduction

Cells provide highly complex reaction environments, where crowding, confinement and interfaces play an important role. In bacteria, around 30% of the intact cytoplasm volume is occupied by macromolecules.[1] The energetics and dynamics of macromolecular reactions in crowded environments differ from dilute solutions due to excluded volume effects and additional weak, non-specific attractive and repulsive interactions with background molecules or large structures that are highly system-dependent.[2-7] A fundamental chemical consequence of volume exclusion is a generalized non-specific force that favours macromolecular compaction and protein-protein association in order to minimize the excluded volume.[8-10] In general, larger and less compact macromolecules are more sensitive to excluded volume effects than smaller and more compact ones. Crowding has a significant effect on the assembly of fibril-forming proteins. Furthermore, crowding favours bundling of filaments leading, under certain circumstances, to spatial self-organization of fibres.[11] For example, a strong enhancement of actin polymerization and bundle formation by crowders has been shown *in vitro*.[12, 13] Crowding appears to affect actin dynamics by slowing down subunit dissociation and decreasing the critical concentration of polymerization of the ADP-actin filaments, potentially enhancing the binding of actin regulatory proteins.[14] The combination of packing constraints and spatial confinement, studied in cell-sized microchambers, enhances actin bundle formation by decreasing the threshold concentration for the isotropic-to-nematic phase transition.[15] Actin network architecture is determined by the size[16] and shape of the spatial boundaries, and therefore myosin-induced contraction will vary with the geometry, as determined using bar-shaped micropatterns.[17] As with actin, geometric conditions have significant effects on the self-organization of tubulin.[18] Microfabricated chambers of defined dimensions have been shown to determine the microtubule aster positioning at the geometric center without the need of molecular motors.[19] This organization becomes highly asymmetric in confined spherical geometries as determined by the relative sizes of microtubules and container, generating cortical bundles.[20, 21]

We are interested in the behaviour of FtsZ polymers in crowded environments. FtsZ, prokaryotic homologue of tubulin, is an essential protein required for septation in most bacteria. It is an early septum component, forming a ring (Z ring) at mid-cell during cell division and is thought to be responsible for initiating and driving cell constriction.[22-25] In the presence of GTP, FtsZ polymerizes in an apparently cooperative manner to form single stranded protofilaments of around 100 monomers under close to physiological conditions[26] highly dynamic *in vivo*[27] and *in vitro.*[28] In the presence of crowding agents, these protofilaments arrange into supramolecular structures that range from flexible single and multi-stranded fibres, to circles, bundles and toroids depending on solution and working conditions.[22, 23, 25, 29, 30] Excluded volume models satisfactorily described, qualitatively and often quantitatively, the behaviour of FtsZ in *in vitro* studies using different crowders.[29, 31] As the assembly of FtsZ to form the structures active in division takes place at the membrane, experimental efforts are being made to study FtsZ in membrane-like systems. A variant of FtsZ, containing an artificial targeting sequence able to bind to the membrane, was able to narrow the region of the liposome in which is located in the absence of the natural anchoring elements. Inside tubular liposomes, this FtsZ mutant located preferentially in certain regions and, eventually, produced constrictions,[32] while their incorporation on the outer face produced the deformation of the lipid surface.[33, 34] The arrangement of these mutant polymers has also been studied inside lipid tubes, revealing ribbon-like structures[35] similar to those formed by wild type FtsZ in the presence of high concentrations of crowders.[29] FtsZ has also been encapsulated in giant vesicles with other elements of the proto-ring (the first protein complex formed in bacterial division) showing deformations of the vesicles formed by lipid,[36-38] not observed with those made of inner membrane isolated from bacteria.[39] A complementary tool to study the reactivity of FtsZ and polymer dynamics inside confined cell-like compartments is the water-in-oil formation of microdroplets in microfluidic devices, resulting in droplets of sizes similar to giant vesicles, but completely monodisperse and easily manipulated (for instance, to change their geometry) inside microfluidic channels.[40] Therefore, microdroplets would allow us to probe and visualize how the complex process of FtsZ bundle formation from GTP-driven polymerization of FtsZ is influenced by flow, crowding and confinement.

In this study we show how FtsZ polymerization in crowded droplets coated with *E. coli* lipids leads to a dense fibrous network, the geometry of which depends on droplet shape, concentration of FtsZ monomers, crowding agent, and flow conditions in the microfluidic channels.

3.2 Results and discussions

3.2.1 Microdroplets in microfluidics

Figure 3. 1 shows a schematic of the flow-focusing microfluidic device for droplet production. Two streams of dispersed aqueous phases in working buffer and Ficoll 70 are mixed in a 1:1 ratio prior to the droplet formation junction. One stream contains FtsZ at the specified concentration; the other stream delivers GTP at a concentration of 6 mM. A well-controlled crowded environment was induced by the addition of Ficoll 70, chosen because of its inert nature.[29, 41] Addition of the crowder induces the arrangement of FtsZ polymers into bundles,[29] suitable for the observation of their organization via confocal microscopy.

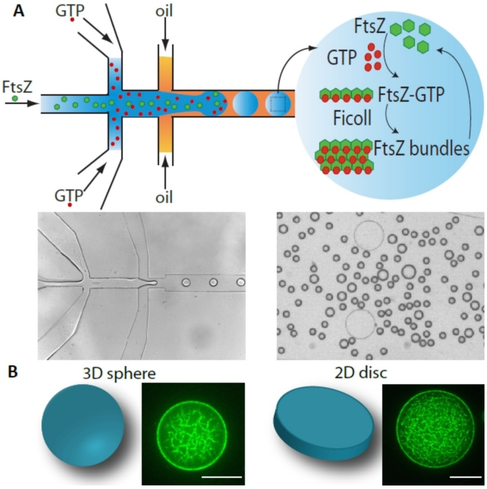

Figure 3. 1 (A) Schematic illustration of the microfluidic chip. Below, images showing typical production and collection of droplets. (B) Geometries obtained with the microfluidic chip and, below, corresponding fluorescence images of droplets containing FtsZ bundles. Scale bar = 20 µm.

In order to find the appropriate oil-surfactant combination to study our system, we first investigated a range of lipids in bulk emulsions. The surfactants tested were monoolein, asolectin and *E. coli* lipids. Monoolein is a lipid widely used for emulsion stabilization due to its biocompatibility and multiple applications in the fields of drug delivery, emulsion stabilization and protein crystallization.[42] *Escherichia coli* lipids are a ternary mixture of the lipids naturally found in the membrane of the bacteria, and in the same relative abundances, and it was chosen to better mimic the boundary that FtsZ founds in the cell. Asolectin was chosen as an alternative lipid mixture, as the ability of the *E. coli* lipids to stabilize microdroplets had not been tested before. Bulk emulsions were prepared by gently pipetting up and down two immiscible solutions: an aqueous phase containing 0.5 g L-1 FtsZ, 100 g L-1 Ficoll, 1mM GTP in working buffer and an oil phase composed of the specified lipids dissolved in oil. Using squalane as the continuous phase and monoolein as the surfactant, at FtsZ and Ficoll 70 concentrations of 0.5 g L^{-1} and 100 g L^{-1}, we found no bundles distributed within the lumen, FtsZ appearing mainly at the oil-water interphase (Figure 3. 2). However, with the same FtsZ and Ficoll 70 concentrations, bundles were present when asolectin or *E. coli* lipids were used to stabilize the droplets.

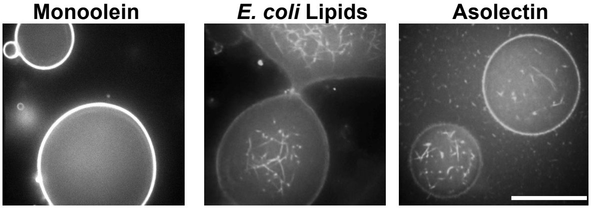

Figure 3. 2 FtsZ bundles were only observed with asolectin and *E. coli* lipids. With monoolein as a surfactant, the high fluorescence intensity at the droplet surface shows that most of FtsZ is adsorbed at the surface explaining the absence of FtsZ bundles in the droplet. Scale bar = 20 µm.

Although asolectin successfully stabilized the water droplets, it proved not suitable for the study of the FtsZ system, as protein was found in the oil phase, which was much less pronounced in the case of *E. coli* lipids. Of the different oils investigated (using *E. coli* lipids as surfactant), fluorinated oils proved unsuitable for bundle formation as all FtsZ adhered to the interface, probably as a result of improper formation of the lipid monolayer at the oil-water interface. Mineral oil, on the other hand, resulted in homogeneous fibre networks in droplets and the lowest fluorescence intensity in oil phase (Figure 3. 3). Although the resulting droplets lack the components and functionalities found in the bacterial membrane, the lipid monolayer provides a more biologically relevant alternative to the triblock copolymer surfactants typically used in droplet-based microfluidics.[43]

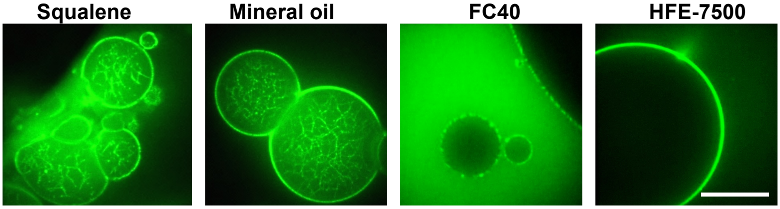

Figure 3. 3 Bulk emulsion of FtsZ bundles in different oil phases containing *E. coli* lipids (25 g L^{-1}). Scale bar = 20 µm

In all microfluidics experiments, we used *E. coli* lipids (25 g L^{-1}) in mineral oil as the continuous phase. To minimize droplet coalescence, a delay channel was added between the flow-focusing junction and the device reservoir (750 µm length), which allowed the lipids to self-assemble at droplet interfaces.[44, 45]

Automated syringe pumps controlled the flow rates inside the microfluidic device, rendering uniform droplet production at a production frequency around 300 droplets/sec. After droplet formation, the flow was stopped by cutting the inlet tubing allowing us to trap droplets in the device reservoir for fluorescence image analysis (Figure 3. 1). Despite some droplet coalescence due to our weak phospholipid surfactant, around 80% of the droplets were monodisperse, which allowed us to get sufficient data for quantitative analysis. The advantage of our technique is that we can induce polymerization and bundle formation of the FtsZ unassembled species (monomers and small oligomers)[46] on chip, confined in droplets of different dimensionality. Figure 3. 4 is a schematic overview of our microchip used for droplet production. The narrow channels in the reservoir (~ 20 µm width and 800 µm long) were meant to study FtsZ behaviour in cylinder shape droplets but fast drying of the droplets when trapped in the channels impaired analysis. Therefore, we focused only on ~20 pL spherical (~30 µm diameter) and disc-shaped droplets (~50 µm diameter) using two devices of different height (28µm and 10 µm), which allowed us to directly relate differences in bundle distribution with the changes in dimensionality and crowder concentrations.

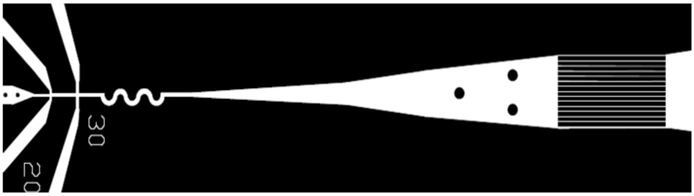

Figure 3. 4 Schematic illustration of the microfluidic chip design

3.2.2 Dynamics of FtsZ bundles

As previously mentioned, FtsZ needs to bind to GTP to polymerize and form protofilaments.[47] In the presence of crowder, these protofilaments rearrange to form bundles. Because droplets are closed systems, the polymerisation will become depleted of nucleotide, at which point the FtsZ bundles depolymerise back to the unassembled species.

Figure 3. 5 shows the emergence and disappearance of FtsZ bundles in microfluidically produced droplets containing concentrations of FtsZ, Ficoll 70 and GTP of 1 g L^{-1}, 100 g L^{-1} and 3 mM respectively. These results show that the formation of the fibrous network is fully reversible, with complete depolymerisation of FtsZ bundles in both spherical and disc-like droplets after approximately 40-50 min, in agreement with turbidity measurements in solution.[29] Interestingly, FtsZ bundle formation is delayed by 5-l0 min, in contrast to bulk solution experiments where bundles are formed instantaneously upon mixing of FtsZ with GTP. These differences might arise from shear forces inside droplets flowing through narrow channels, as well as generated between the different flows of the oil and aqueous phases at the junction, which disrupt the arrangement of polymers into bundles or increase the depolymerisation rates. This delay was not observed at higher Ficoll concentrations, which could be explained by the fact that the higher viscosity of the solutions dampens the shear forces, while at the same time favouring bundle formation through crowding.[29] In all further experiments, droplets were imaged around 20-40 min after formation and stopping flows.

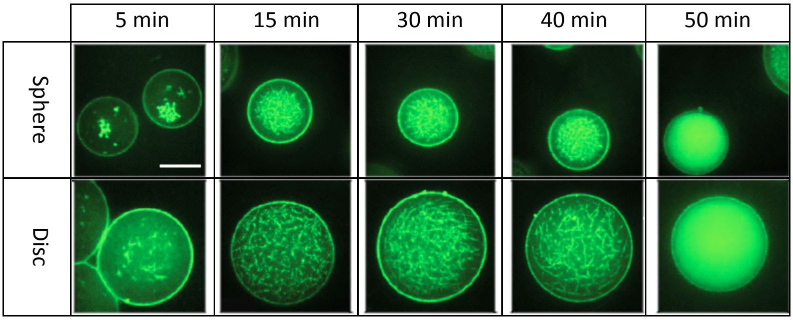

Figure 3. 5 FtsZ bundle stability in time. FtsZ droplets were produced in microfluidics. The final concentrations of FtsZ, Ficoll and GTP were 1 g L^{-1}, 100 g L^{-1} and 3 mM respectively. The droplets with spherical shape were produced in devices with 28 μm height and their diameters were around 30 μm. The droplets with disc shape were produced in a device with 10 μm height and their diameters were around 50 μm. In these conditions, spheres and discs have the same volume. In both cases, it took around 40-50 min for the FtsZ bundles to disassemble. Scale bar = 20 μm.

Further confirmation of the dynamic nature of the FtsZ bundle network comes from FRAP (fluorescence recovery after photobleaching) experiments. Erickson and co-workers have shown that the FtsZ ring in *E. coli* is a highly dynamic structure where interchange of subunits between the ring and the cytoplasm renders structures identical to those observed before photobleaching.[27] We performed FRAP experiments on FtsZ bundles confined in droplets (Figure 3. 6). The graphs show the time-lapse fluorescence recovery of bleached FtsZ bundles (1g L^{-1}) confined in spherical droplets and disc-shaped droplets, at two different crowder concentrations: 100g L^{-1} and 150 g L^{-1} Ficoll 70. An important initial observation is that the bundle arrangement within the droplets before and after photobleaching showed apparently identical structures and bundle organization, which seems to indicate that although the system is dynamic (see below), the overall gel-like structure is maintained for a determined composition and droplet geometry.

We determined the half time of recovery of a bleached region by fitting the corrected fluorescence intensity to the equation given under Materials and methods. For a Ficoll 70 concentration of 100 g L^{-1}, the half time recovery was 25 s ± 2s and 20 s ± 2s in spherical and disc-shape droplets, respectively. These results show that FtsZ bundles confined in droplets are continuously exchanging subunits with free FtsZ in the solution.

The background fluorescence intensity in the droplets can mostly be attributed to FtsZ protofilaments, whose size is below the microscope resolution,[26] as the crowder concentration is around the limit at which bundles form in solution[29] and in emulsion under our experimental conditions (not shown), with a minor contribution of unpolymerised FtsZ plus a minor fraction of free probe.[48]

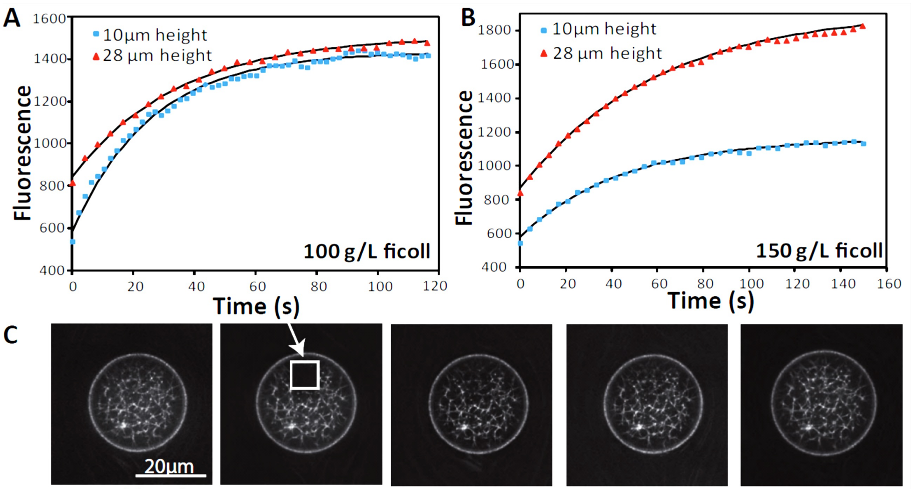

pre- bleach 0 sec 50 sec 100 sec 150 sec

Figure 3. 6 FRAP on FtsZ bundles in spherical and disc-shaped droplets containing the same FtsZ concentration (1 g L^{-1}). The fluorescence intensity of the photobleached region was measured over time in droplets containing (A) 100g L^{-1} Ficoll and (B) 150g L^{-1} Ficoll. (C) Time-lapse series of fluorescence images showing the time course of recovery. The white arrow shows the bleached region.

FRAP experiments on bundles formed using 150 g L^{-1} Ficoll 70 showed a slower exchange of FtsZ monomers, with a half time of recovery of 38 s ± 3s and 29 s ± 2s in spherical and disc-shaped droplets, respectively, although a certain effect on diffusion derived from the increase in the viscosity of the solution by crowder addition cannot be discarded.[41] The background intensity is clearly lower when compared with measurements at 100 g L^{-1} Ficoll 70, suggesting major arrangement of protofilaments into bundles, as this higher concentration falls in the plateau of bundle formation in solution.[29]

The values of half-time recovery are close to the values found by Erickson and co-workers for the Z ring in *E. coli*, around 30 s using the fusion protein FtsZ-GFP.[27] Our FRAP experiments show, therefore, that the crowded environment in the droplets leads to FtsZ bundles with similar exchange kinetics as those found in vivo.

3.2.3 Effect of crowder concentration on FtsZ bundle distribution

We first observed FtsZ bundles in ~20 pL spherical (~30 µm diameter) and disc-shaped droplets (~50µm diameter) for a fixed FtsZ concentration (1 g L^{-1}) at Ficoll 70 concentrations ranging from 100 g L^{-1} to 150 g L^{-1}. Figure 3. 7 A shows representative confocal fluorescence microscopy images. For both droplet shapes, a high fluorescent intensity can be seen at the oil-water interface, which indicates adsorption of FtsZ to the lipid monolayer.

In the spherical droplets, FtsZ bundles formed a network centred in the droplet with a lower bundle density in the vicinity of the oil-water interface; we call this region the depletion zone. The width of this depletion zone is dependent on the Ficoll concentration and reduced by around 40% when increasing Ficoll concentrations from 100 to 150 g L^{-1} (from 4.6 µm ± 0.2 µm to 2.9 µm ± 0.3 µm, Figure 3. 7 B). In disc-shaped droplets, the arrangement of the FtsZ bundles is clearly different from that in the spherical droplets under equivalent conditions. The bundle network is spread in most of the droplet lumen, presenting a larger pore size of the network and a strongly reduced depletion zone which shrinks only modestly upon increasing Ficoll concentration (from 2.8 µm ± 0.2 µm to 2.1µm ± 0.3 µm, Figure 3. 7). It is worth to mention that the size of the bundles and their distribution is similar, within our current experimental resolution, along the networks (that is, no significant difference is observed between the bundles located in the centre and close to the boundary).

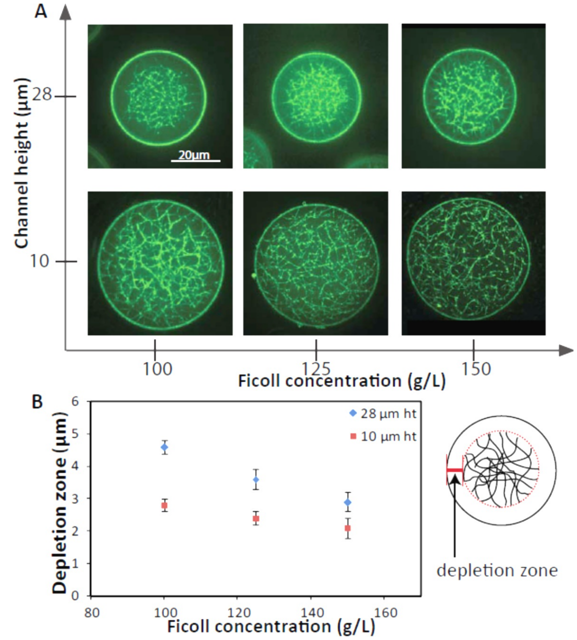

Figure 3. 7 Effect of crowder concentration on FtsZ bundles distribution in confined environment. (A) Representative confocal images of spherical and disc-shaped droplets with the same FtsZ concentration (1g L^{-1}) and different Ficoll concentrations (100g L^{-1} - 150g L^{-1}). (B) Width of the depletion zone versus Ficoll concentration. Error bars represent standard deviation of the mean.

3.2.4 Effect of FtsZ concentration on bundle distribution

Figure 3. 8 shows representative confocal fluorescence images on the dependence of the depletion zone and bundles distribution as a function of FtsZ concentration. Ficoll 70 concentration was kept constant (100 g L^{-1}) while the FtsZ concentration increased from 1 g L^{-1} to 3 g L^{-1}. In the spherical droplets, the depletion zone shrinks from 4.6 µm ± 0.2 µm to 1.6 µm ± 0.2 µm for an FtsZ concentration of 1g L^{-1} and 3 g L^{-1} respectively (Figure 3. 8 B). The depletion zone in the disc-shaped droplet vanished with the increase of FtsZ concentration. At 1 g L^{-1} FtsZ, the depletion zone is around 2.8 µm ± 0.2 µm, dropping to 1.3µm ± 0.3 µm at 2 g L^{-1} FtsZ and disappearing at 3g L^{-1} FtsZ (Figure 3. 8). The background intensity in the disc-shaped droplets is significantly lower at all FtsZ concentrations, indicating that most FtsZ protofilaments within these droplets (but not in the spherical ones) are forming bundles. These results indicate that the shape of the network confinement promotes self-organization of FtsZ polymers.

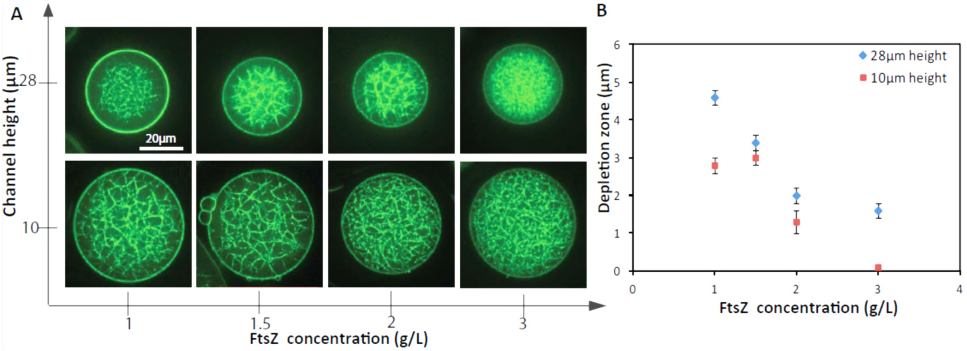

Figure 3. 8 Effect of FtsZ concentration on bundles distribution in confined environment with the same Ficoll concentration and (A) FtsZ concentration ranging from 1-3 g L^{-1} (B) Depletion zone versus FtsZ concentration. Error bars represent standard deviation of the mean.

A similar trend was observed when studying the dependence of FtsZ bundles distribution with a higher Ficoll 70 concentration (150 g L^{-1}) and FtsZ concentrations ranging from 1 – 2 g L^{-1} (Figure 3. 9): the bundle density increased with the FtsZ concentration, but the depletion zone stayed roughly constant for the spherical (2.8 µm ± 0.1 µm) and for the disc-shaped droplets (2.3 ± 0.2 µm). It seems that with a higher Ficoll 70 concentration, the FtsZ bundle structure is more rigid and independent of the FtsZ concentration. Noteworthy, no arrangement of polymers into bundles was observed in the absence of crowder even at FtsZ concentrations as high as 9 g L^{-1} (not shown), in contrast with the self-organization observed in actin filaments, enhanced in cell-sized confinement,[15] and microtubules.[49]

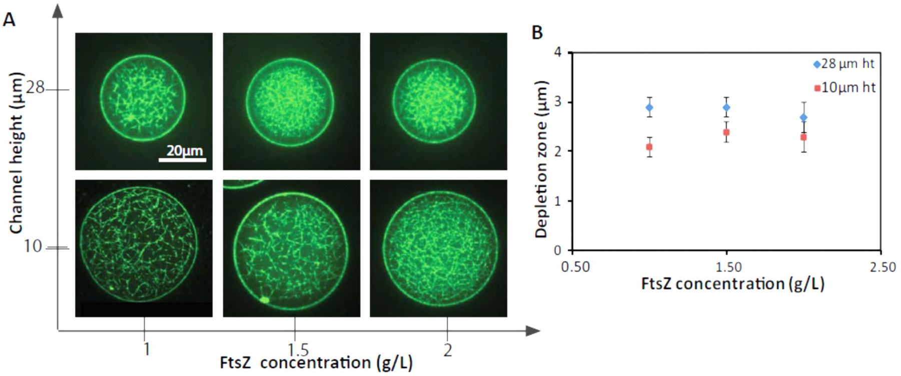

Figure 3. 9 Arrangement of FtsZ bundles in droplets containing 150 g/L Ficoll and (A) FtsZ concentration from 1 to 2 g/L (B) Depletion zone versus FtsZ concentration.

In order to gain more insight into the mechanism by which the depletion zone forms, we studied the network of FtsZ bundles in droplets, before and after passing through narrow channels (~20 µm width and 800 µm long) located in the reservoir of the microfluidic device. A schematic drawing of the chip design is shown in Figure 3. 10 and Figure 3. 4. fluorescence images of spherical and disc-shaped droplets, taken at different locations of the device are represented in Figure 3. 10. The FtsZ bundle network deforms when passing through the channel in both droplet shapes, but in different ways. In the case of spherical droplets, the network is pushed back to the rear end of the droplet, reminiscent of the deformation of fibrin networks in moving droplets reported by Pfohl and co-workers.[50] Interestingly, this compressed network relaxes back to the initial arrangement after passing the channels. In contrast, in disc-shaped droplets, the network is permanently deformed and the FtsZ bundles are clearly aligned with the direction of the flow. Importantly, these effects are only seen with Ficoll concentrations of 100 g L^{-1}, and at higher Ficoll 70 concentrations (125-150 g L^{-1}), the presumably more robust network looks similar before and after the narrow channels.

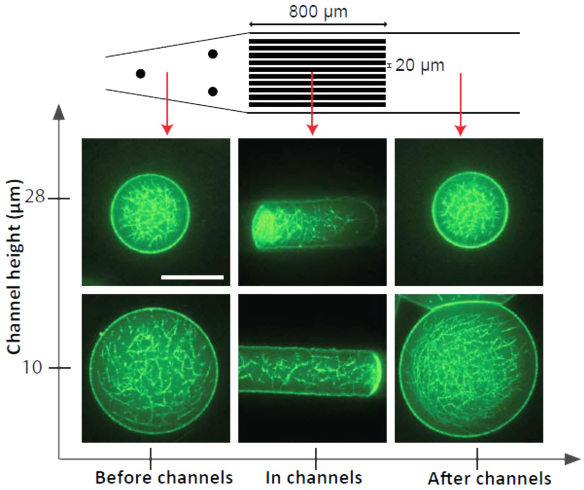

Figure 3. 10 Arrangement of FtsZ bundles in droplets when forced to pass through narrow channels. For a final Ficoll and FtsZ concentrations of 100 g L^{-1} and 1 g L^{-1}, respectively, images of spherical and disc-shaped droplets were taken before, in and after narrow channels. The channels width is ~ 20µm and the length is ~ 800µm. Scale bar = 30µm

3.2.5 Discussion

Using microdroplets in microfluidics we have investigated the structural, spatial and dynamic organization of FtsZ polymer bundles and how these properties are influenced by the composition and the geometry of these confined cell-like compartments. In all droplets, we observe high fluorescence intensity at the oil-water interface and it is likely that as soon as the droplets are formed, the unassembled FtsZ or/and FtsZ protofilaments adsorb to the droplet surface, while in the interior of the droplets filaments aggregate into the bundles making up the observed network. However, the formation of the depletion zone is not obvious, and a number of hypotheses can be proposed to explain it.

Negishi *et al*. described a mechanism based on geometric and entropic arguments: stiff fibres are excluded from the interfacial area where their rotational entropy is reduced. [51] The FtsZ protofilaments under low KCl concentration have rather small persistence lengths (≈ 55 nm) and contour lengths (≈ 196 nm),[52] which are much smaller than the size of the observed depletion zone. The exclusion effect, however, might be determining the distribution of the stiffer FtsZ bundles, although entropic forces would be expected to lead to aligned bundles.

Another possible mechanism would be related with the spontaneous demixing of filament-forming proteins (microtubules or actin) and globular proteins under physiological conditions described by Herzfeld and co-workers,[53, 54] observed in crowded solutions of actin bundles.[13, 55] In contrast to the bundle formation of actin[15, 56, 57] and tubulin[49] in the absence of crowders, FtsZ protofilaments do not arrange into bundles in the absence of crowders under close to physiological buffer conditions, even at very high FtsZ concentrations. The narrow distribution of FtsZ filaments might lower the driving force for bundling,[26, 58] but we do not observe the alignment of the bundles which would be expected upon demixing the rods from the globular proteins. A strong argument in favour of a demixing process is the dependence of the depletion zone on droplet shape. Upon demixing, the ‘dilute’ phase will form a thinner layer in the case of disc-shaped droplets with their larger surface-to-volume ratio compared to spherical droplets. Simple geometrical arguments would give an ~ 3 μm depletion zone for disc-shaped droplets when there is an~ 5 μm depletion zone in spherical droplets, which is in line with experimental results.

However, alternative explanations could be presented. The combination of adsorption to the interface and bundle formation in the interior of the droplet could lead to a local FtsZ concentration that falls below the critical concentration required for the bundle formation. As a consequence, a region close to the droplet surface is depleted from bundles as shown in Figure 3. 7 and Figure 3. 8.

Although working in a completely different field, Whitesides and co-workers have shown the occurrence of such a phenomenon in selective crystal nucleation on patterned self-assembled monolayers.[59] The decreasing trend in the depletion zone thickness with increasing FtsZ concentration in the case of spherical droplets (3D, Figure 3. 8) supports this mechanism. Accordingly, the non-spherically shaped droplets, with their higher surface-to-volume ratio, should have a smaller depletion zone for a fixed FtsZ concentration with respect to their spherical counterparts, as is actually the case as shown in Figure 3. 8.

Finally, we cannot completely discard some effects of the recirculation flows around the droplet pushing the FtsZ network away from the interface, as deformation of the FtsZ network in the narrow channels (Figure 3. 10) shows that shear forces can influence the distribution of the fibres. However, as disc-shaped droplets have larger contact areas with the channel walls, fluid flows inside disc-shaped droplets would be expected to be larger, which does not support the observation that the depletion zone in these droplets is typically smaller. Moreover, variation of the width of the depletion zone with Ficoll and FtsZ concentrations showed that dimensions are stable with time, apparently depending only on the specific composition and geometry of the container.

3.3 Conclusions

The microfluidic based technology developed here, has allowed the reconstitution of dynamic systems inside lipid containers, and enabled the characterization of the modulation of the spatial organization of the FtsZ network under determined geometry constraints. We believe that self-organization of FtsZ bundles might be determined by specific properties inherent to the system and the geometry of the droplet, conferring specific boundary conditions. A number of observations can be drawn on the polymerization of FtsZ into fibrous networks in droplets: 1) bundle formation is delayed in droplets in microfluidic devices at the lowest Ficoll concentration, 2) the polymerization is reversible, and there is exchange of FtsZ monomers with the bundles, yet the gel or network as a whole does not change after formation, and 3) a depletion zone appears near the oil-water interface, where at the lowest Ficoll and FtsZ concentrations very few bundles are seen; this effect is much more pronounced in spherical than in quasi-2D droplets. This microfluidic platform constitutes a very powerful tool to test the properties of FtsZ in the presence of companion cell division elements and site-selection systems which will help to complete our understanding of the precise functional role of FtsZ in cell division.

3.4 Experimental section

Materials

Guanine nucleotides were from Jena, Ficoll 70 and other analytical grade chemicals were from Sigma. In all experiments, final GTP concentration was 3 mM. Polar extract phospholipids from *E. coli* (67 % phosphatidylethanolamine, 23 % phosphatidylglycerol and 10 % cardiolipin; Avanti Polar Lipids, Alabama, USA) and soybean asolectin (phosphatidylcholine, lecithin, cephalin and phosphatidylinositol in around the same amount; Sigma) were stored in chloroform:methanol 1:2 (v/v). Just before use, a determined amount was dried under nitrogen flow, kept under vacuum for at least two hours and resuspended in mineral oil by sonication in a thermostated bath at 37 ºC for 30 min, to get a final concentration of 25 g L^{-1}.

Protein purification and labelling

FtsZ was purified by the calcium precipitation method as described,[60] dialyzed against the working buffer (50 mM Tris-HCl, pH 7.5, 500 mM KCl, 5 mM $MgCl_2$), and aliquots were stored at -80 ºC until used. The protein was covalently labelled in the amine groups with Alexa-488 carboxylic acid succinimidyl ester dye (Molecular Probes, Invitrogen), under conditions to ensure minimal interference of the dye with FtsZ assembly, as in,[29] with some modifications. FtsZ polymers were labelled with Alexa-488 dye (four-fold molar excess regarding FtsZ monomers) and separated from the residual unpolymerized protein and most of the free dye.[48] The labelled protein was stored frozen at -80 ºC in 50 mM Tris-HCl, pH 7.5, 500 mM KCl, 5 mM $MgCl_2$, 10% glycerol buffer. The ratio of labelling, estimated from the molar absorption coefficients of the dye and the protein, was 0.3-0.5. In all the experiments, labelled protein was 1% of total FtsZ concentration.

Microfluidic chip design and fabrication

The first step in any microfabrication protocol is the virtual design of the desired device using computer assisted design (CAD) programs, such as AutoCad (Autodesk Inc.). A high resolution image of the design is then printed on a transparency which will serve as a photomask in contact photolithography to produce a negative relief in photoresist on a glass substrate. The main steps in devices fabrication by photolithography is represented in Figure 3. 1.A. SU-8 negative photoresist (Micro Resist Technology GmbH, Germany) was used for fabrication purposes. The device fabrication started with creating a design in an AutoCAD program. A high resolution commercial image setter then printed this design on a transparency (JD Photo tools, UK). This transparency served as the photomask in contact photolithography to produce a negative relief in photoresist on a glass substrate. SU8-2025 photoresist is spin coated on a round Silicon wafer with 50 mm diameter (Si-Mat silicon materials, Germany). Spin coating parameters were optimized to achieve the desired film thickness. Subsequently, the sample was soft baked for 1 min at 65°C, 3 min at 95°C and 1 min at 65°C in order to evaporate the solvent and densify the film. Then, the samples were exposed to UV light (λ = 365 nm) in the mask aligner (Karl Suss MJB 3 UV 300/400) for 28 seconds through the photomask.

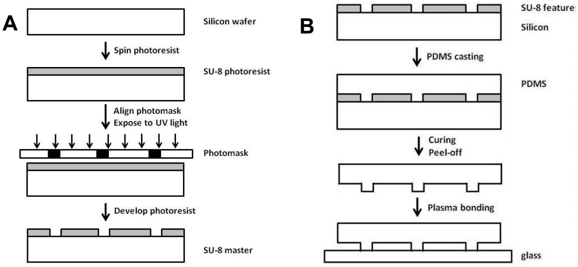

Figure 3. 11 Microfluidic chip fabrication by photolithography. A, spin-coat SU-8 2000 photoresist on a silicon wafer; B soft-bake on a hot plate to evaporate the solvent and harden the photoresist.

After exposure, the sample was post-baked for a time which depended on the thickness of the photoresist (1 min at 65°C, 2 min at 95°C and 1 min at 65°C). The samples were rinsed with developer solution (mr-Dev600, Micro Resist Technology GmbH, Germany) to remove the non-crosslinked regions. Thus the fabrication of the SU-8 mask was accomplished on a silicon wafer which resulted in 28 micron height channels. In order to achieve 10 micron height channels, SU8-2007 photo resist was used with an exposure time of 20 seconds. This master is used as a mold for soft-lithographic technique to have PDMS channels (Figure 3. 11.B). In the next step of device fabrication, PDMS base Sylgard™

184 and curing agent (Dow Corning GmbH, Germany) were mixed in a ratio of 10:1 w/w, degassed and decanted onto the SU-8 master. Once mixed, poured over the master and heated to elevated temperatures, the liquid mixture becomes a solid, cross-linked elastomer in a few hours via the hydrosilylation reaction between vinyl ($SiCH=CH_2$) groups and hydrosilane (SiH) groups. After thermal curing for 2-3 hours in an oven at 65 °C, PDMS facilitates easy peeling from the SU-8 master. In order to use these PDMS structures as microfluidic devices, inlet holes were punched and the channels were sealed by a glass slide. Surface activation by oxygen plasma (Diener electronic GmbH, Germany) was used for PDMS-glass bonding. To improve wetting by the continuous phase, devices were coated with a hydrophobic layer by flushing with Aquapel (Pittsburgh Glass Works, LLC) in the channels and allowing it to dry overnight at 65 °C.

Fluorescence microscopy

Samples were observed with a spinning disk confocal microscope (CSU-X1, Yokogawa Electric Corp.) on an Olympus inverted microscope (IX81). Alexa-488 was excited with 488 nm laser light (λ_{em}= 525 nm) and images were recorded with a temperature controlled EM-CCD camera (iXon3, Andor) using an exposure time of 0.8-1 s and a piezo-driven 100x (1.3 NA) oil immersion objective. All observations were conducted at room temperature.

Data analysis

- Droplet volume

The spherical and disc-shaped droplets (Figure 1) were produced such as their volume is the same (~20 pL). The formula used to calculate the diameter, D, rendering a volume equivalent to the sphere in the disc-shaped droplet is: $(\pi/12) \times [2D^3 - (D-h)^2 (2D+h)]$, where h is the height of the channels. The typical flow rates to obtain spheres with a diameter close to 32 µm are 160 $\mu L\ h^{-1}$ for the oil phase, 20 $\mu L\ h^{-1}$ for the aqueous phases. To obtain disc-shaped droplets of ~ 50 µm diameter, the typical flows were 45 $\mu L\ h^{-1}$ and 20 $\mu L\ h^{-1}$ for the oil and aqueous phases respectively.

- Depletion zone

For all experimental conditions, 3-5 representative droplets were selected for the calculation of the depletion zone. Image J (National Institutes of Health, USA) was used for data analysis. Using the oval tool of the software, a first circle was drawn around the core of the droplet (showing the highest FtsZ bundle density), and a second circle was drawn around the whole droplet. Then, drawing a line through the section defined by both circles, we can have access to the depletion zone depicted in Fig. 3B.

FRAP experiment

The same procedure as reported in reference[27] was followed. Photobleaching was achieved by 3 laser pulses of 25 μs at 50% laser power. Time series after bleaching were taken over 1-3 min with exposures every second. Measurement of integrated intensity in the bleached regions at each time point were made in Image J and exported for data analysis to Excel 2007. For each bleached region, the background intensity was corrected for overall photobleaching of the sample during observation (determined from the intensity of another region of the same droplet over time). Calculation of the half time fluorescence recovery was performed by least-square fitting of the exponential equation $F_\infty - F(t) = [F_\infty - F_0]\, e^{-kt}$, where F_∞ is the fluorescence of the bleached region after maximal recovery, F(t) is the fluorescence at time t, F_0 is the initial fluorescence just after bleaching (t=0), and k is the rate constant, allowing F_∞, F_0 and the half-time ($t_{1/2} = \ln 2/k$), to vary. Results correspond to the average of 2-7 measurements.

3.5 References

1. A. Vendeville, D. Lariviere and E. Fourmentin, *FEMS microbiology reviews*, **2011**, *35*, 395-414.
2. A. P. Minton, *Mol Cell Biochem*, **1983**, *55*, 119-140.
3. A. P. Minton, *Int J Biochem*, **1990**, *22*, 1063-1067.
4. A. P. Minton, *J Cell Sci*, **2006**, *119*, 2863-2869.
5. H. X. Zhou, G. Rivas and A. P. Minton, *Annual review of biophysics*, **2008**, *37*, 375-397.
6. Y. Phillip and G. Schreiber, *FEBS Lett*, **2013**.
7. A. H. Elcock, *Curr Opin Struct Biol*, **2010**, *20*, 196-206.
8. R. J. Ellis, *Trends in Biochemical Sciences*, **2001**, *26*, 597-604.
9. A. P. Minton, *Current Opinion in Structural Biology*, **2000**, *10*, 34-39.
10. A. P. Minton, *J. Biol. Chem.*, **2001**, *276*, 10577-10580.
11. J. Herzfeld, *Journal of molecular recognition : JMR*, **2004**, *17*, 376-381.
12. R. A. Lindner and G. B. Ralston, *Biophys Chem*, **1997**, *66*, 57-66.
13. A. Suzuki, M. Yamazaki and T. Ito, *Biochemistry*, **1989**, *28*, 6513-6518.
14. K. B. Frederick, D. Sept and E. M. De La Cruz, *J Mol Biol*, **2008**, *378*, 540-550.
15. M. Soares e Silva, J. Alvarado, J. Nguyen, N. Georgoulia, B. M. Mulder and G. H. Koenderink, *Soft Matter*, **2011**, *7*, 10631-10641.

16. L. Limozin and E. Sackmann, *Phys Rev Lett*, **2002**, *89*, 168103.
17. A. C. Reymann, R. Boujemaa-Paterski, J. L. Martiel, C. Guerin, W. Cao, H. F. Chin, E. M. De La Cruz, M. Thery and L. Blanchoin, *Science*, **2012**, *336*, 1310-1314.
18. T. Vignaud, L. Blanchoin and M. Thery, *Trends Cell Biol*, **2012**, *22*, 671-682.
19. T. E. Holy, M. Dogterom, B. Yurke and S. Leibler, *Proc Natl Acad Sci U S A*, **1997**, *94*, 6228-6231.
20. M. Cosentino Lagomarsino, C. Tanase, J. W. Vos, A. M. Emons, B. M. Mulder and M. Dogterom, *Biophys J*, **2007**, *92*, 1046-1057.
21. M. Pinot, F. Chesnel, J. Z. Kubiak, I. Arnal, F. J. Nedelec and Z. Gueroui, *Curr Biol*, **2009**, *19*, 954-960.
22. D. W. Adams and J. Errington, *Nat Rev Microbiol*, **2009**, *7*, 642-653.
23. H. P. Erickson, D. E. Anderson and M. Osawa, *Microbiol Mol Biol Rev*, **2010**, *74*, 504-528.
24. W. Margolin, *Curr Biol*, **2000**, *10*, R328-330.
25. J. Mingorance, G. Rivas, M. Vélez, P. Gomez-Puertas and M. Vicente, *Trends in microbiology*, **2010**, *18*, 348-356.
26. B. Monterroso, R. Ahijado-Guzmán, B. Reija, C. Alfonso, S. Zorrilla, A. P. Minton and G. Rivas, *Biochemistry*, **2012**, *51*, 4541-4550.
27. J. Stricker, P. Maddox, E. D. Salmon and H. P. Erickson, *Proceedings of the National Academy of Sciences*, **2002**, *99*, 3171-3175.
28. Y. Chen and H. P. Erickson, *J Biol Chem*, **2005**, *280*, 22549-22554.
29. J. M. González, M. Jiménez, M. Vélez, J. Mingorance, J. M. Andreu, M. Vicente and G. Rivas, *J Biol Chem*, **2003**, *278*, 37664-37671.
30. D. Popp, M. Iwasa, A. Narita, H. P. Erickson and Y. Maeda, *Biopolymers*, **2009**, *91*, 340-350.
31. G. Rivas, J. A. Fernández and A. P. Minton, *Proceedings of the National Academy of Sciences of the United States of America*, **2001**, *98*, 3150-3155.
32. M. Osawa, D. E. Anderson and H. P. Erickson, *Science*, **2008**, *320*, 792-794.
33. M. Osawa, D. E. Anderson and H. P. Erickson, *EMBO J*, **2009**, *28*, 3476-3484.
34. M. Osawa and H. P. Erickson, *Mol Microbiol*, **2011**, *81*, 571-579.
35. S. L. Milam, M. Osawa and H. P. Erickson, *Biophys J*, **2012**, *103*, 59-68.
36. A. Martos, M. Jiménez, G. Rivas and P. Schwille, *Trends Cell Biol*, **2012**, *22*, 634-643.
37. H. P. Erickson, *Proc Natl Acad Sci U S A*, **2009**, *106*, 9238-9243.
38. G. Rivas, C. Alfonso, M. Jiménez, B. Monterroso and S. Zorrilla, *Biophysical Reviews*, **2013**.
39. M. Jiménez, A. Martos, M. Vicente and G. Rivas, *J Biol Chem*, **2011**, *286*, 11236-11241.
40. A. B. Theberge, F. Courtois, Y. Schaerli, M. Fischlechner, C. Abell, F. Hollfelder and W. T. Huck, *Angew Chem Int Ed Engl*, **2010**, *49*, 5846-5868.
41. J. R. Wenner and V. A. Bloomfield, *Biophys J*, **1999**, *77*, 3234-3241.
42. C. V. Kulkarni, W. Wachter, G. Iglesias-Salto, S. Engelskirchen and S. Ahualli, *Physical chemistry chemical physics : PCCP*, **2011**, *13*, 3004-3021.

43. J. C. Baret, *Lab Chip*, **2012**, *12*, 422-433.
44. J. C. Baret, F. Kleinschmidt, A. El Harrak and A. D. Griffiths, *Langmuir*, **2009**, *25*, 6088-6093.
45. L. Frenz, K. Blank, E. Brouzes and A. D. Griffiths, *Lab Chip*, **2009**, *9*, 1344-1348.
46. A. Martos, C. Alfonso, P. Lopez-Navajas, R. Ahijado-Guzman, J. Mingorance, A. P. Minton and G. Rivas, *Biochemistry*, **2010**, *49*, 10780-10787.
47. A. Mukherjee and J. Lutkenhaus, *EMBO J*, **1998**, *17*, 462-469.
48. B. Reija, B. Monterroso, M. Jiménez, M. Vicente, G. Rivas and S. Zorrilla, *Anal Biochem*, **2011**, *418*, 89-96.
49. A. L. Hitt, A. R. Cross and R. C. Williams, Jr., *J Biol Chem*, **1990**, *265*, 1639-1647.
50. H. M. Evans, E. Surenjav, C. Priest, S. Herminghaus, R. Seemann and T. Pfohl, *Lab Chip*, **2009**, *9*, 1933-1941.
51. M. Negishi, T. Sakaue, K. Takiguchi and K. Yoshikawa, *Phys Rev E*, **2010**, *81*, 051921.
52. S. Huecas, O. Llorca, J. Boskovic, J. Martin-Benito, J. M. Valpuesta and J. M. Andreu, *Biophys J*, **2008**, *94*, 1796-1806.
53. D. T. Kulp and J. Herzfeld, *Biophys Chem*, **1995**, *57*, 93-102.
54. T. L. Madden and J. Herzfeld, *Biophys J*, **1993**, *65*, 1147-1154.
55. J. Goverman, L. A. Schick and J. Newman, *Biophys J*, **1996**, *71*, 1485-1492.
56. C. M. Coppin and P. C. Leavis, *Biophys J*, **1992**, *63*, 794-807.
57. A. Suzuki, T. Maeda and T. Ito, *Biophys J*, **1991**, *59*, 25-30.
58. J. M. González, M. Vélez, M. Jiménez, C. Alfonso, P. Schuck, J. Mingorance, M. Vicente, A. P. Minton and G. Rivas, *Proc Natl Acad Sci U S A*, **2005**, *102*, 1895-1900.
59. J. Aizenberg, A. J. Black and G. M. Whitesides, *Nature*, **1999**, *398*, 495-498.
60. G. Rivas, A. López, J. Mingorance, M. J. Ferrándiz, S. Zorrilla, A. P. Minton, M. Vicente and J. M. Andreu, *J Biol Chem*, **2000**, *275*, 11740-11749.

Chapter 4

Reconstitution of the divisome system in *E. coli*: from droplets to liposomes

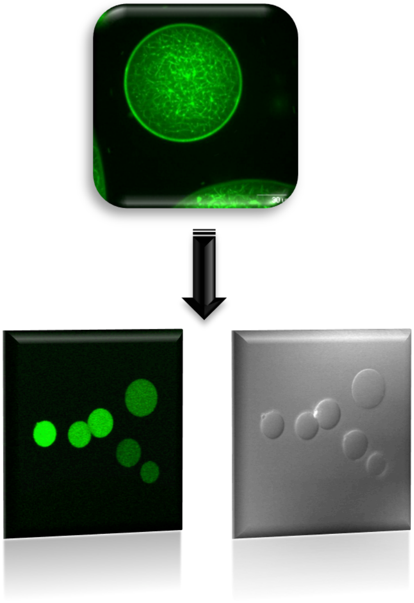

4.1 Introduction

The cell division in *E. coli* involves complex mechanisms, leading to the formation of two identical cells.[1] Cytokinesis is initiated by the formation of a ring at mid-cell by, among others, the essential GTPase protein FtsZ (a tubulin homologue), which is called the Z ring and which can generate constrictive forces. More than 20 proteins are involved in the bacterial cell division and together constitute the divisome, localized at mid-cell and interacting with each other.[2] Among the essential proteins of the divisome, FtsZ, FtsA and ZipA proteins have been described to form the initial proto-ring complex directing the formation of the Z ring at mid-cell.[3] FtsA is an amphitropic protein that belongs to the actin family and ZipA is a membrane protein, which are both able to interact with FtsZ. It is thought that the Z ring localisation at mid-cell is achieved by the Min system and the nucleoid occlusion. The Min system is composed of three proteins MinC, MinD, and MinE, that generates a dynamic oscillation of FtsZ protein inhibition between the two bacterial poles with a higher concentration at the poles compared to that in the mid-cell. In these conditions, the formation of the Z ring is only possible at mid-cell generating identical daughter cells.[4, 5] The nucleoid-associated protein SlmA binds to specific DNA sequences of the bacterial chromosome and stimulates the disassembly of FtsZ filaments in the vicinity of the nucleoid.[6]

Details on how the essential proteins of the divisome system function and interact with each other are not fully understood. FtsZ is a protein of around 45 kDa that assembles into single-stranded filaments using GTP to couple FtsZ monomers head to tail, similar to those in microtubules. FtsZ filaments *in vitro* are one subunit thick and, depending on the solution conditions, up to 200 nm long (50 subunits), which can associate further through lateral interactions into bundles under crowded conditions.[7-9] The question of how FtsZ filaments are attached to the bacteria inner membrane was first answered by Lutkenhaus and co-workers.[10] The authors showed that either ZipA or FtsA supports the formation and stabilization of Z rings, tethering FtsZ to the bacterium lipid bilayer but Z rings were unable to assemble in the absence of both. It was hypothesised that FtsZ, constituting the Z ring, is able to generate constrictive forces all by itself.[11] The change in conformation of FtsZ filaments primarily attached to the membrane from straight to curved conformation might produce the force to generate constriction. This hypothesis was confirmed when the Z ring was reconstituted *in vitro* using liposomes.[12] An FtsZ fusion protein, able to tether itself to the membrane though an amphipathic helix onto the C-terminal, has been described to assemble into multiple Z rings inside tubular multilamellar liposomes in the absence of FtsA or ZipA. The Z rings coincided with visible constriction on the liposomes walls showing that FtsZ can form a ring and generate constrictions without the help of any other proteins. When the same FtsZ fusion protein was added to the outside of liposomes, a deformation was observed producing concave depressions and membrane tubules.[13] In a recent study, FtsZ and a soluble form of ZipA with its transmembrane domain substituted by a histidine tag (sZipA), induced the shrinkage of giant unilamellar vesicles.[14] The vesicles were prepared using the droplet transfer method with EPC lipids (egg phosphatidylcholine) containing 10 % of DOGS-NTA-Ni to anchor sZipA to the inner membrane. The pore-forming protein α-haemolysin was added after vesicle formation to trigger FtsZ polymerization by addition of GTP, resulting in vesicle shrinkage in a concentration ratio of FtsZ/sZipA at least lower than two. Two models were proposed to describe the arrangement of FtsZ into the Z ring: the patchy band model for overlapping short filaments with weak interactions and the lateral interaction model for one or few long filaments with strong interactions.[15, 16] The patchy band model was recently supported using photoactivated localization microscopy (PALM) to investigate the nanoscale organization of FtsZ in live *Caulobacter crescentus*.[17]

We are interested in the interactions between FtsZ and FtsA or ZipA, the proto-ring elements in confined and crowded environment. The size and nature of the cell-like container is a critical parameter that should be taken into account. Even if Z rings were reconstituted in liposomes by Osawa and co-workers,[12] no cases of constriction had proceeded all the way to liposome division, probably due to the rigidity of the membrane of the multilamellar liposomes. Also, those constrictions were only observed in tubular liposome with a diameter below 5 µm, which shows the importance of the container geometry. Microdroplets are easy to produce in microfluidics and their size and shape can be tuned by the flow rates and the chip design. First, using droplet microfluidics, we studied the influence of FtsA or ZipA on the arrangement and organization of FtsZ bundles in lipid coated droplets. Then, combining microfluidics and the droplets transfer method, we worked on the production of giant unilamellar vesicles (GUV) encapsulating FtsZ and ZipA anchored to the membrane. The added value of this method compared to those to produce GUV[18] is the fact that we can produce monodisperse droplets and thereafter vesicles having the same size and composition, allowing for quantitative and statistical measurements. The main questions we want to address are: what is the distribution of the proteins depending on the interaction with their partners? What is the effect on the lipid membrane derived from the interaction between the proto-ring elements? What is the stability of FtsZ bundles in time in the presence/absence of their partners? What is the effect of the cell-like container (sphere, disc, cylinder) on the stability and arrangement of FtsZ?

4.2 Results and discussion

4.2.1 Emulsion droplets containing proteins of the divisome

Droplets of water in oil (W/O) coated with phospholipids are suitable models to mimic living cells as the arrangement of the lipids with the hydrophilic part oriented towards the inner water phase can be assumed to be very similar to the lipid content in the bacterial membrane.[19-21] Compared to liposomes, microdroplets in oil are easy to prepare and less sensitive to osmotic or mechanical stress, making possible the encapsulation of biological molecules without being denatured. We therefore used this cell-like container to encapsulate and study the components of the divisome system in *E. coli*.

4.2.1.1 FtsZ and FtsA in lipid coated droplets

FtsA is an amphitropic protein of the actin family that interacts with FtsZ via a domain located on the opposite side with respect to the C-terminal domain, the latter being an amphipathic helix which can associate to the cytoplasmic membrane.[22, 23] In this work, the FtsA used has a His-tag at the N-terminal domain.

First, bulk emulsions of water droplet in oil containing FtsZ and FtsA were produced by gently pipetting up and down the aqueous protein solution with the immiscible mineral oil solution containing 25 g/L of *E. coli* lipids (67 % phosphatidylethanolamine, 23 % phosphatidylglycerol and 10 % cardiolipin). A well-controlled crowded environment was induced by the addition of the inert polymer ficoll 70,[24] which forces the arrangement of FtsZ polymers into bundles suitable for the observation of their organization via fluorescence microscopy.[9] Figure 4. 1 shows representative confocal fluorescence microscopy images of droplet containing 2.5 µM FtsA labelled with Alexa 647 (red) in the absence and presence of 12 µM FtsZ labelled with Alexa 488 (green) in working buffer with 120 g/L Ficoll and 3 mM GTP. In all fluorescent images, a high fluorescent intensity can be seen at the oil/water interface, which indicates adsorption of proteins to the lipid monolayer. When only FtsA was present in the droplet, the protein was mainly located at the interface as shown by the relative fluorescent intensity profile, with higher intensities at the droplet interface compare to that of the droplet lumen. However, when both FtsA and FtsZ were present in the droplet, FtsA was still present at the interface but also colocalized with FtsZ bundles in the droplet lumen. The respective fluorescent intensity profiles demonstrate that FtsA was not only present at the droplet interface when FtsZ was present.

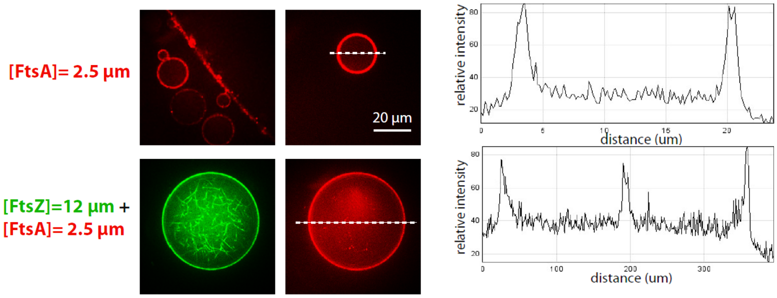

Figure 4. 1 Fluorescent images of bulk emulsion containing FtsA (red) alone or FtsZ (green) and FtsA (red), in the presence of ficoll 70 and GTP in working buffer (left). Respective fluorescent intensity profiles of FtsA at a white dotted line in the center of droplets (right). In the presence of FtsZ, FtsA was dislodging from the droplet interface and colocalized with FtsZ bundles in the lumen of the droplet.

Using microdroplet in microfluidics (as in chapter 3), the same experiment was performed in monodisperse droplets. The microfluidics device had 3 inlets and a large reservoir where droplets can be stored and imaged in time (Figure 4. 2, left). One stream contains FtsZ and FtsA at 24 µM and 5 µM, respectively in the presence of 120 g/L ficoll 70 and working buffer, the other stream delivers GTP at a concentration of 6 mM. Both streams were mixed in a 1:1 ratio prior to the droplet formation junction where it joined the oil containing lipids. Figure 4. 2 (right) shows representative fluorescent images of droplets containing FtsZ and FtsA at final concentrations of 12 µM and 2.5 µM, respectively. In the top two images, the same droplet is shown with FtsZ having the green label and FtsA the red one. In the bottom two images, the proteins have the opposite labels. As previously observed in bulk experiment, FtsA is dislodged from the droplet interface in the presence of FtsZ. It seems that when using FtsA with a green label, the colocalization with FtsZ bundles is more pronounced but since the images are taken in the mid plane, bundle distribution might be different. In a similar study, using giant unilamellar vesicles instead of droplets, FtsA had the same behaviour in the presence of FtsZ dislodging from the inner face of the vesicle membrane to colocalize with FtsZ polymers.[25] These observations show that FtsZ, in a polymerized form, can modulate and have an influence on the FtsA membrane interactions.

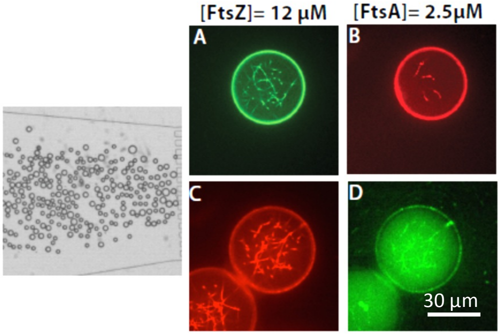

Figure 4. 2 Microdroplets production in microfluidics (left) containing 12 µM FtsZ and 2.5 µM FtsA with different labels (right). A and B represent a droplet containing FtsZ with Alexa-488 label and FtsA with Alexa-647 label. C and D contain the same proteins with opposite labels.

4.2.1.2 FtsZ and sZipA in lipid coated droplets

ZipA is a membrane protein present at the *E. coli* inner membrane which C-terminal globular domain binds the C-terminal alpha-helix of FtsZ.[26] We used a soluble mutant of ZipA (sZipA, lacking the transmembrane region and having a histidine tag instead), that presents the same binding affinity for FtsZ.[27, 28] The attachment of sZipA via its His-tag has been conducted by adding 10% DOGS-NTA-Ni to the *E. coli* lipids (25 g/L). This amount, in excess regarding the protein concentration employed, sufficed to attach sZipA at low concentrations and ensured results will be comparable in terms of surface composition in the event that higher content of sZipA were required.

First, we produced bulk emulsions in order to find the right conditions to observe changes in FtsZ bundle organization, with protein concentrations close to those used by Cabre and co-workers.[14] The authors demonstrated that sZipA had a great effect on FtsZ giant unilamellar vesicles containing FtsZ bundles, leading to shrinkage of the vesicle presumably due to interaction between the two proteins. The effect exerted in the membrane by the pulling action of FtsZ bundles through their interaction with sZipA was demonstrated by the use of the inhibitor peptide, which inhibits interactions between both proteins.

Similar to the experiment in the previous section with FtsA, we needed to verify the attachment of sZipA in the presence of 10 mol % DOGS-NTA mixed with *E. coli* lipids in mineral oil (Figure 4. 3). With 2 µM sZipA the attachment of the protein to the droplet interface is more important than that with 10 µM sZipA, as shown by the relative fluorescent intensity. Inside the droplets, the mean intensity went from around 20 to 60 a.u with 2 µM and 10 µM, respectively. The results show that the attachment of sZipA at the droplet interface is efficient as the increase of relative fluorescent intensity is proportional to the sZipA concentration. At every sZipA concentration, DOGS-NTA lipids are in large excess and most of sZipA should be attached to the interface. As vesicle shrinkage was observed with concentration above 5 µM sZipA and 12 µM FtsZ,[14] we decided to continue with 10 µM sZipA.

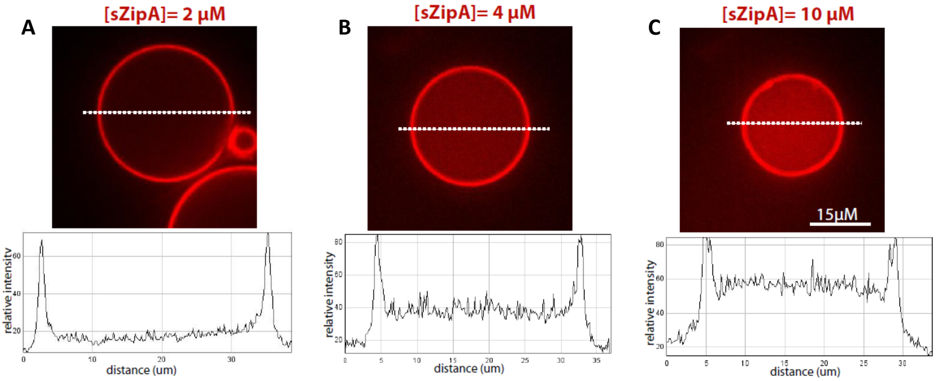

Figure 4. 3 Representative confocal images of droplets containing A. 2 µM B. 4µM or C.10 µM sZipA with 10% DOGS-NTA. Below, the respective fluorescent intensity profiles of sZipA at a white dotted line in the center of droplets showed that the over 2 µM, sZipA is also present in the lumen.

Figure 4. 4 shows representative fluorescent images of droplets containing 10 µM sZipA in working buffer with or without 10 % DOGS-NTA in the *E. coli* lipids, alone or in the presence of FtsZ bundles. We used a GTP regenerating system (RS) in order to follow bundle arrangement and eventual interactions between the two proteins. It is composed of acetate kinase and acetyl phosphate at final concentrations of 2 u/mL and 15 mM, respectively, which allowed the regeneration of GTP to obtain stable bundle for around 2h.[29] When no RS was used, FtsZ bundles started to disassemble after 40 min (Chapter 3-Figure 3.5). Without DOGS-NTA and in the absence of FtsZ, sZipA was evenly distributed at the interface and in the droplet lumen. When FtsZ was present, sZipA colocalized with FtsZ bundles in the droplets, indicating soluble ZipA was interacting with FtsZ as expected. With DOGS-NTA, sZipA is mainly at the droplet interface either in the absence or presence of FtsZ bundles and no major changes are visible in FtsZ bundles arrangement in time, meaning no interactions were observed between the two proteins other than at the lipid interface. It could be that at the concentration tested, the effect in bundle distribution and/or in the lipid monolayer cannot be observed and we decided to further optimize our system to determine the proper conditions by changing some parameters.

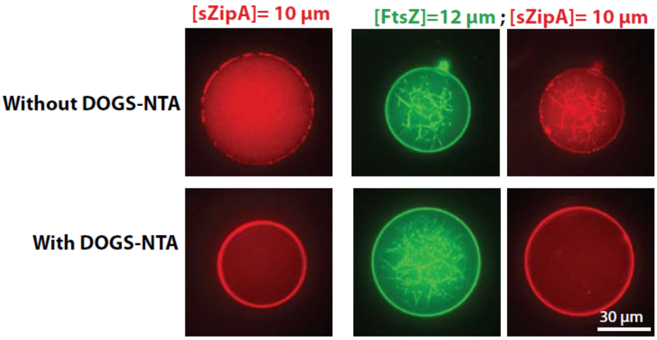

Figure 4. 4 Bulk emulsion containing 10 µM ZipA alone in the droplet (left) or 12 µM FtsZ (green) and 10 µM ZipA (red) in the same droplet (right), with or without 10 mol % DOGS-NTA in the *E. coli* lipid solution. With DOGS-NTA, sZipA is mainly at the droplet interface, while colocalizing with FtsZ when DOGS-NTA was absent.

The first parameter we changed was the protein concentration combinations. Bulk emulsions were produced with 10 mol% DOGS-NTA mixed with *E. coli* lipids in mineral oil. For the same sZipA concentration at 4 µM or 10 µM, FtsZ was present in the droplet at concentrations of 12 µM or 24 µM (Figure 4. 5). At a low sZipA concentration of 4 µM, the protein is mainly located at the droplet interface, independently from the FtsZ concentration. When the sZipA concentration is increased to 10 µM, a strong fluorescent intensity can be observed in the lumen of the droplet, probably due to an excess of protein compared to free NTA groups attached in the inner face of the droplet. Since both FtsZ and sZipA are spontaneously adsorbing to the droplet interface during droplet formation, the presence of FtsZ could block the NTA groups that might no longer be available for the attachment of sZipA. A careful examination of the droplet in time in those different conditions did not show any noticeable changes in FtsZ or sZipA arrangement and organization. Moreover, the depletion zone observed in FtsZ confocal images,[30] where no bundles are present between the droplet interface and the FtsZ network might make the interaction between FtsZ and sZipA at the interface difficult.

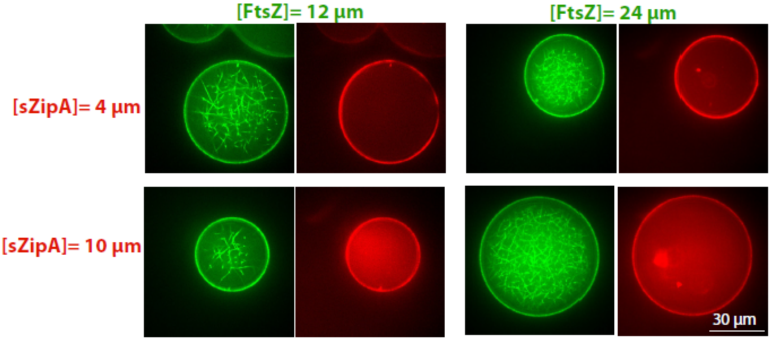

Figure 4. 5 Bulk emulsions containing different concentration combinations of FtsZ (green) and ZipA (red) present in the same droplet. Observation in time did not reveal any changes in the FtsZ bundle arrangement implying that the interaction between the two proteins is weak or inexistent.

The second parameter we modified was the droplet shape in order to reduce the depletion zone. Using the same device as described in section 4.2.1.1 but containing narrow channels in the device reservoir, we were able to trap and follow in time plug shaped droplets. *E. coli* lipids (25 g/L) in mineral oil were mixed with 10 mol% DOGS-NTA and the FtsZ and sZipA concentrations were 24 µM and 4µM, respectively. A higher FtsZ concentration was used to obtain a denser and more spread network, presenting a smaller depletion zone. Figure 4. 6 shows representative images of plug shaped droplets of different size, trapped in narrow channels of 15 µm width and 30 µm height. Two plug shaped populations were selected according to their different length of around 50 µm (plug 1) and 30 µm (plug 2). The longer plugs corresponded to droplet fusion occurring before the narrow channels. In both cases, the concentration of proteins inside the droplets is the same but the volume is different. Imaging the two droplet populations in time and after 80 min we did not see any deformation of the droplet membrane or any changes in the arrangement of FtsZ bundles.

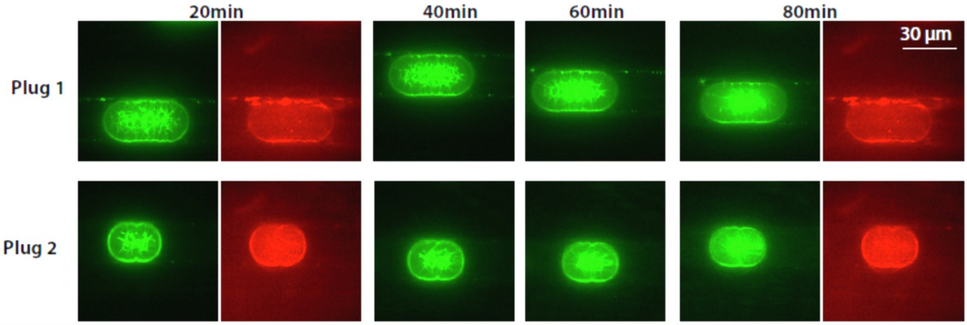

Figure 4. 6 Confocal images of plug shaped droplets containing 24 µM FtsZ (green) and 4 µM sZipA (red). Plug 1 corresponds to fused droplets having twice the volume of plug 2. The depletion zone seemed smaller but there was no effect on the droplet membrane or FtsZ bundle arrangement in time.

The last parameter we investigated was the number of NTA groups present at the droplet inner face. Considering a droplet of 30 µm in diameter, presenting at its interface 10 mol% DOGS-NTA lipids mixed with *E. coli* lipids then the number of mole of NTA would be 6.6 10^{-16}. Now, if the sZipA concentration encapsulated in the same size droplet is around 4 µM, its number of moles would be 5.65 10^{-17} which is around one order of magnitude lower than the NTA groups at the interface. In other words, in these conditions there is a large excess of NTA groups compared to that of sZipA. However, since FtsZ is also going to the droplet interface this could reduce the number of NTA groups available for sZipA and therefore we decided to increase the percentage of DOGS-NTA from 10 mol% to 30 mol%. Figure 4. 7 shows representative fluorescent images of droplets containing sZipA (4µM) alone or in the presence of FtsZ (24 µM) with different DOGS-NTA mol% at the droplet interface. When only sZipA is present in the droplet, no significant changes of fluorescent intensity in the droplet lumen was observed from 10 mol% to 50 mol% DOGS-NTA, indicating that NTA groups were indeed already in excess at 10 mol%. When both sZipA and FtsZ are present in the droplet, no major differences in the arrangement of FtsZ bundles and droplet interface was observed.

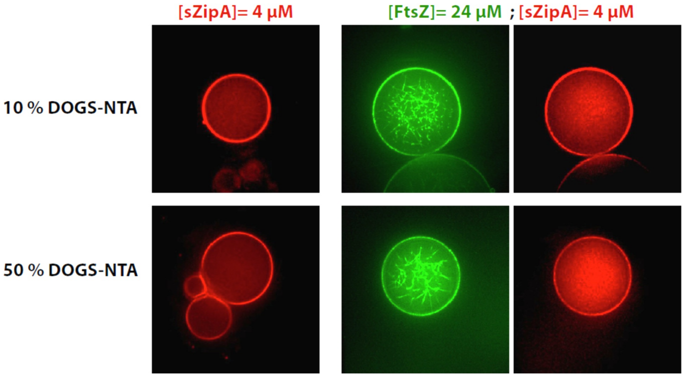

Figure 4. 7 Confocal images of bulk emulsions containing 4 µM sZipA alone in a droplet (left) or 24 µM FtsZ (green) and 4 µM sZipA (red) in the same droplet (right), with 10 % or 50 mol % DOGS-NTA in the *E. coli* lipid solution. No major differences were observed due to the increase of possible attachment to the droplet interface.

From all the parameters we investigated, we came to the conclusion that although allowing the encapsulation of native protein retaining their ability to interact with each other, droplets were not an adequate platform for the study of possible effect in the lipid membrane. Several factors can justify this result; first the dynamic properties of a monolayer can be quite different from those of a bilayer. Also, the high surface tension and the low flexibility induced in aqueous droplets by the external oil phase could be hampering the observation of any possible effect. We therefore decided to proceed with our study using liposomes as a cell-like container.

4.2.2 Liposomes formation for divisome encapsulation

A liposome is a spherical vesicle that consists of a lipid bilayer that is artificially made. The lipids can be artificial of natural amphiphilic lipids (predominantly phospholipids), which form a bilayer similar to those found in bio-membranes. Liposomes are often classified by the number of lamellae and their size. Small unilamellar vesicles (SUV) and large unilamellar vesicles (LUV) with diameters ranging from 20 to about 100 nm can be used as a drug delivery system,[31] whereas giant unilamellar vesicles (GUV, diameter above 1 µm) are often used as a cell like model.[32, 33] Multilamellar vesicles (MLV) have a diameter above 500 nm and multivesicular vesicles (MVV) which contain vesicles in a large vesicle are above 1 µm in diameter.

The appropriate type of liposome for our study would be the GUV, which can have a suitable size for microscopy visualization. There are a large variety of methods for the formation of GUV[18] such as the phospholipids film hydration or electroformation method, which yields polydisperse vesicles with no control over the content and the membrane composition. Compared to bulk experiments, microfluidics offers the possibility to have a total control over the size, composition and shape. Some existing methods use microfluidics as a tool for GUV formation like the double emulsion W/O/W where the oil phase is a volatile solvent.[34] The drawbacks of this method are that the device fabrication and the complete removal of the solvent by evaporation might not be easy. Below are described two methods of vesicle production we selected for our system, one on chip and another one combining on and off chip approaches.

4.2.2.1 Liposomes production in chip

An elegant method to produce liposomes in microfluidics was described by Paegel and co-workers.[35] The technique is based on a layer-by-layer phospholipid membrane assembly on droplets in microfluidics. The microfluidic device contained a droplet production part (water in oil) followed by a long delay line channel allowing the lipids to equilibrate at the droplet interface and then a reservoir part containing cup arrays in order to trap the droplets. Subsequently, the oil phase was flushed out by the buffer solution yielding unilamellar liposomes. As this seemed a very easy method for liposome formation, we decided to use it for our system.

First, we tried a similar chip with the production, delay line and traps in the same microfluidic device. With three inlets, we were able to separate the FtsZ flow from the GTP flow (both in working buffer in the presence of 150 g/L ficoll 70) before droplet production when meeting the oil flow composed of *E. coli* lipids in mineral oil. In that way, FtsZ polymerization into bundles is happening in-line, only when the droplet is formed. After the droplet production part (30 µm) a short delay line followed, ending in a lager reservoir containing around a hundred traps. Since it usually takes around 5 min before the flows are stabilized and the droplets are monodisperse, we used inverted traps in order to only trap monodisperse droplets flushing with the oil flow from the outlet of the device (Figure 4. 8). Once the droplet production was stabilized, the flow was stopped by cutting the inlet tubing, which led to uncontrolled droplet fusion (Figure 4. 8 B). Then, the oil tubing was connected to the outlet to flow the droplet into the cup arrays and get trapped. However, as show in Figure 4. 8 C, since a lot of droplets fused and contained FtsZ bundles, this led to clogging of the production part making it impossible to trap the droplets.

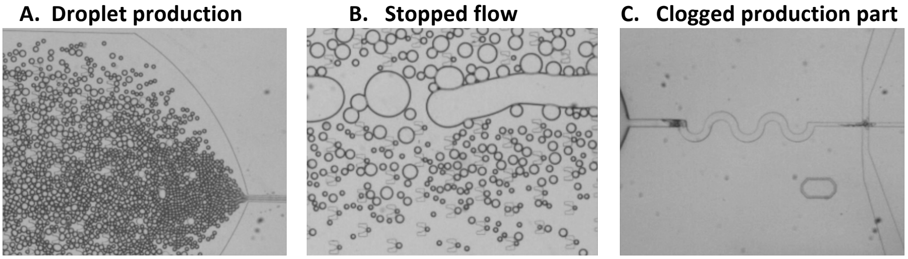
A. Droplet production **B. Stopped flow** **C. Clogged production part**

Figure 4. 8 Liposome formation in chip. A. Droplet production with droplet fusing in the reservoir. B. When the flow is stopped, droplet fusion is more pronounced. C. Trapping of the droplets was not possible and led to the clogging of the production channels.

Secondly, we tried to use two different devices to separate the droplet production part from the droplet trap part in order to have a better control on the droplet production and avoid the clogging of the device. As previously, the droplet production device also contained three inlets followed by a short delay line but now containing a gradually wider reservoir that allowed us to obtain monodisperse droplets (around 80 %). Once the droplet production was stable and monodisperse (Figure 4. 9 A), a piece of tubing was connected from the outlet to the inlet of a second chip only containing traps to allow the droplet to travel from on device to the second. When most of the traps were occupied with droplets, the piece of tubing was gently disconnected to stop the droplet flow. The tubing was then replaced by another one containing the working buffer and around 10 cm of oil/lipids solution at its end to remove the excess of droplets around the traps (Figure 4. 9 B).

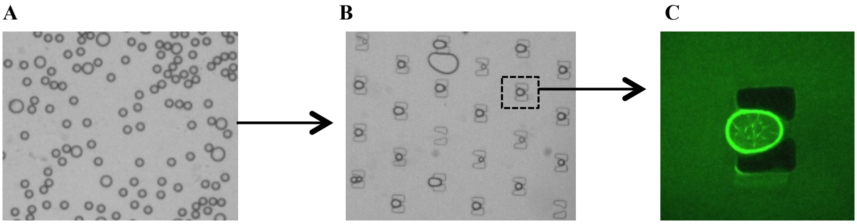

Figure 4. 9 Droplet production and trapping in two different devices. A. Droplets produced were monodisperse and then transfered to a second device via a tubing to be trapped in cup arrays (B). C. A confocal image of a trapped droplet shows the presence of FtsZ bundles.

Confocal images of the trapped droplets in oil showed that all contained FtsZ bundles as represented in Figure 4. 9 C. After the working buffer replaced the oil flow, some droplet fusion was observed but a relatively high amount of droplets remained stable until liposome formation. Figure 4. 10 shows a representative liposome in a trap, on the left a representative confocal image and on the right a bright field image confirming the presence of a liposome. Compared to droplet in oil, there is no difference of diffraction index between the inner solution of a liposome and the surrounding buffer. When the same experiment was performed with addition of 10 mol% DOGS-NTA mixed in E. coli lipids and 4 µM sZipA, no deformation or changes in bundle arrangement was observed (not shown here).

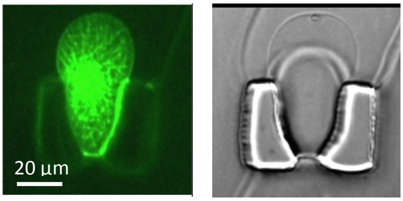

Figure 4. 10 Representative liposome in trap device. Left: confocal image with FtsZ bundles inside the liposome. Right: bright field image confirmed the presence of a liposome, showing no difference of contrast with the external solution.

From these images, it can be seen that the liposome formation in chip is not complete. During liposome formation, the droplet goes from a monolayer to a lipid bilayer and during this process the unassembled FtsZ is dislodge from the interface. Trapped droplets are initially spherical and barely touching the traps, but since the working buffer is flushed with a much higher flow rate to remove the oil around the droplets, this led to squeezing of the droplet on the traps. The consequence is that a layer of oil remains between the traps and the droplets and cannot be removed yielding ‘semi-liposomes’. Moreover, swelling of the droplets during the liposome formation was observed which leads to a dilution of the droplet content. The liposomes seemed to strongly adhere to the PDMS traps since it was impossible to flush them out of the device. Despite the promising report in the literature, this method does not seem to produce high-quality liposomes in our hands, and we therefore decided to try another method for liposome production described below.

4.2.2.2 Liposomes production by combining on and off chip methods

To produce liposomes in a more controlled way, Yomo and co-workers combined a microfluidic approach with a droplet transfer method.[36] Water droplets in oil were produced in a flow-focusing device using a mixture of span 80 and tween 80 (9:1 volume ratio in paraffin) and another oil phase containing lipids (POPC:POPG:Chol at 9:1:1 in paraffin) was injected downstream to dilute the detergent. The collected droplets were then transferred in an Eppendorf tube through an oil/buffer interface yielding to vesicle formation. The authors demonstrated that 80 % of lipids were present at the vesicle interface using fluorescently tagged lipids. In a similar way, we decided to first produce monodispersed lipid droplets in microfluidics and thereafter produce vesicles with the droplet transfer method as described in Figure 4. 11. When FtsZ droplet production in microfluidics is stable and gives monodisperse droplets, droplets can be collected via a piece of tube from the outlet to a 2 mL Eppendorf tube containing two immiscible phases: the working buffer with 100 mM glucose and lipids in mineral oil sitting on top. Centrifugation allows the droplets to migrate through the lipid saturated oil/water interface, which could lead to monodisperse unilamellar giant vesicles.

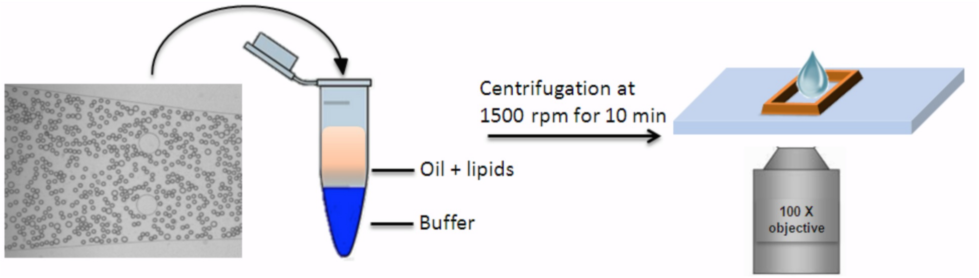

Figure 4. 11 Protocol for monodisperse liposome production. Monodisperse droplet produces in microfluidic device are collected via a piece of tubing to a tube containing the working buffer and an lipid/oil mixture. Centrifugation can lead to monodisperse giant vesicles of around 35 µm and can be easily observed by microscopy.

The microfluidic and droplet transfer methods were tested separately for different lipid compositions. The selected lipids were POPC (1-palmitoyl-2-oleoyl-sn-glycero-3-phosphocholine), EPC (L-α-phosphatidylcholine from egg yolk) and *E. coli* lipids, common lipids used for vesicle formation.[18, 37] Every lipid solution was prepared in mineral oil since it was previously concluded that it was the best condition for FtsZ observation.[30] For the droplet transfer method, we tested all three lipids in order to know which lipid composition would provide the highest yield and most stable liposomes. The concentrations of POPC and EPC were 0.5 g/L and for *E. coli* lipids of 25 g/L in mineral oil. FtsZ solution was prepared with an initial concentration of 12 µM with 120 g/L ficoll 70, 3mM GTP and 100 mM sucrose in working buffer with GTP-regenerating system.

The droplet transfer method used is fully described in the experimental section of this chapter. Figure 4. 12 shows representative fluorescent images of bulk emulsion (A), droplet transfer liposomes (B) and bright field images of the liposomes (C). Comparing the emulsion droplets, a difference in FtsZ bundle arrangement and attachment to the interface can be seen. With *E. coli* lipids, as previously observed, FtsZ is strongly adsorbing to the interface showing a higher affinity compared to that of the other lipids. This strong affinity could explain why it was not possible to obtain vesicle formation using *E. coli* lipids, preventing the bilayer to form and only water droplets in oil in water were observed. An alternative explanation might lie in the different hydrocarbon tails mixture, leading to different interactions with the oil phase and making liposome formation more challenging. In the case of POPC and EPC, liposome formation succeeded with a higher yield for POPC. However, no bundles were observed in any of the liposomes even when a GTP-regenerating system was used, which implies that the procedure for liposome formation could induce the depolymerization of the FtsZ bundles.

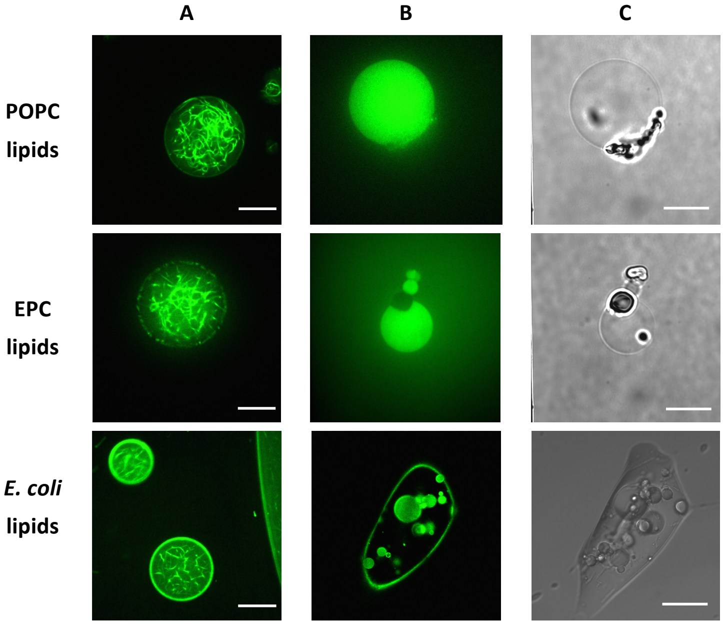

Figure 4. 12 Liposome formation with droplet transfer method using different lipids in mineral oil. A. Bulk emulsion containing FtsZ bundles showed differences in bundle arrangement and protein adsorption at the droplet interface. B. After centrifugation, liposomes were only obtained with POPC and EPC lipids. C. Bright field images corresponding to B. Scale bar = 20 µm.

When POPC and EPC (0.5 g/L in mineral oil) were used to produce FtsZ droplets in microfluidics, it resulted in wetting of the water flow on the channels wall resulting in droplet fusion (Figure 4. 13 A and B). However, the droplet production with 25 g/L *E. coli* lipids gave very stable and monodisperse droplet and no wetting was observed. Lower concentration of *E. coli* lipids in mineral oil were tested (15g/L and 5 g/L) and no wetting were observed.

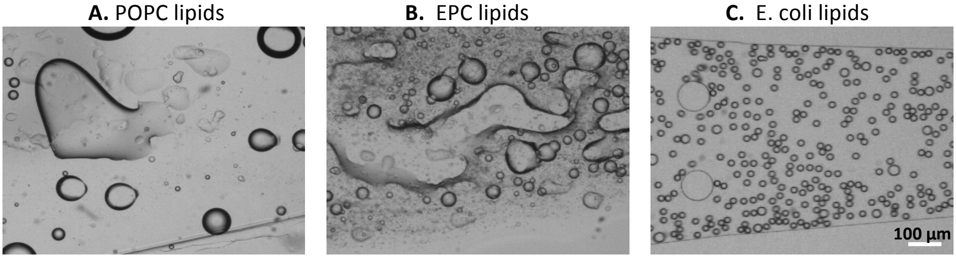

Figure 4. 13 Lipids coted droplet formation in microfluidic device. A , B. Droplet formation was not possible with POPC and EPC in mineral oil at 0.5 g/L, respectively. Wetting of the water flow on the device channels could be due to a low droplet stability or an inadequate device coating. C. droplet production with 20 g/L *E. coli* lipids in mineral oil resulted in stable and monodisperse droplets.

A good compromise would be to use a different lipid composition for the inner layer and outer layer of the liposome. *E. coli* lipids could constitute the inner lipid face since it allowed obtaining stable and monodisperse droplet in microfluidics, and POPC could constitute the outer lipid face of the bilayer since it showed successful liposome formation with the droplet transfer method.

4.2.3 Mimicking the nucleoid occlusion

In *E. coli* cells, the genetic material is packaged in a chromosome decorated with the nucleoid-associated protein SlmA that is believed to lead to so-called nucleoid occlusion. It was shown that SlmA leads to disassembly of FtsZ in vitro and was therefore modulating the formation of the Z ring.[6, 38, 39] In order to mimic the nucleoid occlusion system, we started with a simplistic model using commercial agarose beads encapsulated in droplets containing FtsZ bundles.

As a control experiment, we first studied the polymerization of FtsZ bundles in time, encapsulated in microdroplets. The droplets production was done in microfluidics, using a droplet production device as previously described, with concentration of FtsZ and

Ficoll 70 below the critical concentration of the bundle formation, at 10 µM and 80 g/L, respectively. We also used a GTP regenerating system to make sure that the GTP concentration was roughly constant during the course of the experiment. Once the flow was stable and the droplets were monodisperse the inflows were stopped by cutting the inlet tubing. Figure 4. 14 shows representative images of FtsZ polymerization in time, triggered by an increase of concentration while the droplet was shrinking. Since the initial droplet size was around 40 µm and that the height of the microfluidic device was around 30 µm, the droplets were immobile when the flow was stopped. It was then easy to select droplets for imaging in time and follow the polymerization. For the first 10 min after droplet production, no FtsZ bundles were present in the droplets and high fluorescence intensity was observed inside and at the droplet interface. After around 30 min, most of the droplets contained FtsZ bundles which did not change in arrangement and shape during the following hour. The final droplet size allowed us to estimate the final concentration of the components encapsulated in the droplets: around 12 µM FtsZ, 100 g/L Ficoll 70 and 3 mM GTP.

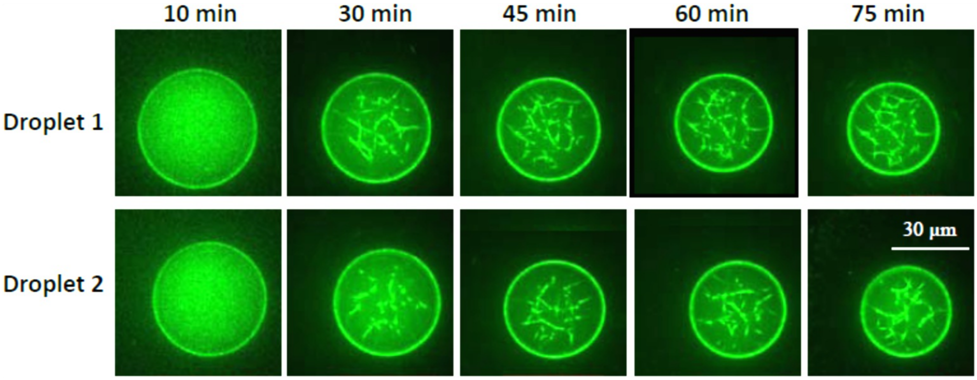

Figure 4. 14 FtsZ polymerization in shrinking droplets. Droplet 1 and 2 are representative droplets showing FtsZ bundle formation in time during droplet shrinkage in microfluidic device due to evaporation.

The second control experiment consisted in checking the encapsulation efficiency of the commercial agarose beads. The beads are highly crossed-linked agarose beads of about 10 µm in diameter and diluted five times in working buffer (20 % v/v bead solution). Using a three inlets device, the agarose beads flow was further diluted by two inflow of working buffer before meeting the oil/surfactant flow, which consisted of 25 g/L of *E. coli* lipids in mineral oil. During the droplet formation, some fusion occurred but most of the droplets remained monodisperse and all contained at least one agarose bead (Figure 4. 15). On the 10 X objective image, the beads can be seen by their lower contrast in the middle of the droplet, which is more evident on the 40 X objective image. Since the bead encapsulation was successful, we proceeded with bead and FtsZ encapsulation in microdroplets.

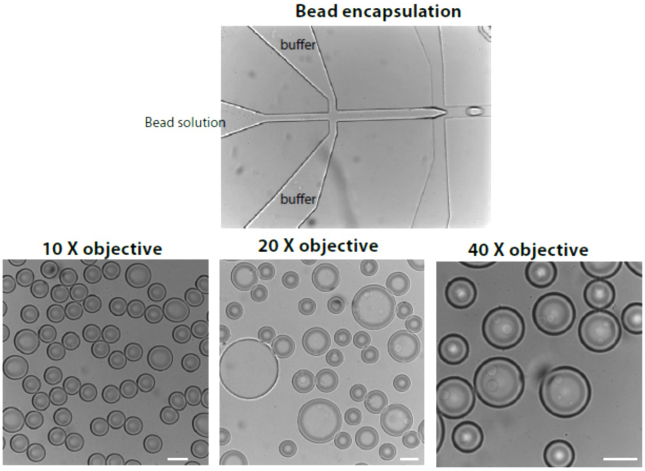

Figure 4. 15 Commercial agarose bead encapsulation in microdroplets. Top: 3 inlets device with one inlet containing the bead solution, another one the buffer to dilute the beads before droplet formation when meeting the oil/surfactant flow. Bottom: bright filed images of the collected droplets using different objective magnification showed the presences of at least one bead per droplets. Scale bar correspond to 30 µm.

The third control experiment was performed to check the unspecific adsorption of FtsZ on the agarose beads. Mixing GDP-FtsZ with agarose beads in working buffer, it appeared that FtsZ is adsorbing on the bead. Since at the working pH FtsZ has a negative charge, we decided to coat the agarose beads with BSA (Bovine Serum Albumin), of similar isoelectric point, in order to repel FtsZ. The coating of the beads with BSA was achieved by incubating the beads with 10 g/L BSA solution in working buffer for at least one hour at 4°C. Figure 4. 16 shows fluorescence images of droplets containing unpolymerized FtsZ with beads with or without BSA coating. On the coated beads, it is clear that no FtsZ is adsorbing to the bead surface and this system can be used for further experiments.

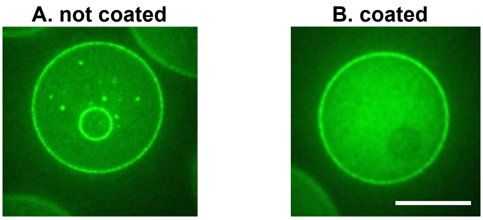

Figure 4. 16 Confocal images of unpolymerized FtsZ droplets containing agarose beads. A. non coated beads led to FtsZ monomers adsorption. B. BSA coated beads showed no FtsZ monomers adsorption and can be used as nucleoid mimic. Scale bar = 20 µm.

With a successful bead encapsulation, bead coating and FtsZ polymerization in time contained in microdroplets, we could combine all three control experiments into one. The idea was to monitor the FtsZ polymerization in time, encapsulated in microdroplets containing BSA coated beads which is represented in Figure 4. 17. Using a three inlet microfluidic device, one flow contained the *E. coli* lipids in mineral oil (25 g/L) and two others separate flows containing FtsZ or GTP and agarose beads, mixed before meeting the oil flow. The monodisperse droplets had a starting diameter of around 40 µm at initial concentrations of 10 µM FtsZ, 80 g/L Ficoll 70, 2.5 mM GTP and 10 X bead solutions. Most of the droplets contained at least one agarose bead and as the droplets started to shrink in time the concentration of the different components increased to reach a concentration at which bundle formation is possible. Interestingly, FtsZ bundles started to appear after 25 min nucleating from the agarose beads. It seemed that the beads facilitated the bundle formation, which started from the bead to the droplet interface. A 3D reconstruction made from Z-stack images shows that bundles are mainly surrounding the beads.

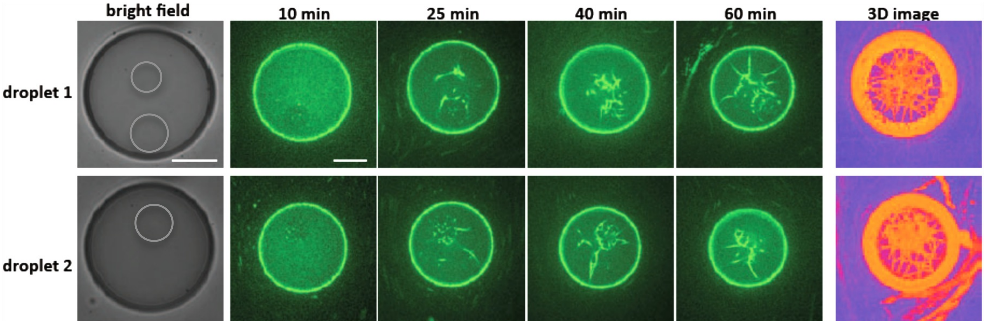

Figure 4. 17 FtsZ polymerization in shrinking droplets containing agarose beads. Droplet 1 and 2 are representative droplets containing FtsZ and Ficoll at critical concentrations of 10 µM and 80 g/L, respectively. While droplets are shrinking due to evaporation, the concentrations inside the droplets

increased and FtsZ bundles appeared first on the encapsulated bead. Grey circles are surrounding the beads in the bright field images. Scale bar = 15 µm.

4.3 Conclusions

The behaviour of three essential divisome proteins in *E. coli* was investigated in 'cell-like' containers. Using droplet microfluidics, FtsZ and FtsA were successfully encapsulated revealing protein interactions, with FtsA remaining at the droplet interface when alone in the droplet. These results illustrate that FtsZ bundles have a great influence on FtsA membrane interactions. The encapsulation of sZipA in microdroplets with different DOG-NTA % mol mixed with *E. coli* lipids in mineral oil revealed an increasing membrane attachment efficiency of the protein. When both FtsZ bundles and sZipA were present in the droplet, no significant changes in bundles arrangement was observed even when the droplet shape or sZipA membrane attachment were modified. However, it was demonstrated by Cabre and co-workers that the encapsulation of the two proteins in giant unilamellar led to shrinkage of the vesicle presumably due to interaction between the two proteins. We concluded that despite the encapsulation of the protein retained their ability to interact with each other, microdroplets were not an adequate platform for the study of possible effect in the lipid membrane. The factors which can have an influence are the different physico-chemical properties between droplets and liposomes: the dynamics of a monolayer differ from those of a bilayer and the high surface tension and the low flexibility of aqueous droplets in oil could be hampering the observation of any possible effect.

Since studies of the divisome proteins encapsulated in liposomes were already reported in the literature,[14] we tried to develop a new method for the formation of monodisperse liposomes. Focusing on the formation of giant unilamellar vesicles, suitable size for microscopy visualization, we investigated two approaches: one on chip and another one combining on and off chip. The on chip approach led to uncontrolled droplet fusion while the combining method appeared to be promising. The production of FtsZ bundles droplets in oil containing *E. coli* lipids was monodisperse and stable. However, when droplets were collected and transferred through a two phases solution (top: *E. coli* lipids in oil, bottom: buffer), vesicle formation was not possible. Bulk experiments revealed that with EPC or POPC lipids, liposome formation by droplets transfer was successful. Therefore, droplet formation with *E. coli* lipids in microfluidics followed by droplet transfer with POPC lipids could lead to the formation of monodisperse and stable liposomes. Since it was reported that the size and nature of the cell-like container is a critical parameter for the divisome study,[12] optimisation of our system could lead to a controlled method for liposome formation and study protein behaviour under confinement.

4.4 Experimental section

Materials

Reagents, salts, mineral oil and buffer components were from Sigma. Polar extract phospholipids from *E. coli*, L-α-phosphatidylcholine from egg yolk (EPC), 1-palmitoyl-2-oleoyl-sn-glycero-3-phosphocholine (POPC) and 1,2-dioleoyl-sn-glycero-3-[(N-(5-amino-1-carboxypentyl)iminodiacetic acid)succinyl] nickel salt (DOGS-NTA-NI) were purchased from Avanti polar lipids (Alabama, USA) and were stored in chloroform:methanol 2:1 (v/v). Just before use, a determined amount was dried under nitrogen flow, kept under vacuum for at least two hours and resuspended in mineral oil by sonication in a thermostated bath at 37 ºC for 30 min, to get the desired final concentration (0.5 to 25 g L^{-1}). Fluorescent dyes (Alexa 488, Alexa 647) were from Molecular probes. Agarose beads were purchased from ABT (agarose bead technologies) and were 4% highly crosslinked beads with an average diameter of 10 µm.

Protein purification and labelling

The proteins used were wild type proteins except for ZipA, a soluble mutant was used instead (sZipA, lacking the its hydrophobic N-terminal domain), that presents the same binding affinity for FtsZ.[27, 28] *E. coli* FtsZ was purified by the calcium precipitation method as described previously.[40] sZipA and FtsA, both harbouring a His tag, were overexpressed in *E. coli* strain BL21(DE3) and purified as described.[27, 41] The proteins were dialyzed against the **working buffer** (50 mM Tris-HCl, pH 7.5, 500 mM KCl, 5 mM $MgCl_2$), and aliquots were stored at -80 ºC until used.

All three proteins were labelled with Alexa probes (1:10 molar ratio) in 50 mM Hepes/HCl (pH 8), 100 mM KCl and 5 mM $MgCl_2$ at room temperature for about 10 min.[14, 25] For FtsZ, labelling occurred in conditions promoting protein polymerization as described.[9] Labelled proteins were separated from free probes using a gel filtration column.[42] The labelled proteins were stored frozen at -80 ºC in working buffer with 10% glycerol buffer. The ratio of labelling, estimated from the molar absorption coefficients of the dye and the proteins, was 0.3-0.5. In all the experiments, labelled protein was 2% of total protein concentration

Droplet formation

The microfluidic chip design and fabrication was the same as in Chapter 3 – Experimental section. The microfluidics device had 3 inlets and a large reservoir with channels. One stream contains FtsZ at the specified concentration with or without one of the other two proteins FtsA or sZipA; the other stream delivers GTP at a concentration of 6 mM. They were mixed in a 1:1 ratio prior to the droplet formation junction where it joined the oil containing lipids.

Droplet transfer method

FtsZ (12-25 µM) solution was equilibrated in working buffer with 120 g/L Ficoll 70, 3mM GTP and 100 mM sucrose. Emulsions were produced by mixing 15 µL of protein solution with 500 µL of oil/lipids solution by gently pipetting up and down until the emulsion was homogeneously cloudy. In the meantime, 500 µL of the oil lipid mixture was placed on top of a buffer containing 100 mM glucose in working buffer and allowed to equilibrate for around 1h. After that time, the emulsion was placed on top of the 2 phase solution and centrifuged for around 10 min at 1500 rpm. The oil phase was removed and the liposomes were collected at the bottom of the tube with a 1 mL pipette. Around 200 µL of the liposome solution was poured in a press-to-seal well placed on a coverslip.

Note: glucose and sucrose are used to create a difference of density between the liposomes and the outer buffer which will force them to sink and allow easy observation by microscopy.

Agarose bead solution preparation

From a stock solution of beads in 20% ethanol, 500 µL were centrifuged in a spin column (0.22µm cellulose acetate), at 900 rpm for 90 s then at 4000 rpm for 90 s. The beads were washed 3 times with 300 µL 1X PBS solution at 4000 rpm for 3min and resuspended in 300 µL of working buffer yielding to a 2X diluted bead solution. Subsequently, 200 µL of 10 g/L BSA was added to 100 µL of the 2 X diluted bead solution and incubated at 4°C for around 1h. After three washing steps with working buffer at 1000 rpm for 10 min, the supernatant was removed and 200 µL of working buffer was added to the beads yielding a 5X diluted agarose bead solution coated with BSA.

Fluorescence microscopy

Samples were observed with a spinning disk confocal microscope (CSU-X1, Yokogawa Electric Corp.) on an Olympus inverted microscope (IX81). Alexa-488 was excited with 488 nm laser light (λ_{em}= 525 nm) and Alexa-647 with 620 nm laser light (λ_{em}= 675 nm). Images were recorded with a temperature controlled EM-CCD camera (iXon3, Andor) using an exposure time of 0.8-1 s and a piezo-driven 100x (1.3 NA) oil immersion objective. All the images shown below correspond to confocal fluorescence images taken at mid plane that is an equatorial section of the droplets, and are representative of the behaviour observed in all droplets tested under each particular condition. All observations were conducted at room temperature.

4.5 References

1. A. J. F. Egan and W. Vollmer, *Ann Ny Acad Sci*, **2013**, *1277*, 8-28.
2. A. I. Rico, M. Krupka and M. Vicente, *J Biol Chem*, **2013**, *288*, 20830-20836.
3. M. Vicente and A. I. Rico, *Mol Microbiol*, **2006**, *61*, 5-8.
4. V. W. Rowlett and W. Margolin, *Curr Biol*, **2013**, *23*, R553-R556.
5. S. Arumugam, Z. Petrasek and P. Schwille, *P Natl Acad Sci USA*, **2014**, *111*, E1192-E1200.
6. H. B. Cho, H. R. McManus, S. L. Dove and T. G. Bernhardt, *P Natl Acad Sci USA*, **2011**, *108*, 3773-3778.
7. M. A. Oliva, S. C. Cordell and J. Lowe, *Nat Struct Mol Biol*, **2004**, *11*, 1243-1250.
8. D. Popp, M. Iwasa, A. Narita, H. P. Erickson and Y. Maeda, *Biopolymers*, **2009**, *91*, 340-350.
9. J. M. González, M. Jiménez, M. Vélez, J. Mingorance, J. M. Andreu, M. Vicente and G. Rivas, *J Biol Chem*, **2003**, *278*, 37664-37671.
10. S. Pichoff and J. Lutkenhaus, *Embo J*, **2002**, *21*, 685-693.
11. H. P. Erickson, *Trends Cell Biol*, **1997**, *7*, 362-367.
12. M. Osawa, D. E. Anderson and H. P. Erickson, *Science*, **2008**, *320*, 792-794.
13. M. Osawa, D. E. Anderson and H. P. Erickson, *Embo J*, **2009**, *28*, 3476-3484.
14. E. J. Cabre, A. Sanchez-Gorostiaga, P. Carrara, N. Ropero, M. Casanova, P. Palacios, P. Stano, M. Jimenez, G. Rivas and M. Vicente, *J Biol Chem*, **2013**, *288*, 26625-26634.
15. S. L. Milam, M. Osawa and H. P. Erickson, *Biophys J*, **2012**, *103*, 59-68.
16. Z. Li, M. J. Trimble, Y. V. Brun and G. J. Jensen, *Embo J*, **2007**, *26*, 4694-4708.
17. S. J. Holden, T. Pengo, K. L. Meibom, C. F. Fernandez, J. Collier and S. Manley, *P Natl Acad Sci USA*, **2014**, *111*, 4566-4571.
18. P. Walde, K. Cosentino, H. Engel and P. Stano, *Chembiochem*, **2010**, *11*, 848-865.
19. M. Hase, A. Yamada, T. Hamada, D. Baigl and K. Yoshikawa, *Langmuir*, **2007**, *23*, 348-352.

20. A. Tsuji and K. Yoshikawa, *Chembiochem*, **2010**, *11*, 351-357.
21. A. V. Pietrini and P. L. Luisi, *Chembiochem*, **2004**, *5*, 1055-1062.
22. P. Szwedziak, Q. Wang, S. M. V. Freund and J. Lowe, *Embo J*, **2012**, *31*, 2249-2260.
23. S. Pichoff and J. Lutkenhaus, *Mol Microbiol*, **2005**, *55*, 1722-1734.
24. J. R. Wenner and V. A. Bloomfield, *Biophys J*, **1999**, *77*, 3234-3241.
25. M. Jimenez, A. Martos, M. Vicente and G. Rivas, *J Biol Chem*, **2011**, *286*, 11236-11241.
26. L. Mosyak, Y. Zhang, E. Glasfeld, S. Haney, M. Stahl, J. Seehra and W. S. Somers, *Embo J*, **2000**, *19*, 3179-3191.
27. A. Martos, C. Alfonso, P. Lopez-Navajas, R. Ahijado-Guzman, J. Mingorance, A. P. Minton and G. Rivas, *Biochemistry-Us*, **2010**, *49*, 10780-10787.
28. V. M. Hernandez-Rocamora, B. Reija, C. Garcia, P. Natale, C. Alfonso, A. P. Minton, S. Zorrilla, G. Rivas and M. Vicente, *J Biol Chem*, **2012**, *287*, 30097-30104.
29. E. Small and S. G. Addinall, *Microbiol-Sgm*, **2003**, *149*, 2235-2242.
30. S. Mellouli, B. Monterroso, H. R. Vutukuri, E. te Brinke, V. Chokkalingam, G. Rivas and W. T. S. Huck, *Soft Matter*, **2013**, *9*, 10493-10500.
31. T. M. Allen and P. R. Cullis, *Adv Drug Deliver Rev*, **2013**, *65*, 36-48.
32. T. Oberholzer and P. L. Luisi, *J Biol Phys*, **2002**, *28*, 733-744.
33. A. Saha, G. Mondal, A. Biswas, I. Chakraborty, B. Jana and S. Ghosh, *Chem Commun*, **2013**, *49*, 6119-6121.
34. H. C. Shum, D. Lee, I. Yoon, T. Kodger and D. A. Weitz, *Langmuir*, **2008**, *24*, 7651-7653.
35. S. Matosevic and B. M. Paegel, *Nat Chem*, **2013**, *5*, 958-963.
36. K. Nishimura, H. Suzuki, T. Toyota and T. Yomo, *J Colloid Interf Sci*, **2012**, *376*, 119-125.
37. I. Lopez-Montero, P. Lopez-Navajas, J. Mingorance, M. Velez, M. Vicente and F. Monroy, *Biochim Biophys Acta*, **2013**, *1828*, 687-698.
38. T. G. Bernhardt and P. A. de Boer, *Mol Cell*, **2005**, *18*, 555-564.
39. N. K. Tonthat, S. T. Arold, B. F. Pickering, M. W. Van Dyke, S. D. Liang, Y. Lu, T. K. Beuria, W. Margolin and M. A. Schumacher, *Embo J*, **2011**, *30*, 154-164.
40. G. Rivas, A. López, J. Mingorance, M. J. Ferrándiz, S. Zorrilla, A. P. Minton, M. Vicente and J. M. Andreu, *J Biol Chem*, **2000**, *275*, 11740-11749.
41. A. Martos, B. Monterroso, S. Zorrilla, B. Reija, C. Alfonso, J. Mingorance, G. Rivas and M. Jimenez, *Plos One*, **2012**, *7*.
42. B. Reija, B. Monterroso, M. Jiménez, M. Vicente, G. Rivas and S. Zorrilla, *Anal Biochem*, **2011**, *418*, 89-96.

Chapter 5

Microtubules dynamics in crowded and confined environment

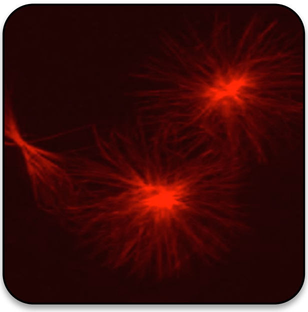

Microtubule asters

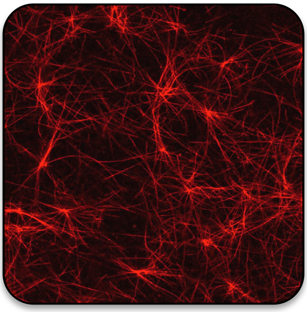

Microtubules in bulk

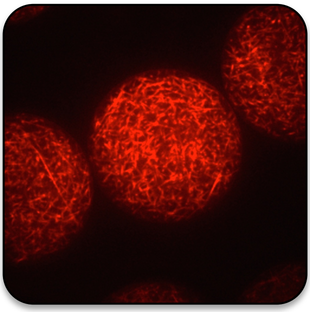

Microtubules in emulsion

5.1 Introduction

Microtubules are essential protein assemblies present in the cytoplasm of eukaryotic cells. They are hollow cylinders of about 25 nm in diameter and a few micrometres long, composed of α and β-tubulins (each about 55 kDa MW), which are homologous but not identical. Both have a nucleotide binding site which can bind to guanosine triphosphate (GTP) but only β-tubulin can hydrolyse its bound GTP to GDP plus P_i (inorganic phosphate), release the P_i, and exchange the GDP for GTP.[1] The atomic structure of tubulin (Figure 5. 1) was first obtained by Nogales *et al.* at 3.5 Å resolution maps from electron crystallography of zinc-induced tubulin sheets stabilized with taxol[2]. The authors noted another significant difference between α and β-tubulin: the globular domain of β-tubulin has a binding site for Taxol and other drugs.

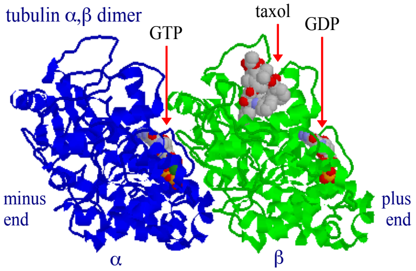

Figure 5. 1 Structure of the α,β-tubulin heterodimer, subunit of microtubules. β-tubulin is able to hydrolyse GTP to GDP upon microtubule polymerization and present a binding site for taxol and other drugs, contrary to α-tubulin.

Along the microtubule axis, α,β-tubulin heterodimers (stable once formed) are joined head-to-tail to form protofilaments in a polar fashion: the end exposing α-tubulin is slow growing and called minus end; the fast growing end exposing β-tubulin is called plus end. In vivo, microtubules usually have 13 protofilaments but in vitro, it is possible for purified tubulin to assemble with a range of diameters containing between 9 and 16 protofilaments.[3] During microtubule polymerization, each heterodimer carries two GTP molecules and associate to form a protofilament or microtubule (Figure 5. 2)[4]. Upon addition of a new dimer at the plus end, the catalytic domain of α-tubulin contacts the nucleotide exchangeable site (E site) of the previous β subunit and the GTP is hydrolysed to GDP when the tubulin dimers are added to the plus end of the growing microtubule. Such GTP hydrolysis is not mandatory for microtubule formation, but it appears that only

GDP-bound tubulin molecules are able to depolymerize. Thus, a GTP-bound tubulin serves as a cap at the tip of microtubule to protect from depolymerization and once the GTP cap is stochastically lost, the microtubule begins to depolymerize and shrinks rapidly.[5] Microtubules are temperature-sensitive and the hydrolysis of GTP is facilitated at a temperature of 37 °C and stopped at temperatures of around 4 °C.

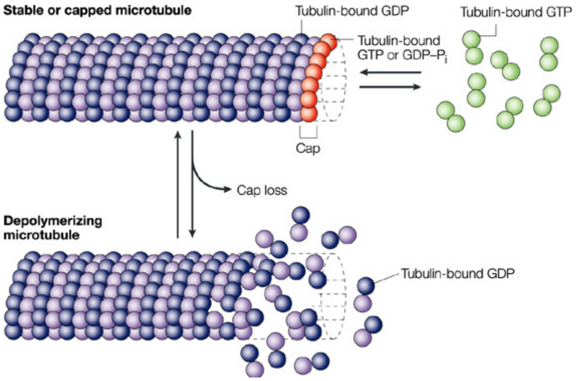
Stable or capped microtubule
Tubulin-bound GDP
Tubulin-bound GTP
Tubulin-bound GTP or GDP–P_i
Cap
Cap loss
Depolymerizing microtubule
Tubulin-bound GDP

Figure 5. 2 Polymerization dynamics of microtubules. Tubulin heterodimers add up to microtubule ends leading to GTP hydrolysis with release of inorganic phosphate Pi. A microtubule end containing tubulin-bound GTP or GDP–Pi is stable, or ‘capped’, against depolymerization. When the GTP cap is hydrolyses, conformational changes in the tubulin molecules destabilize the microtubule polymer, resulting in catastrophe and shortening of the microtubule.[4]

Microtubules are extremely important components involved in essential cell processes, affecting cell shape, cell mobility, cell transport and cell division.[4, 6] In vivo, the minus end of microtubules is associated with the centrosome located near the centre of the cell, whereas the plus end is peripheral. The polymerization of microtubules occurs in three phases: nucleation, elongation and steady state (Figure 5. 3)[7]. It is important to emphasise that microtubules are highly dynamic, growing and shrinking depending on their biological function in the cell. Microtubules show two kind of non-equilibrium behaviour, both *in vivo* and *in vitro*. The first kind of dynamic behaviour, called dynamic instability,[8] is a process in which the individual microtubule ends switch between phases of growth (rescue), shortening (catastrophe) and attenuated dynamic (steady state). The second dynamic behaviour, called treadmilling,[9] is a net growth at one microtubule end and balanced by net shortening at the opposite end. Dynamic instability and treadmilling are compatible, and a specific microtubule population can show a mixture of both behaviours.

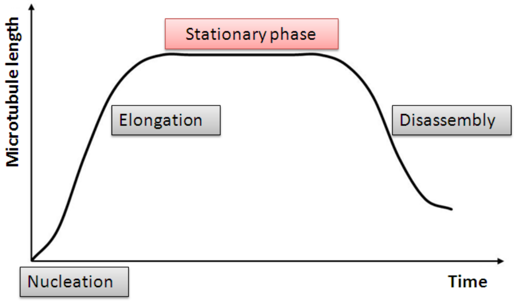

Figure 5. 3 Diagram representing microtubules dynamics. The microtubule length versus time starts with nucleation then elongation, followed by a stationary phase where microtubules are still dynamic. Once GTP is depleted, microtubule will depolymerize.[7]

Microtubule dynamics *in vivo* are regulated by microtubule-associated proteins, stabilizing or destabilizing microtubules.[10] As an example, kinesins and dyneins are molecular motors that move along microtubules in a directed manner. Confinement and crowding are also important parameters involved in microtubule dynamics with cell boundary properties affecting microtubules organization. In animal cells, microtubules organize into distinct patterns that can be categorized in three classes: bundles, asters and antiparallel overlaps.[11] However, the precise interplay between the cell's confinement/crowding and microtubule polymerization/organization/assembly, are not well understood.

We are interested in understanding the influence of spatial confinement and crowding on microtubules dynamics. It is known that microtubules and motor protein kinesin confined in microfabricated chambers (~2 μm depth, 90 μm diameter), organize into asters.[12] By varying the relative concentration of the components, different structures have been obtained, ranging from bundles, vortices to asters. Using similar fabricated microscopic chambers that simulate the closed environment of cells, Leibler and co-workers studied the positioning of microtubule asters.[13] The authors showed that pushing forces generated by growing microtubules are enough to drive the asters to the middle of the chamber. When dynein motor proteins were attached to the edges of the chamber, the same result was observed.[14] However, the experiments mentioned above with microtubules in microfabricated chamber do not take into account the flexibility of the confining geometry. Many living cells can change their shape in response to intra-cellular forces.[15, 16] In earlier work, microtubules encapsulated in lipid vesicles resulted in a deformation of the lipid container in the direction of the growing microtubules.[17-19] Using emulsion droplets and vesicles of different stiffness encapsulating *Xenopus* egg extracts, Gueroui and co-workers demonstrated that both the size and flexibility of the container are critical for the self-organization of microtubules.[20] Interestingly, using droplet microfluidics, two recent papers showed that the size of *Xenopus* spindles directly scaled with the volume of the cytoplasmic extract droplet, with tubulin as a limiting component.[21, 22] Keeping the droplet volume constant, a change in droplet shape from spherical and elongated to compressed shape did not give any differences in spindle length.

In this chapter, we studied microtubules organization/assembly inside confined cell-like compartments, using water-in-oil microdroplets formed in microfluidic devices and allowed the production of monodisperse droplets that can be easily manipulated. Therefore, microdroplets would allow us to probe and visualize how microtubules behavior is influenced by flow, crowding and confinement in droplets of different shapes. The questions we want to address are: what are the critical conditions for microtubule bundle formation? What are the differences in microtubule arrangement depending on the droplet shape or crowder? Is there an effect of the confinement on microtubule bundle arrangement compared to that of bulk experiment?

5.2 Results and discussion

5.2.1 Preparation of stabilized microtubules

The protocol for the preparation of stabilized microtubules is described in the experiment section of this chapter and is based on the supplier procedure (Cytoskeleton). Briefly, rhodamine labelled tubulin was mixed with unlabeled tubulin solution (15 % labelling ratio) and warmed in a water bath for around 20 min at 37 °C. Tubulin polymerized into microtubules and was stabilized by the addition of taxol solution (20 µM). When following the Cytoskeleton kit protocol, we were not able to obtained stable microtubules. Therefore, we decided to optimize the system investigating the influence of three parameters: tubulin, taxol and GTP concentrations (Figure 5. 4). In experiment 1, the GTP concentration is very low due to a dilution by addition of the taxol solution. In experiment 2, GTP was added to the taxol buffer to obtain a final concentration of 1.5 mM in the microtubule solution. However, both experiments 1 and 2 did not yield stable microtubules, only some 'aster' like microtubules. In the third experiment, we decided to increase both the tubulin and taxol concentrations leading indeed to stable and dense microtubule solution. In the next experiments, the taxol and the GTP concentrations were kept constant and the tubulin concentration was decreased. The presence of microtubule bundles at very low tubulin concentrations (0.3 µM) shows that the tubulin concentration is not a critical parameter. Therefore, the optimum concentrations for obtaining stable microtubules are at least 1 mM GTP and 20 µM taxol. Noteworthy: the size of a single microtubule is around 25 nm and it is most likely that we observe microtubule bundles.

Experiment number	1	2	3	4	5
Final tubulin concentration (µM)	1.4	2.5	**3.8**	**1.3**	**0.3**
Final Taxol concentration (µM)	19	18	21.5	22.5	22.5
Final GTP concentration (mM)	0.03	1.5	1.1	1.1	1.1
Confocal mages	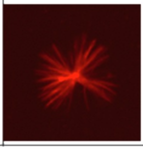	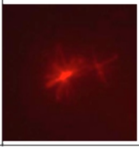	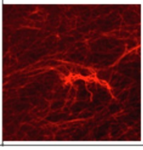	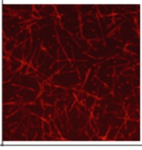	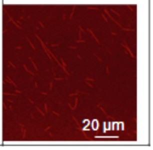

Figure 5. 4 Confocal images of microtubule solutions in different conditions. The optimum concentration for preparation of taxol stabilized fluorescent microtubules is 20 µM taxol, 1 mM GTP and above 0.2 µM tubulin.

5.2.2 Stabilized microtubules in bulk emulsions

The protein encapsulation efficiency in droplets depends on the nature and combination of the oil and surfactant.[23] In order to find the appropriate oil/surfactant combination to study microtubules, we investigated a range of surfactants in bulk emulsions as depicted in Figure 5. 5. The surfactants tested were span 80, monoolein, cithrol and a custom-made block copolymer (SS1), all at a concentration of 2 % in oil (wt/wt). Span 80 is a commonly used nonionic surfactant, which usually offers good emulsion stability and biocompatibility. Monoolein is a lipid widely used for emulsion stabilization due to its biocompatibility and multiple applications.[24] A commercially available (Cithrol)[24] and custom-made Krytox®-based (SS1) block copolymer[25] surfactants were chosen for their proven biocompatibility and formation of very stable emulsions. Bulk emulsions were prepared by gently pipetting up and down two immiscible solutions: an aqueous phase containing taxol-stabilized microtubules in buffer and an oil phase composed of the specified surfactant dissolved in oil (Figure 5. 5). Using mineral oil and span 80, microtubules were nicely encapsulated in droplets but when the emulsion was imaged the day after, it showed that microtubules formed thicker bundles and mainly accumulated at the droplet interface. The same was observed when using the same oil but cithrol as a surfactant or the combination squalane/monoolein. On the other hand, the custom-made tri-block copolymer (SS1) in HFE 7500 resulted in homogeneous microtubules distributed in droplets, with no microtubules present at the interface even after one day of incubation. This oil surfactant combination seemed to be the best but all the oil/surfactant combinations will be further investigated in droplet microfluidics.

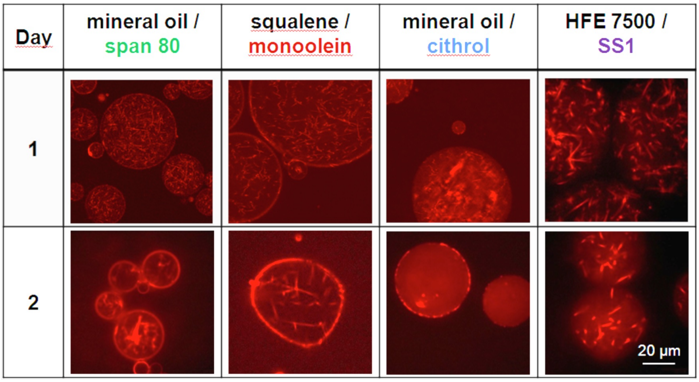

Figure 5. 5 Stability of microtubule bulk emulsions using different oil/surfactant combinations. The optimum condition to produce microtubule bulk emulsion is with HFE 7500 oil and SS1 surfactant.

5.2.3 Stabilized microtubules in droplet microfluidics

Droplet microfluidics offers many advantages, which makes it ideal for studying microtubules. Compared to bulk experiment, the production of microdroplets reduces the volume of reagent required for assays, the size of sample required, and the size of the equipment itself. Moreover, microdroplets can be seen as ‘cell-like’ containers that can be manipulated by changing the shape, size and composition.

Microfluidic devices were prepared as previously described (chapter 3 - Experimental section). In order to further confirm the choice of our oil/surfactant system, we produced droplets in microfluidics devices consisting of a 20 µm droplet production part (30 µm height) followed by a large reservoir for droplet storage. By means of syringe pumps, the stream of water solution and oil/surfactant solution were kept the same for the different production part devices, at 5 and 10 µL/h, respectively. From Figure 5. 6 it is clear that the custom-made surfactant (SS1) dissolved in HFE 7500 gave the most stable and monodisperse droplets. When Cithrol or Span 80 in mineral oil was used, droplet fusion was observed resulting in bigger droplet sizes or in streams of water flows in the reservoir. With monooleine in squalane, droplets were not completely monodisperse but little droplet fusion was observed. Therefore, both SS1 and Monooleine surfactant in oil were further investigated in order to find the best microtubule encapsulation in droplet microfuidics.

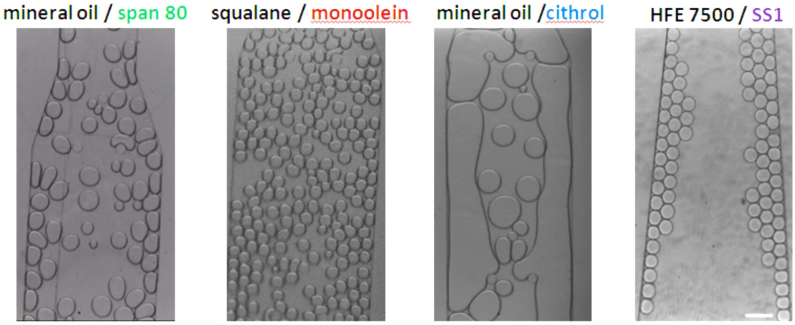

Figure 5. 6 Water droplet production in 20 µm production device (30 µm height) with different oil/surfactant. Monoolein and SS1 surfactants in squalane and HFE 7500, respectively, gave monodisperse and stable droplets. With cithrol or span 80 in mineral oil, droplets fusion was observed. Scale bar = 100 µm.

A solution of stabilized microtubules was prepared as previously described (section 5.2.1), with a final tubulin concentration of around 0.5 g/L (Figure 5. 7). Microtubules droplets with monoolein or SS1 as a surfactant were produced with flow of 10 and 1 µL/h for the oil and microtubule flows, respectively. Microtubules droplets formed with monoolein in squalane were monodisperse (around 30 µm in diameter) and interestingly formed lipid bilayers when droplets were getting into contact.[6] This resulted in droplet clusters sharing a lipid bilayer, boundary comparable to the cell membrane. From the confocal images, microtubule bundles seem to arrange uniformly in the droplet lumen but when a video was taken, microtubules disappeared with a highest intensity at the droplet boundary. The reason of this behaviour could be attributed to microtubule adsorption at the droplet interface as the confocal images show only fluorescent intensity at the interface compare to that in the droplet lumen. This phenomenon was not observed with HFE 7500 and SS1 as an oil/surfactant combination, showing that microtubules have a higher affinity for monoolein lipids or squalane oil (Figure 5. 7. C). In this case, droplets were formed with water and oil flow set at 15 and 115 µL/h, respectively (Figure 5. 7. A).

Droplet were stable, monodisperse and from the confocal images, microtubules are spread over the droplets with no fluorescence intensity observed at the droplet boundaries. From these results, it seems obvious that the best oil/surfactant combination for the investigation of microtubule dynamics in confined environment is HFE 7500/SS1 and will be used throughout this study.

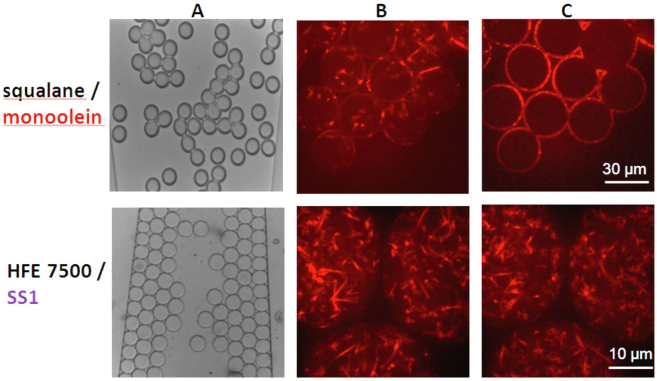

Figure 5. 7 Microtubules droplets produced in microfluidics with monoolein in squalane or SS1 in HFE 7500 as oil/surfactant combination. **A,** droplet production in 25 µm height device and 20 µm production part. **B**, confocal images of microtubules in microdroplets of around 30 µm diameter. **C**, confocal images of the same emulsion after having taken a video (20s, exposure time 0.2 sec).

Because the droplet diameter is a lot higher than microtubule bundles length, one cannot follow their behaviour in time. The shear force created during the droplet production creates mixing in the droplet, resulting in bundle floating around at a high speed making it impossible to follow microtubules in a single plane.[8] Therefore, we decide to produce droplet in a microfluidic device of 10 µm height instead of 25 µm height to force microtubule bundles to stay in one focal plane. Figure 5. 8 show the differences in droplet production and in confocal images of microtubules bundles using devices of two different heights. With both devices, the droplets production size was around 60 µm and a stable microtubule solution was prepared as previously mention (section 5.2.1) at a final concentration of 0.5 g/L. The bright field images were taken after the droplet production was stopped by cutting the inlet tubings to stop the flows. Using a microfluidic device of 10 µm height, the production of droplet was stable and homogeneous and when the flow was stopped, most of the droplets were monodisperse even if some fusion was observed. Comparing the confocal images in the 10 and 25 µm height devices, single microtubule bundles can be observed and follow in time which is not possible in the spherical droplets with microtubule bundles floating around and changing focal plane. Therefore, we decided to study the microtubule dynamics in confined environment by producing squeezed droplets in microfluidic devices of around 10 µm height.

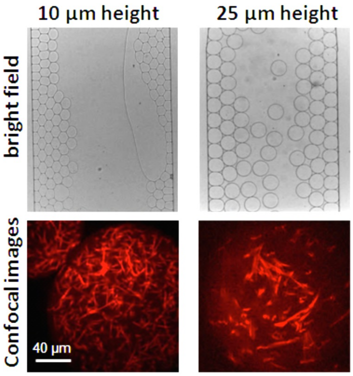

Figure 5. 8 Comparison of microfluidic device height for microtubules droplet observation in HFE 7500/ SS01. Microtubule bundles are stable and static in 10 µm height devices, allowing to follow their dynamics in time which is not possible in spherical droplets where bundles are moving around.

5.2.4 Dynamics of microtubules in crowded environment: bulk versus bulk emulsion

Theoretical predictions demonstrated that assemblies of macromolecules are stabilized in crowded conditions,[26, 27] confirmed experimentally for filament of tubulin. In the presence of various concentrations of 10 kDa dextran or 6 kDa PEG, tubulin formed microtubules in polymerization buffer in the absence of microtubule associated proteins, presumably through a depletion attraction mechanism.[28] No tubulin assembly was observed in the absence of crowder, increasing upon increase of crowder concentration and lowering the critical tubulin concentration at 0.25 mg/ml with 15 % of 10 kDa dextran or 4.5 % 6 kDa PEG. In a more recent study, the effect of 35 kDa PEG on microtubule bundling and pattern formation was studied.[29] Using a static magnetic field and in the absence of PEG, microtubules formed striated birefringence bundle buckling. However, with a sufficiently high PEG concentration (0.5 wt%), no pattern was observed that was attributed to the loss of the dispersed microtubule network. The authors proposed that PEG associated osmotic forces driving microtubules together are the result of enhanced bundling.

In an attempt to investigate the effect of crowding and confinement on microtubules dynamics, we compared their behavior in bulk solution and in bulk emulsion in the presence of crowders. These control experiments were performed to determine the critical crowding and tubulin concentrations for microtubule bundle observation. Taxol–stabilized microtubules can be stable for at least 24 h and up to two weeks at room temperature. Since the goal of our study is to investigate microtubule dynamics, tubulin solution must be prepared without taxol, polymerized at temperature close to 35 °C. Following the protocol for microtubules formation as previously mentioned (section 5.2.1), tubulin and rhodamine tubulin were polymerized in the presence of crowder agents in an Eppendorf tube placed in a water bath at 37 °C (Figure 5. 9). After 30 minutes, the microtubule solution was split in two: one for bulk solution observation and the other one was mixed with SS1/ HEF 7500 for bulk emulsion observation. The crowding agent chosen for this study were ficoll 70 (semi-rigid spherical) and dextran 70 (linear coil).[9, 11] Both are inert, neutral and hydrophilic polysaccharide crowders, which can therefore be described using pure excluded-volume models.[30]

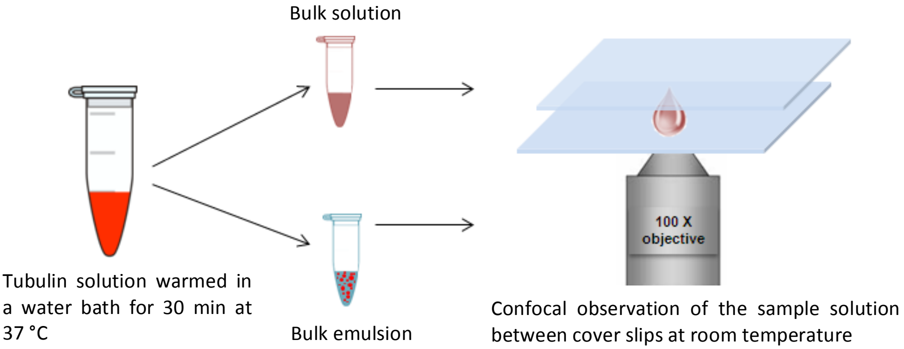
Bulk solution
Tubulin solution warmed in a water bath for 30 min at 37 °C
Bulk emulsion
100 X objective
Confocal observation of the sample solution between cover slips at room temperature

Figure 5. 9 Preparation of microtubule bulk solutions and bulk emulsions in the presence of crowders.

Figure 5. 10 shows representative images of microtubule bulk solutions on a cover slip, in the presence of crowder concentrations ranging from 100 g/L to 300 g/L and an initial tubulin concentration of 1.3 g/L. Bundle dimensions are difficult to analyze since a network of fiber is always formed making it impossible to determine their length or width with accuracy. However, qualitative analysis can be done by comparing width and length in different conditions. With ficoll 70, microtubule bundles are randomly distributed, become thinner with an increase of crowder concentration and showing a higher bundle density at 200 g/L. In comparison with dextran 70, a random network of thick microtubule bundles was observed, which became thinner and shorter with an increase of crowder concentration and interestingly started to align in the same direction. This significant difference in alignment between both crowders can be attributed to their different shape: ficoll is usually modeled as a sphere whereas dextran as rod-like crowding agent.[31] Also, it might indicate that the network of fibers with dextran 70 is perhaps more connected and therefore better able to transmit any external force, leading to some kind of global alignment of the fibrils. At 300 g/L of crowder, only aggregates or very short microtubules were observed meaning that a high crowder concentration can hamper or slow dawn bundle formation.[32]

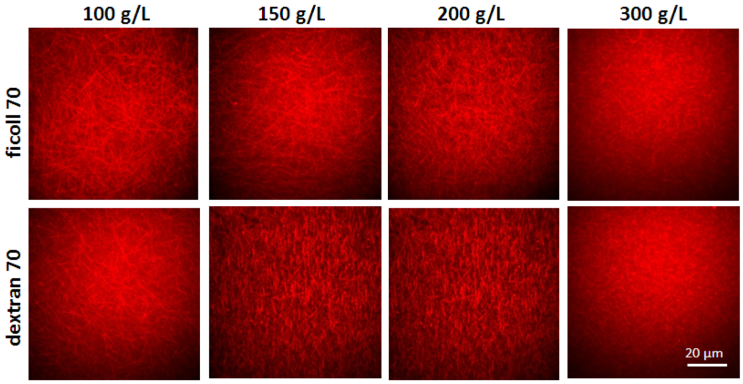

Figure 5. 10 Effect of crowder on microtubules bundles arrangement in bulk solution (1.3 g/L tubulin). Microtubule bundles are thinner and shorter with dextran 70 compared to that of ficoll 70 and started to align at 150-200 g/L. At 300 g/L, no microtubule bundles were observed, only aggregates were present.

The same tubulin solution was used to produce microtubules bulk emulsions, with HFE 7500 and SS1 as the oil and surfactant, respectively (Figure 5. 11). The emulsion was prepared by gently pipetting up and down the microtubule solution and three times its volume in HFE 7500-SS1 in an Eppendorf tube. The floating emulsion was then collected with a pipette and placed between two cover slips. The shear forces involved in the emulsion preparation led to mixing inside the droplet and therefore it was not possible to measure the orientation and anisotropy of microtubule bundles. Comparing bulk emulsion images, microtubule bundle length and thickness show a large difference whether ficoll 70 or dextran 70 was used. Microtubule bundles are thicker and longer with ficoll 70 compared to those with dextran 70. An increase of ficoll 70 led to a higher bundle density with a shorter length. However, an increase of dextran 70 repressed the formation of microtubule bundles with aggregates formed from 200 g/L of crowder.

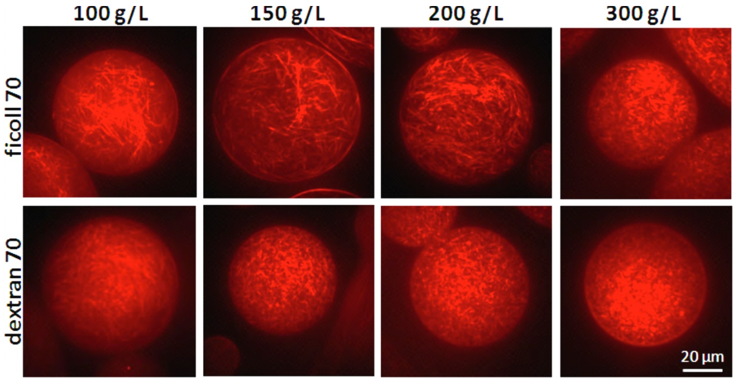
100 g/L
150 g/L
200 g/L
300 g/L
ficoll 70
dextran 70
20 µm

Figure 5. 11 Effect of crowder on microtubules bundles arrangement in bulk emulsion (1.3 g/L tubulin). Bundles arrangement was similar to that of bulk solution and confinement seemed to have no effect.

Figure 5. 12 shows microtubule bulk solutions and emulsions with lower initial tubulin concentration at 0.5 g/L and increasing ficoll 70 concentrations from 100 to 300 g/L. No microtubule bundles were observed with 100 g/L ficoll 70 meaning that the tubulin is below the critical concentration in these specific crowder conditions. At 150 and 200 g/L ficoll 70, microtubules were observed and formed a network of thin and long microtubule bundles in bulk solution, getting thicker in bulk emulsion. Interestingly, almost no microtubule bundles were observed at 300 g/L ficoll 70 as previously observed, probably due to a repression of the bundle formation by high crowder concentrations. Similar results were observed when dextran 70 was used as a crowder (not shown here).

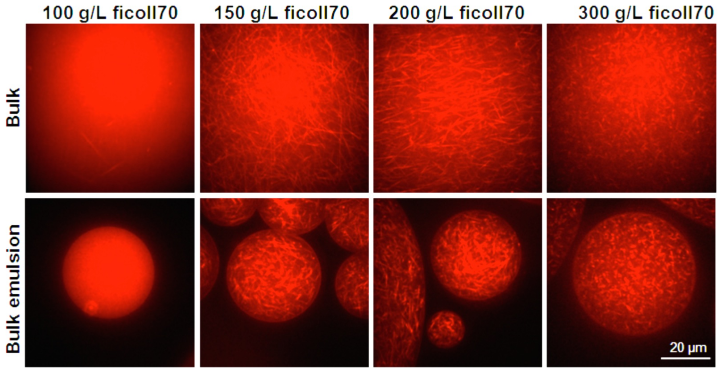
100 g/L ficoll70
150 g/L ficoll70
200 g/L ficoll70
300 g/L ficoll70
Bulk
Bulk emulsion
20 µm

Figure 5. 12 Microtubules in bulk and bulk emulsion (0.5 g/L tubulin) with different ficoll 70 concentrations from 100 to 300 g/L. No microtubule bundles were present at 100 g/L and 300 g/L crowder, only a uniform fluorescent signal or aggregates were observed, respectively. At 150 or 200 g/L, microtubules bundles similar in bulk and bulk emulsion and distributed uniformly.

In order to follow microtubules in time, confined in microdroplets of different shapes in the presence of crowders, the tubulin concentrations should be as low as possible so the bundle density is good enough for quantitative measurements. In conclusion from the control experiment above, the best conditions for microtubule observation in time, confined in microdroplets would be at 0.5 g/L tubulin and between150-200 g/L of crowder.

5.2.5 Microtubules dynamics in temperature controlled microfluidic devices

Microtubules polymerize at 37 °C and quickly depolymerize at 4 °C. Therefore, the study of microtubules dynamics requires temperature control. Tran and co-workers proposed an elegant technique for high-resolution live cell imaging under microfluidic temperature control.[33] Using a bilayer polydimethylsiloxane (PDMS) device, the bottom layer contained cells and the top one the water channels. The water flow was connected to a Peltier system for temperature control, capable of reversible temperature switch from 5 °C to 45 °C. A complete microtubule depolymerization in Cdc25-55 cells was observed at 6 °C, followed by a quick repolymerization at 22 °C.

The experimental setup we used to study microtubule dynamic confined in droplet is described in Figure 5. 13. The bilayer PDMS device was prepared using soft lithography and the details of the fabrication procedure can be found in the Experiment section of this chapter. Briefly, the top layer consisted of deep winding channels (160 μm) with 100 μm width and the bottom layer consisted of a droplet production part ending in a large reservoir of 10 μm height. The PDMS top layer, prepared as a regular device, was carefully aligned and bond on the bottom layer, which was prepared by spin coating PDMS mix on the master, by plasma treatment. The bilayer assembly was then peeled off from the master to be bond on a cover slip after a second plasma treatment. Inlet punched in both PDMS layers allowed to separate inflows and outflows in the different layers.

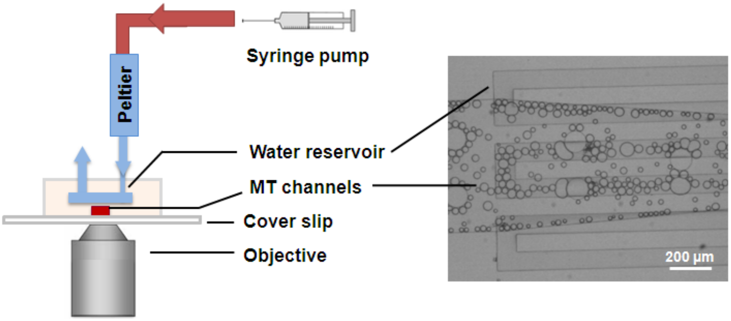

Figure 5. 13 Temperature control system. Left: The PDMS double layer device is constituted of a bottom layer for microtubule observation and a top layer for temperature regulated water using a Peltier system. Right: bright field image of the doubles layer device with microtubules droplets trapped in the bottom layer and the water channel sitting on top, separated by a 25 µm PDMS layer.

Microtubule droplets were produced from a cold solution of 1.5 g/L tubulin concentration, 200 g/L Ficoll and 3 mM GTP in tubulin buffer using HFE 7500/SS1 as the oil/surfactant, while a warm flow of water was running in the top layer set at 35 °C with the Peltier system. The flow of droplets was stopped by cutting the inlet tubing and after microtubule polymerization, the water flow in the top layer was cooled down to 5 °C. Figure 5. 14 shows representative confocal images of microtubule droplets in time during the cooling process. Interestingly, microtubules bundles were present from the beginning while the droplets were produce from a cold tubulin solution. This could be explained by a combination of factors: the droplet production was done at room temperature which might be enough for tubulin polymerization and the high tubulin and crowder concentration could increase the polymerization speed. Images at 5 and 10 min showed a decrease of bundle density with an increase of background intensity. Also, a high fluorescent intensity at the droplets interface implied affinity of tubulin for the oil/surfactant. After 30 min of cooling, microtubule bundles are not visible anymore and only high background intensity is present probably corresponding to tubulin monomers of oligomers.

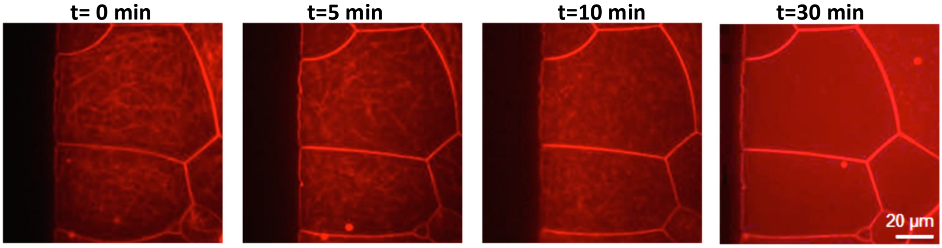

Figure 5. 14 Microtubules depolymerization in bulk emulsion with 1.5 g/L tubulin and 200 g/L Ficoll, using a bilayer device. 10 min after cooling the system to 4 °C, microtubules started to depolymerize and no microtubule bundle was observed after 10 min.

The use of double layer device for microtubule polymerization can be a powerful tool to study polymerization/depolymerization in time depending on different conditions however the droplets are sensitive to temperature and shrinkage which could lead to errors. Droplets can evaporate or swell depending on their location in the device compared the water device channels above. Evaporation in time is illustrated in Figure 5. 15, where droplets produced in a single layered device were imaged in time while the device was heated on a hot plate set at 40 °C. Droplets contained 0.5 g/L tubulin, 200 g/L dextran in the presence of GTP regenerating system. Monodisperse droplet after 5 min show a uniform distribution of the tubulin protein that moves to the interface as the droplet is shrinking in time. After 45 min, no microtubule bundles were observed and droplet seemed to stick to the channel walls.

To conclude from these experiments, the optimum experimental set up to study the arrangement and organization of microtubules in droplets was first to generate polymerization in bulk then to produce monodisperse droplet containing microtubules in microfluidic device. In that way, tubulin will not go to the droplet interface, as mainly microtubules will be present after bulk polymerization

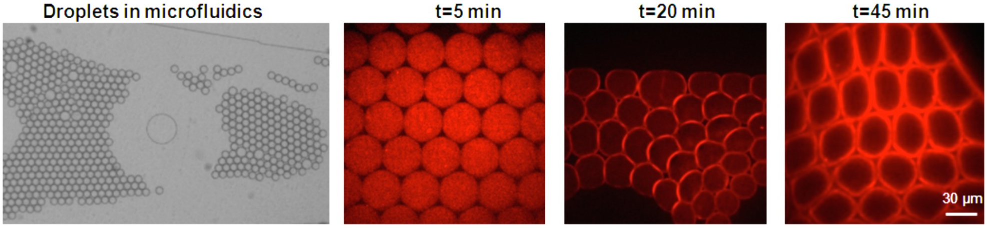

Figure 5. 15 Droplet evaporation in time. Monodisperse droplets containing 0.5 g/L tubulin and 200 g/L dextran were trapped in microfluidic a device and left on a hot plate at 40 °C. At first, droplets had a uniform distribution of the protein but while the solvent is evaporating, the protein is going to the interface and no microtubule bundle was observed.

5.2.6 Microtubules dynamics in droplet microfluidics

Taxol stabilized microtubules are stable for at least 24 h at room temperature but quickly depolymerize at 0°C. Without taxol, microtubules show dynamic behaviour characterized by stochastic growing and shrinking at microtubules ends. Tubulin is a GTP-ase protein and as soon as GTP is depleted, microtubules will depolymerize. In the conditions described in the previous section, microtubules are stable for around 40 min before starting to disassemble. In order to mimic the condition present in the cell with a stable GTP concentration, we decided to use a GTP regenerating system (RS) with phosphoenolpyruvate (PEP) and pyruvate kinase (PK). The enzyme PK catalyses the transfer of a phosphate group from PEP to GDP, yielding one molecule of pyruvate and one molecule of GTP. Figure 5. 16 show representative fluorescent images of microtubule bulk emulsions containing 0.5 g/L tubulin, 150 g/L ficoll 70, with and without RS. In the absence of RS, microtubules started to depolymerize after 25 min as shown by the high background intensity in the droplets. With RS, it took more than 60 min before microtubules began to depolymerize and this system was therefore used to produce and image droplets in microfluidics in time.

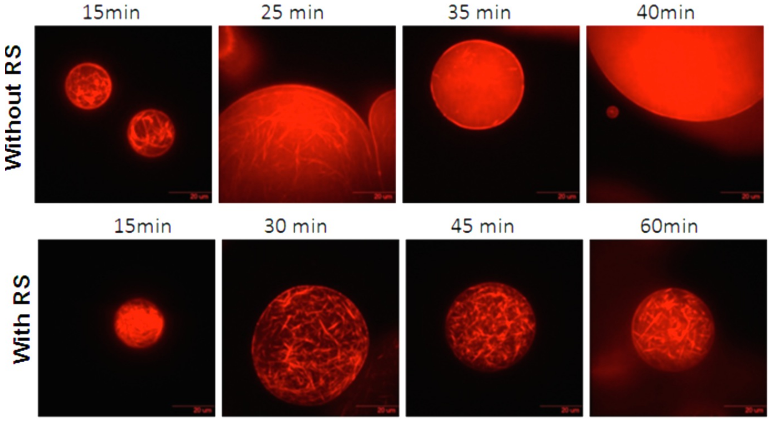

Figure 5. 16 Comparison of microtubules stability on bulk emulsion, with and without regenerating system (RS). With RS, microtubule bundles are stable for more than 60 min while were quickly depolymerizing after 25 min without RS.

The microfluidic device was prepared as previously described in the Experimental section of Chapter 3. The flow-focussing device is composed of two inlets, a droplet production part and a reservoir containing long and narrow channels. The height of the devices was 10 µm, allowing microtubule observations and the width of the channels was around 15 µm. The tubulin flow is separated from the oil/surfactant flow constituted of HFE 7500/SS1 before meeting at the droplet production part where microtubules droplets in oil were formed. Once droplet production was stable and monodisperse, the flow was stopped by cutting the inlet tubings forcing the droplets to stop and be trapped in different parts of the reservoir. Hence, droplets trapped in the reservoir will have a quasi 2D shape and droplets trapped in the narrow channels will have an elongated shape also called plug shaped as showed in Figure 5. 17. Compared to bulk emulsion, droplets in microfluidics were monodisperse and had a well-defined size. The narrow channel height of 10 µm allowed obtaining squeezed droplets containing microtubule bundles fixed in a quasi 2D plane, allowed to follow microtubules in time.

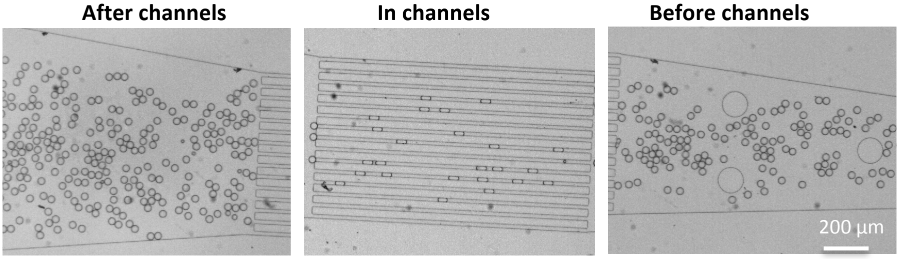

Figure 5. 17 Droplet production device showing droplets trapped in different part of the device yielding to 2D or plug shape droplets.

The quantification of the imaged droplets in different condition was done using the software 'Microfilament analyser' or MFA.[34] This image analysis tool allows quantification of fibril orientation and a description of the software as well as the data analysis is described in the Experimental section of this chapter. Briefly, a section image (mid-plane) and a z-stack of a droplet are saved in a same file then uploaded in the MFA software. After alignment of the mid-plane image with the z-stack project appearing semi-transparent on top, the droplet was selected by manually drawing the outline contour. When the image contrast and the filament detection settings were adjusted (minimal filament length, filament diameter, threshold value and step size of the optical polarizer), the detected filaments appeared in yellow on the images.

The parameters were adjusted such that the detected filaments would coincide with the existing filament in the droplet. The MFA detection is based on an approach called 'virtual rotating polarizer' with a virtual line grid placed in a horizontal start position over the image as showed in Figure 5. 18 A. The filaments that lie on top of the grid line thus having the same orientation are detected and then the grid is slightly rotated in an angle step of 3°. As the detected filaments have a direction but no sense, analysis from 0° to 180 ° give the same results as 180° to 360° range. For every line, the connectivity of every pixel is successively studied on an orthogonal cross-section though the line. A pixel is part of a filament if its intensity value is above the set threshold, minimal length and diameter values. Once the number of filaments and their orientation are known, a circular graph displays the output grouped into transversal, longitudinal and oblique orientations according to the angle limits described in Figure 5. 18 B.[35] When more than three orientations are detected it is defined as random while two detected orientations correspond to a combined orientation.

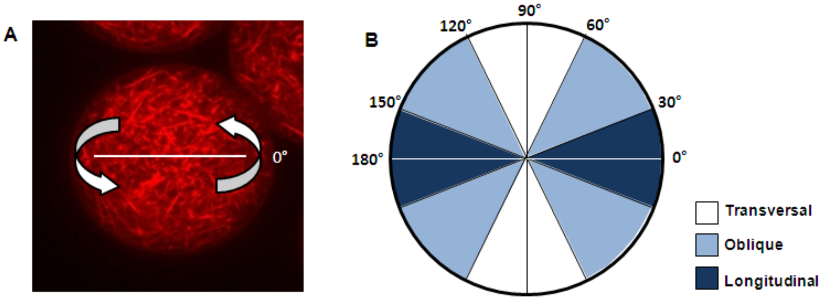

Figure 5. 18 A. Confocal image of microtubule bundles in a droplet with the white arrow showing the rotational plane of the virtual polarizer. B. Schematic representing the limits of the different orientations related to the positioning of the virtual polarizer on the image (MFA detection module).[34, 35]

As a starting tubulin concentration, we used 0.5 g/L in the presence of 200 g/L of crowder in tubulin buffer. Images of droplets at three different locations were taken: before channels, in channels and after channels. We were interested to investigate the influence of crowding and container shape on microtubules arrangement, in disk or plug shaped droplets. The droplets after channels were imaged in order to study the influence of shear force and mixing on microtubules arrangement, after passing through the narrow channels. Figure 5. 19 shows the output data of the MFA when 200 g/L of Ficoll 70 was used as a crowder. Before the channels, only two main orientations were observed (two green asterisks), a transversal and longitudinal which can be attributed to a combined orientation. Interestingly, when droplets are trapped in narrow channels, the main orientation was still combined but with an increase of oblique and transversal detected filaments. The same was observed with droplets after the channel and can be attributed to the shear forces while passing through the channel at a high speed creating a rapid internal mixing. The microtubule bundles seem to cluster and did not disassemble into homogeneous bundle even after 30 min. Future experiments could optimize crowder concentration or other methods to alter microtubule stability in order to observe more dynamic processes.

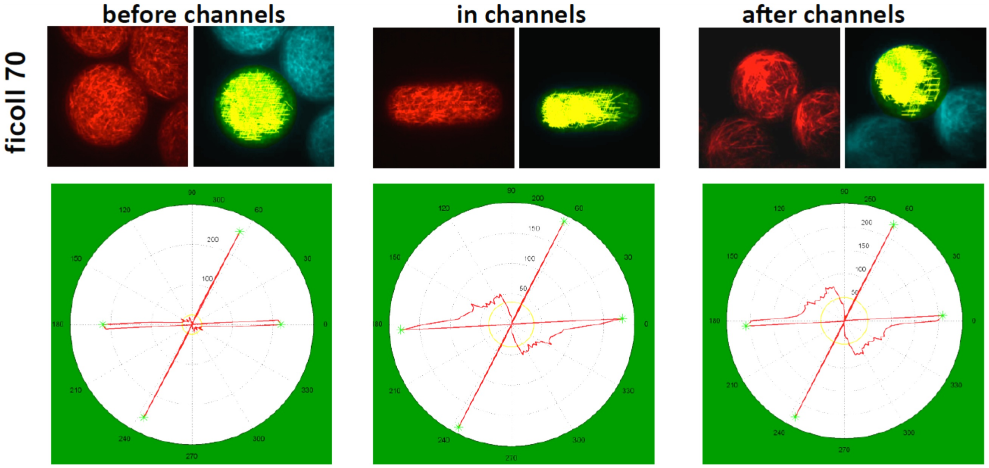

Figure 5. 19 Microtubule visualization and detection using MFA. Analyzed droplets contained 0.5 g/L tubulin and 200 g/L ficoll 70, and detected microtubules are represented in yellow. Below, circular plot represent the output data, with the main orientation of microtubules.

The same experiment was performed with 0.5 g/L of tubulin but using dextran 70 as a crowder at a concentration of 200 g/L. In that case, two main orientations were also identified as transversal and longitudinal (green asterisks) constituting a combined orientation. Surprisingly, the microtubule bundles orientation seemed different after channels whether ficoll 70 or dextran 70 was used as a crowder. Previously, it was shown that with droplet containing ficoll 70, microtubule bundles aggregates or clustered together probably due to the shear forces and mixing passing through the narrow channels. However, no clustering was observed with dextran 70, and microtubules bundle arrangement was similar before and after channels. Pfohl and co-workers showed similar behavior with deformation of fibrin networks in moving droplets passing through narrow channels that relaxed back to the initial arrangement after passing the channels.[36].

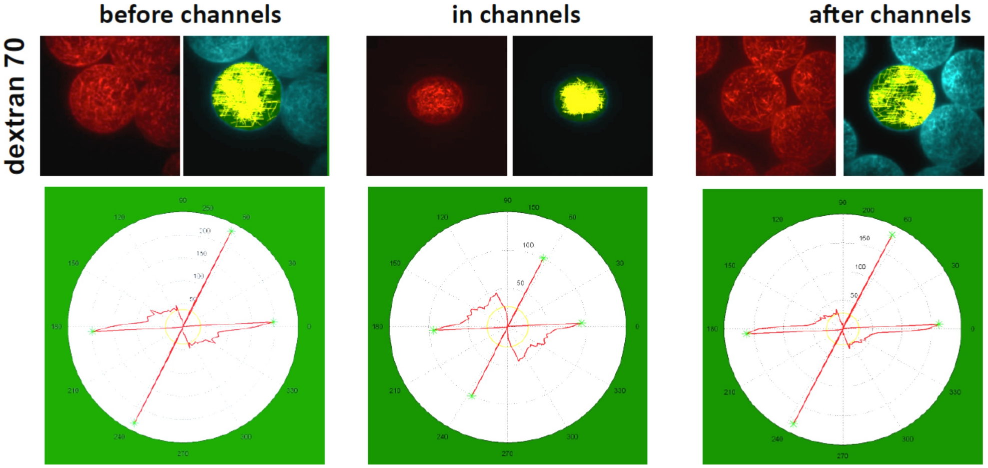

Figure 5. 20 Microtubule visualization and detection using MFA. Analyzed droplets contained 0.5 g/L tubulin and 200 g/L dextran 70, and detected microtubules are represented in yellow. Below, circular plot represent the output data, with the main orientation of microtubules.

5.3 Conclusions

We have described an approach for the investigation of microtubules behaviour and arrangement in crowded and confined environment. Monodisperse droplets were generated in a flow-focusing device of 10 µm height, suitable for microscopy observation. Despite the high shear forces involved during the droplet production, microtubules retained their capability to assemble. The critical parameter for microtubule bundle formation and observation with fluorescence microscopy were the GTP, crowder and tubulin concentration. For an initial tubulin concentration of 0.5 g/L, GTP and crowder concentration should be at least 1 mM and 150 g/L, respectively. The roles of physical constraints on microtubules were investigated by a control of the droplet size and geometry. Using ficoll 70 or dextran 70 as a crowder, microdroplets containing microtubules passing through a narrow channel showed different behaviour. Microtubules bundles were more connected and robust and led to aggregation into droplets while passing the channel when ficoll 70 was used, which was not observed with dextran 70. Further experiments changing the droplet volume or crowder nature need to be investigated. This approach should in principle allow for a detailed study of microtubule bundles behaviour and conformation under confinement and crowding, possible with precise droplet production in microfluidics. In our system, the bundles are not very dynamic and hence we did not observed strong dependencies on flow rates, droplet sizes and droplet shapes. In the future, the stability of the microtubule bundles could be tuned in order to access a richer set of behaviours. We believe that this assay can be useful for quantitative studies of biological systems in confined environment.

5.4 Experimental section

Materials

Tubulin and rhodamine tubulin were purchased from Cytoskeleton Inc. in a kit containing general tubulin buffer, cushion buffer, taxol and DMSO. Proteins were used as received without any extra purification. Guanine nucleotides, Ficoll 70, Dextran 70 and other analytical grade chemicals were from Sigma. In all experiments, final GTP concentration was 2 mM. Droplets were produced using different oil/surfactant combinations. Mineral oil, span 80, monoolein and squalane were purchased from Sigma, the fluorinated oil (HFE 7500) was purchased from 3M and cithrol was generously offered by Croda. The custom-made tri-block surfactant[25,37] was prepared as previously described.[38]

Preparation of stabilized microtubules

The protocol utilized for the preparation of fluorescent microtubules was based on the supplier procedure (Cytoskeleton). Because tubulin protein is highly labile, the whole preparation was done on ice to prevent tubulin polymerization. First, 20 µg of lyophilized Rhodamine labelled tubulin were resuspended in a solution mixture containing general tubulin buffer (80 mM PIPES pH 6.9, 2 mM $MgCl_2$ and 0.5 mM EGTA), 1mM GTP and cushion buffer (general tubulin buffer with 60 % glycerol). The final concentration of glycerol was around 5 % and is believed to improve tubulin polymerization.[39, 40] The second step consisted in preparing a solution of unlabelled tubulin in the same way as previously, dissolving the lyophilised tubulin in general tubulin buffer and cushion buffer. In the final step, a certain volume of rhodamine tubulin solution is mixed with unlabeled tubulin solution (with a labelling ratio usually around 15 %) and warmed in a water bath for around 20 min at 37 °C. Since tubulin is not stable to many rounds of freeze/thawing, the rest of the tubulin solution was divided into aliquots of 5 µL and stored at – 80 °C. After 20 min, most of the tubulin was polymerized into microtubules, which can be stabilised by the addition of a taxol solution (20 µM). After 20 min, most of the tubulin was polymerized into microtubules, which can be stabilised by the addition of a taxol solution and GTP to a final concentration of 20 µM and 1 mM, respectively. In these conditions, microtubules are stable at room temperature for more than a week but will immediately depolymerize when the temperature of storage is decreased to 4 °C.

Microfluidic chip design and fabrication

The devices used in this study were constructed by conventional soft lithographic techniques as described in chapter 3 - Experimental section. To improve wetting by the continuous phase, devices were coated with a hydrophobic layer by flushing with Aquapel (Pittsburgh Glass Works, LLC) in the channels and allowing it to dry overnight at 65 °C.

Double layer device fabrication

The PDMS device is composed of two layers: the bottom one contains channels for microtubule observation in microdroplets and the top one contains winding channels to flow temperature controlled water.

The bottom layer will be called ‘thin slab’ and was prepared by mixing PDMS and curing agent at 21:1 ratio, stirred for about 3 min and degased under vacuum to remove the air bubbles. Once the mixture was transparent, it was poured on top of the silica wafer (master) containing channels to cover around 30 % of the surface followed by spin coating. The program used for spin coating was 10 sec at 1000 rpm followed by 60 sec at 1250 rpm allowed getting an even layer of around 25 µm. The master was then placed on a hot plate at 90 °C until the thin layer of PDMS was cured which took around 15 min.

The top layer will be called ‘thick slab’ and was prepared using PDMS:curing agent mixture with a ratio of 5:1, mixed and degased as previously. The more curing agent, the stiffer the cured PMDS will be and since high water flow rates will occur in the thick slab channels, it needed to be stiffer than the thin slab. Once the mixture was bubble free, it was poured on top of the master placed in a petri dish and cured at 65 °C for at least 3h. Afterwards, the thick slab was cut, peeled off from the petri dish and holes were pushed for the inflow and outflow of water using a 1.5 mm puncher.

Subsequently, the thick layer was carefully aligned and bond on the thin layer using plasma treatment (65 % power for 9 sec). The bilayer assembly was then placed in the oven at 90 °C for around 2h. The PDMS bilayer assembly was peeled off the master, inlet and outlet holes were punched for the thin layer (1 mm puncher) and bond on a cover slip after plasma treatment at 65 % power for 9 sec.

Fluorescence microscopy

Samples were observed with a spinning disk confocal microscope (CSU-X1, Yokogawa Electric Corp.) on an Olympus inverted microscope (IX81). Rhodamine was excited with 561 nm laser light (λ_{em}= 547 nm) and images were recorded with a temperature controlled EM-CCD camera (iXon3, Andor) using an exposure time of 0.8-1 s and a piezo-driven 100x (1.3 NA) oil immersion objective. Observations were conducted at temperatures between 4°C and 37°C using a temperature control system.

Quantification

-Microfilament analyser

The manual and the MicroFilament Analyser program were downloaded from http://www.ua.ac.be/bimep/MFA, freely available for research and education purposes. The MFA program is written in Matlab code but runs a user-friendly interface which comprises the different steps of data analysis. For every droplet, a mid-plane image and a z-stack project were saved as tiff in a same file, with an extension for the z-stack. As an example, the mid-plane image was saved as droplet1 and the z-stack as droplet1zsk. It is important to mention that the z-stack correspond to a maximum projection of a set of successive optical sections through the droplet. First, the mid-plane images was loaded in the software and aligned with the z-stack image, which appears semi-transparent on top. Then, the droplet was selected by drawing manually a region of interest to outline the droplet contour. An automatic selection is also possible but did not give accurate results in droplet selection. Afterwards, the contrast was adjusted to 1.3 in order to reduce the background intensity. The final step consists in the filament detections adjusting four parameters: the minimal length was set to 30 pixels, the filament diameter to 4 pixels (nothing was detected below); the threshold value was set between 20 and 25 (depending on the detection accuracy) and the step size of the optical polarizer to 3° (smallest meaningful and detectable increment). The detected microtubule bundles appeared in yellow and a circular plot gave their main orientation. Also, the data can be exported on an excel file, like the number of filament detected and the detected main angles.

5.5 References

1. E. Nogales, *Annu Rev Bioph Biom*, **2001**, *30*, 397-420.
2. E. Nogales, S. G. Wolf and K. H. Downing, *Nature*, **1998**, *391*, 199-203.
3. L. A. Amos, *Org Biomol Chem*, **2004**, *2*, 2153-2160.
4. M. A. Jordan and L. Wilson, *Nat Rev Cancer*, **2004**, *4*, 253-265.
5. G. Brouhard and D. Sept, *Curr Biol*, **2012**, *22*, R802-R803.
6. A. Desai and T. J. Mitchison, *Annu Rev Cell Dev Bi*, **1997**, *13*, 83-117.
7. O. Valiron, N. Caudron and D. Job, *Cell Mol Life Sci*, **2001**, *58*, 2069-2084.
8. T. Mitchison and M. Kirschner, *Nature*, **1984**, *312*, 237-242.
9. V. I. Rodionov and G. G. Borisy, *Science*, **1997**, *275*, 215-218.
10. A. W. Hunter and L. Wordeman, *J Cell Sci*, **2000**, *113*, 4379-4389.
11. M. Dogterom and T. Surrey, *Curr Opin Cell Biol*, **2013**, *25*, 23-29.
12. F. J. Nedelec, T. Surrey, A. C. Maggs and S. Leibler, *Nature*, **1997**, *389*, 305-308.
13. T. E. Holy, M. Dogterom, B. Yurke and S. Leibler, *P Natl Acad Sci USA*, **1997**, *94*, 6228-6231.
14. L. Laan, N. Pavin, J. Husson, G. Romet-Lemonne, M. van Duijn, M. P. Lopez, R. D. Vale, F. Julicher, S. L. Reck-Peterson and M. Dogterom, *Cell*, **2012**, *148*, 502-514.
15. B. Diagouraga, A. Grichine, A. Fertin, J. Wang, S. Khochbin and K. Sadoul, *J Cell Biol*, **2014**, *204*, 177-185.
16. A. Diz-Munoz, D. A. Fletcher and O. D. Weiner, *Trends Cell Biol*, **2013**, *23*, 47-53.
17. D. K. Fygenson, J. F. Marko and A. Libchaber, *Phys Rev Lett*, **1997**, *79*, 4497-4500.
18. T. Kaneko, T. J. Itoh and H. Hotani, *J Mol Biol*, **1998**, *284*, 1671-1681.
19. V. Emsellem, O. Cardoso and P. Tabeling, *Phys Rev E*, **1998**, *58*, 4807-4810.
20. M. Pinot, F. Chesnel, J. Z. Kubiak, I. Arnal, F. J. Nedelec and Z. Gueroui, *Curr Biol*, **2009**, *19*, 954-960.
21. J. Hazel, K. Krutkramelis, P. Mooney, M. Tomschik, K. Gerow, J. Oakey and J. C. Gatlin, *Science*, **2013**, *342*, 853-856.
22. M. C. Good, M. D. Vahey, A. Skandarajah, D. A. Fletcher and R. Heald, *Science*, **2013**, *342*, 856-860.
23. M. Kaltenbach, S. R. A. Devenish and F. Hollfelder, *Lab Chip*, **2012**, *12*, 4185-4192.
24. C. V. Kulkarni, W. Wachter, G. Iglesias-Salto, S. Engelskirchen and S. Ahualli, *Phys Chem Chem Phys*, **2011**, *13*, 3004-3021.
25. A. M. Jimenez, M. Roche, M. Pinot, P. Panizza, L. Courbin and Z. Gueroui, *Lab Chip*, **2011**, *11*, 429-434.
26. H. X. Zhou, G. N. Rivas and A. P. Minton, *Annu Rev Biophys*, **2008**, *37*, 375-397.
27. S. B. Zimmerman, *Biochimica et biophysica acta*, **1993**, *1216*, 175-185.
28. W. Herzog and K. Weber, *European journal of biochemistry / FEBS*, **1978**, *91*, 249-254.

29. Y. Guo, Y. Liu, R. Oldenbourg, J. X. Tang and J. M. Valles, Jr., *Physical review. E, Statistical, nonlinear, and soft matter physics*, **2008**, *78*, 041910.
30. A. P. Minton, *Journal of Biological Chemistry*, **2001**, *276*, 10577-10580.
31. D. Homouz, L. Stagg, P. Wittung-Stafshede and M. S. Cheung, *Biophysical Journal*, **2009**, *96*, 671-680.
32. L. A. Munishkina, A. Ahmad, A. L. Fink and V. N. Uversky, *Biochemistry-Us*, **2008**, *47*, 8993-9006.
33. G. V. Casquillas, C. H. Fu, M. Le Berre, J. Cramer, S. Meance, A. Plecis, D. Baigl, J. J. Greffet, Y. Chen, M. Piel and P. T. Tran, *Lab Chip*, **2011**, *11*, 484-489.
34. E. Jacques, J. Buytaert, D. M. Wells, M. Lewandowski, M. J. Bennett, J. Dirckx, J. P. Verbelen and K. Vissenberg, *Plant J*, **2013**, *74*, 1045-1058.
35. E. Jacques, M. Lewandowski, J. Buytaert, Y. Fierens, J. P. Verbelen and K. Vissenberg, *Plant Signal Behav*, **2013**, *8*, e24821.
36. H. M. Evans, E. Surenjav, C. Priest, S. Herminghaus, R. Seemann and T. Pfohl, *Lab Chip*, **2009**, *9*, 1933-1941.
37. J. C. Baret, *Lab Chip*, **2012**, *12*, 422-433.
38. V. Chokkalingam, J. Tel, F. Wimmers, X. Liu, S. Semenov, J. Thiele, C. G. Figdor and W. T. S. Huck, *Lab Chip*, **2013**, *13*, 4740-4744.
39. R. A. B. Keates, *Can J Biochem Cell B*, **1981**, *59*, 353-360.
40. M. J. Schilstra, P. M. Bayley and S. R. Martin, *Biochem J*, **1991**, *277*, 839-847.

Chapter 6

Conclusions and future perspectives

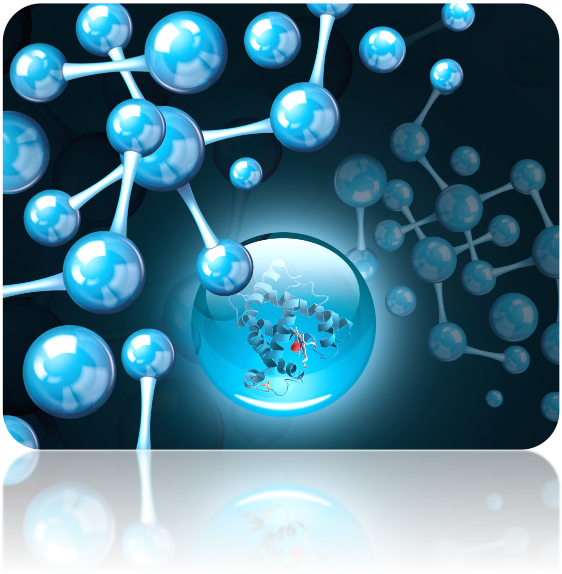

6.1 Conclusions and outlook

For decades, water has for the most part been ruled out as a solvent for synthetic organic chemistry. A key reason is of course the insolubility of the reactants and the incompatibility of the intermediates with water. However, numerous synthetic organic reactions have been found to be accelerated and sometimes more (stereo)selective (relative to organic solvents) in environments described as ‘on water’ reactions.[1] Research aiming to clarify water’s behaviour in aqueous reactivity could lead to new applications of water as a viable alternative solvent for organic chemistry. Water is cheap and a non-toxic solvent, frequently promoted as an ideal solvent in green chemistry which led to an industry perspective. Water is used for homogeneous catalysed processes such as hydrogenation and hydroformylations. Moreover, a selected number of ‘on water’ reactions can have potential implications in prebiotic synthetic chemistry[2,3] and in synthetic biology approaches for the design of minimal biomimetic systems having specific synthetic functions such as oscillator systems.[4] Using droplet microfluidics, we have studied the hypotheses that have been proposed to explain the ‘on water’ effect on some chemical reactions.[5-7] Unfortunately, a lot of the work on synthetic chemistry ‘on water’ did not include a rigorous analysis of the kinetics of the reactions. When we screened many of the reactions reported to be enhanced in the literature, we could not attribute any enhancement to interfacial effects. For two reactions, we were able to determine ‘on water’ reaction rates and confirm the rate enhancements predicted. To develop ‘on water’ conditions as a synthetic tool, more work will have to be done in order to predict which reactions will be catalysed under these conditions.

The bacterial division system of *E. coli* comprises around 15 essential proteins, most of them membrane proteins. In the early stages of division, the first multiprotein complex formed is the proto-ring composed by FtsZ, FtsA and sZipA. Efforts toward understanding the mechanisms involved in the division process are undergoing. A very interesting concept is the ‘bottom-up’ approach,[8] which consists in the construction of biological parts, devices and systems with increasing levels of complexity towards a minimal cell-like scaffold. Liposomes have proven to be suitable platform for the study of the divisome but few reports presented complex systems with more than two encapsulated proteins.[9] The next step would be to incorporate a mimic of the nucleoid occlusion in order to force FtsZ to adopt a ring-shaped structure. This can be achieved by decorating gel beads with SlmA, a nucleoid-associated inhibitory protein. Furthermore, a potentially very different way of organizing the bacterial divisome assemblies inside liposomes could be achieved by a lipid phase separation of the DOGS-NTA at the interface. It was shown that mixture of lipids composed of phosphatidyl cholin lipids, cholesterol and sphingolipids could lead to phase separation.[10-12] This approach would lead to symmetry breaking of the chemical composition inside the container, and thus localized assembly of the FtsZ fibers to anchor ZipA proteins.

Microtubules organize *in vivo* into different patterns with the help of associated molecules to form asters, antiparallel overlaps or bundles. The basic mechanisms by which these patterns arise are not fully known and effort toward the understanding of this phenomenon can be achieved by the use of a bottom-up approach.[13] In vitro experiments of increasing complexity were mainly performed in microfabricated chamber and do not take into account the flexibility of the confining geometry. Droplet and liposomes seem to be a better approach to investigate the effect of the confining space. Additions of microtubule associated proteins in such containing space could lead to similar patterns found in living cells. The volume of the container had proved to be a critical parameter of the spindle size while encapsulating Xenopus egg extracts.[14, 15] More effort should be done toward the change of size and volume of the ‘cell-like’ container.

6.2 References

1. A. Chanda and V. V. Fokin, *Chemical Reviews*, **2009**, *109*, 725-748.
2. I. A. Chen and M. A. Nowak, *Acc Chem Res*, **2012**, *45*, 2088-2096.
3. A. Fallah-Araghi, K. Meguellati, J. C. Baret, A. El Harrak, T. Mangeat, M. Karplus, S. Ladame, C. M. Marques and A. D. Griffiths, *Phys Rev Lett*, **2014**, *112*, 028301.
4. I. R. Epstein, V. K. Vanag, A. C. Balazs, O. Kuksenok, P. Dayal and A. Bhattacharya, *Acc Chem Res*, **2012**, *45*, 2160-2168.
5. R. Breslow, *Accounts of Chemical Research*, **1991**, *24*, 159-164.
6. A. Lubineau, J. Auge and Y. Queneau, *Synthesis-Stuttgart*, **1994**, 741-760.
7. Y. Jung and R. A. Marcus, *Journal of the American Chemical Society*, **2007**, *129*, 5492-5502.
8. A. Martos, M. Jimenez, G. Rivas and P. Schwille, *Trends Cell Biol*, **2012**, *22*, 634-643.
9. M. Jimenez, A. Martos, E. J. Cabre, A. Raso and G. Rivas, *Environ Microbiol*, **2013**, *15*, 3158-3168.

10. H. J. Kaiser, D. Lingwood, I. Levental, J. L. Sampaio, L. Kalvodova, L. Rajendran and K. Simons, *Proc Natl Acad Sci U S A*, **2009**, *106*, 16645-16650.
11. K. Bacia, P. Schwille and T. Kurzchalia, *Proc Natl Acad Sci U S A*, **2005**, *102*, 3272-3277.
12. K. Oglecka, J. Sanborn, A. N. Parikh and R. S. Kraut, *Front Physiol*, **2012**, *3*, 120.
13. M. Dogterom and T. Surrey, *Curr Opin Cell Biol*, **2013**, *25*, 23-29.
14. J. Hazel, K. Krutkramelis, P. Mooney, M. Tomschik, K. Gerow, J. Oakey and J. C. Gatlin, *Science*, **2013**, *342*, 853-856.
15. M. C. Good, M. D. Vahey, A. Skandarajah, D. A. Fletcher and R. Heald, *Science*, **2013**, *342*, 856-860.

Summary

Interfaces and confinement are important parameters to take into account when investigating the influence of the intracellular environment on chemical or biochemical reactions. The chemical reactivity at liquid interfaces is very important in a wider context in chemistry, whether processes are happening at liquid/solid, liquid/gas or liquid/liquid interfaces. Interfaces can dramatically increase or decrease chemical reaction rates. In biological systems, the cell membrane is a complex biochemical interface, critical to its health and functioning. The cell membrane contains proteins which allow the cell to transport small molecules in and out, or act as catalysts/enzymes for some specific reactions. In addition to the importance of interfaces, confinement and crowding are thought to have profound implications for cell function.

Chapter 1 provides an overview of the importance of interfaces, confinement and compartmentalization with respect to specific chemical and biological systems. In this thesis, we used microdroplets in microfluidics as a tool for mimicking the cell, and we studied the effect of crowding and the shape of the container on the behaviour of cytoskeleton proteins (FtsZ and tubulin). In parallel, we studied enhanced chemical reaction rates at water interfaces, of particular relevance for prebiotic chemistry.

The research described in **Chapter 2** was aimed at the development of a new method in order to shed light on the cause of the increase in reaction rate for the 'on water' reactions and quantify its effect for the first time. Droplet microfluidics allowed a precise control over the interfacial area between the water and the oil phase, which is not possible in bulk emulsions. Using two model reactions, we conducted a series of experiments and our data corresponded well with the model proposed by Jung and Marcus in which hydrogen bonds stabilize the transition state of the reaction thereby accelerating it. The drawback of our method is that even if reactions were accelerated initially, the effect became less pronounced with longer reaction times. This might be due to saturation of the interface by the product formed that is not the case in bulk emulsions where droplets are continuously formed, exposing 'fresh' interfaces.

FtsZ and the divisome system constitute the essential proteins involved in the cell division in *E. coli*. In **Chapter 3**, we investigated the effect of crowding and confinement on the polymerization of FtsZ into filament bundles. FtsZ polymerization in crowded droplets coated with *E. coli* lipids led to a dense fibrous network, the geometry of which depended on droplet shape, concentration of FtsZ monomers, crowding agent, and flow conditions in the microfluidic channels. At the lowest ficoll 70 concentrations, bundle formation was delayed in droplet microfluidics and once formed, the network did not change as a whole even though FtsZ monomer exchange with the bundles was observed. Furthermore, a depletion zone appeared near the oil-water interface, where very few bundles were seen and a number of hypotheses were described to explain this phenomenon. This microfluidic platform constitutes a very powerful tool and was further explored in **Chapter 4**, in which the properties of FtsZ were investigated in the presence of companion cell division elements FtsA and sZipA to complete our understanding of the precise functional role of FtsZ in cell division. However, although the proteins retained their ability to interact with each other upon encapsulation, microdroplets were not an adequate platform for the study of possible effect in the lipid membrane. We therefore decided to use liposomes instead, developing a new method for the formation of monodisperse liposomes. The on-chip method was unsuccessful, whereas droplet formation in microfluidics followed by droplets transfer seemed promising, using *E. coli* lipids in the inner face and POPC lipids in the outer face of the liposomes.

Chapter 5 describes an approach for the investigations of microtubule organization/assembly inside microdroplets, under conditions of crowding and confinement. We first conducted bulk emulsion experiment in order to find the best surfactant/oil combination and the critical concentrations for microtubule bundle formation. Then, droplets were produced in a 10 µm height device with a custom-made surfactant which allowed the successful visualisation and encapsulation of microtubules retaining their ability to assemble, despite the high shear forces involved during the droplet production. The roles of physical constraints on microtubules were investigated by a control of the droplet size and geometry comparing different crowders. The alignment of microtubule bundles inside the droplets did not vary between rod shaped and disc shaped droplets. Ficoll 70 led to more robust and connected microtubules compared to dextran 70 that gave a more uniform microtubule distribution, which was explained by the different nature of crowder.

Samenvatting

Grensvlakken en “confinement” (het fysiek beperken van de bewegingsvrijheid van een molecuul) zijn belangrijke parameters waarmee rekening gehouden dient te worden als men de invloed van de intracellulaire omgeving op (bio)chemische reacties onderzoekt. De reactiviteit van chemische verbindingen aan vloeistofgrensvlakken is ook van belang in een bredere context, aangezien processen kunnen plaatsvinden aan een vloeistof-vastestof-, vloeistof-gas-, of vloeistof-vloeistofgrensvlak. Het is bekend dat grensvlakken een zeer groot effect kunnen hebben op reactieconstanten. In biologische systemen vormt de celmembraan een complex biochemisch grensvlak dat essentieel is voor het gezond functioneren van de cel. De celmembraan bevat speciale eiwitten die ervoor zorgen dat de cel kleine moleculen kan uitwisselen met zijn omgeving, of die functioneren als signaalreceptoren of als katalysator voor chemische reacties. Naast de rol van grensvlakken zijn confinement en “crowding” (een beperking van het beschikbare volume dankzij een hoge concentratie van macromoleculen) vermoedelijk van grote invloed op cellulaire functies.

Hoofdstuk 1 geeft een overzicht van het belang van grensvlakken, confinement en compartementalisatie voor specifieke chemische en biologische systemen. In dit proefschrift zijn microdruppels in microfluïdica toegepast om de cellulaire omgeving na te bootsen, waardoor onderzocht kon worden wat de invloed is van crowding en de vorm van de microdruppel op het gedrag van eiwitten uit het cytoskelet (FtsZ en tubuline). Parallel hieraan werd de verhoging van reactiesnelheden aan watergrensvlakken bestudeerd, wat in het bijzonder van belang is voor prebiotische chemie.

Het onderzoek beschreven in **Hoofdstuk 2** was gericht op het ontwikkelen van een nieuwe methode om de oorzaak van verhoogde reactiesnelheden in zogenaamde “on-water”-reacties te achterhalen en om dit effect voor het eerst te kwantificeren. Met behulp van druppelmicrofluïdica kon de oppervlakte van het grensvlak tussen de olie- en waterlaag precies worden gecontroleerd, iets wat niet mogelijk is met emulsies in bulk. Twee modelreacties werden onderzocht en de verkregen data voldeden goed aan het model van Jung en Marcus, waarin stabilisatie van de overgangstoestand door waterstofbruggen de reactie versnelt. Echter, het nadeel van onze methode is dat het “on-water”-effect kleiner werd naarmate de reactietijd toenam, zelfs als reacties initieel sneller verliepen. Een mogelijke verklaring hiervoor is de verzadiging van het grensvlak met het gevormde product. In bulkemulsies vormt dit geen probleem, omdat er continu nieuwe druppels en dus onverzadigde grensvlakken worden gevormd.

FtsZ en het divisoomsysteem vormen de essentiële eiwitten voor celdeling in de bacterie *E. coli*. In **Hoofdstuk 3** laten we zien wat het effect is van crowding en confinement op de polymerisatie van FtsZ tot filamentbundels. FtsZ polymerisatie in microdruppels met een hoge concentratie macromoleculen en gecoat met vetten uit *E. coli* leidde tot een dicht netwerk van vezels. De geometrie van het netwerk hing af van de vorm van de druppel, concentratie van FtsZ monomeren, welk macromolecuul werd gebruikt als crowder en de vloeistofstroomcondities in de microkanalen. Bij de laagste concentraties van de crowder ficoll 70 was de bundelvorming vertraagd in de microdruppels gemaakt in microkanalen. Wanneer de bundels eenmaal gevormd waren, veranderde het netwerk niet, hoewel de bundels wel FtsZ monomeren uitwisselden met de buffer. Daarnaast ontstond er een verarmingszone vlak bij het olie-watergrensvlak waar zeer weinig bundels werden waargenomen en een aantal hypotheses werd aangedragen om dit fenomeen te verklaren.

Het gebruik van microfluïdica voor het onderzoeken van bundelvorming werd voortgezet in **Hoofdstuk 4**, waarin de eigenschappen van FtsZ werden onderzocht in de aanwezigheid van FtsA en sZipA, twee eiwitten die ook betrokken zijn bij de celdeling. Het doel van deze studie was om vast te stellen wat de precieze rol is van FtsZ tijdens de celdeling. Echter, hoewel de eiwitten nog steeds interacties aan konden gaan na compartementalisatie bleken microdruppels niet het geschikte platform om een mogelijk effect op het vetmembraan te onderzoeken. In plaats daarvan werden liposomen gebruikt, waarvoor eerst een nieuwe methode moest worden ontwikkeld om monodisperse vesikels te verkrijgen. De aanpak waarbij de liposomen direct op de microfluïdische chip werden gemaakt bleek onsuccesvol, maar microdruppelformatie in microkanalen gevolgd door druppeltransfer was een veelbelovende methode. Bij deze laatstgenoemde methode bekleedden vetten uit *E. coli* de binnenzijde van de liposomen, terwijl de buitenkant bestond uit POPC.

Hoofdstuk 5 beschrijft een aanpak om de organisatie en assemblage van microtubuli te onderzoeken in microdruppels onder condities van crowding en confinement. Eerst werden experimenten uitgevoerd in bulkemulsies om de beste surfactant/olie combinatie te vinden en de kritische microtubuliconcentraties voor bundelvorming te bepalen. Daarna werden druppels geproduceerd in kanalen met een hoogte van 10 µm, gebruikmakend van een surfactant gesynthetiseerd in ons eigen laboratorium. De microtubuli werden succesvol geëncapsuleerd en gevisualiseerd en behielden de mogelijkheid te assembleren, ondanks de hoge schuifkrachten tijdens druppelproductie. De rol van fysieke beperkingen op microtubuli werd onderzocht door te variëren in crowder, druppelgrootte en –geometrie. De uitlijning van verschillende microtubulibundels in staaf- of schijfvormige druppels verschilde niet. Tevens bleek dat het gebruik van ficoll 70 leidde tot robuustere en meer verbonden microtubuli in tegenstelling tot dextran 70 dat resulteerde in een meer uniforme verdeling van microtubuli, wat werd verklaard door de verschillende eigenschappen van de crowders.

Acknowledgements

It is a pleasure to thank all of the people who have helped and supported me during my PhD research. First, I would like to thank my supervisor Wilhelm Huck for giving me the opportunity to be a member of his research group and for his help, guidance and motivation throughout the time of my research. I also would like to thank Ashleigh Theberge for helping me getting started with the 'on water' reactions project, teaching me how to produce microdroplets and contributing in the redaction of my first manuscript.

My sincere thanks go to Germán Rivas for the opportunity to work in collaboration with his group in Madrid. I enjoyed our conversations and your passion for your research was a real inspiration. The few visits I made in the CIB of Madrid were very useful and I would like to thank you and your group for the warm welcome and kindness. Special thanks go to Begoña Monterroso for her contribution, help and guidance with the FtsZ project. Dear Begoña, it was a pleasure to meet you and work with you! I am grateful for your support, for your help planning my research and for your careful and detailed corrections of my manuscript chapters.

Thank you to the staff of the organic chemistry department: Desiree van der Wey, Peter van Dijk, Marieke Egbertzen, Paula Willems, Theo Peters and Jan Dommerholt. I bothered you so many times to ask you something but you were always kind and happy to help. Thanks to Ad Swolfs, Helene Amatjais-Groenen and Peter van Galen in the assistance of the analysis of my compounds.

I would like to thank my student Lise Bousekkine who did an amazing job during her internship and helped me getting my first paper published. Your enthusiasm, your will to work and learn was outstanding. I also thank Venkat, Rao, and Esra for their contribution and help to my research.

Thank you to my colleagues of the Physical-organic chemistry group for the help, discussions and support over the past four years. I really feel fortunate to have worked in a group with such kind people, in a fun and pleasant atmosphere. Thanks to Venkat, Aigars, Kate, Sergey and Julian, first members of the group who helped ordering equipment and getting familiar with microfluidics and fluorescence microscopy. Also, thanks to Ilya,

Sjoerd (merci pour la traduction du resume), Albert, Maike, Emilien, Marlies, David (thanks for helping me with protein handling), Joost, Agata and Stephanie.
Special thank to my dear friends Yujie and Sophie, with whom I enjoyed spending time and talking to. Thanks you for your help and support, it was a pleasure to have you around.

I would like to thank the manuscript committee for accepting being part of it and for their critical comments: Roeland Nolte, Sijbren Otto and Germán Rivas.

J'aimerais remercier ma famille pour son soutien tout au long de mes études. Chers papa et maman, vous êtes des parents formidables. C'est grâce à vous que je suis la personne que je suis aujourd'hui et c'est à vous que je dois ma réussite. Alors, un grand merci à tous les deux pour votre soutien, encouragements et amour. Cher Hamdi, merci de m'avoir convaincu de changer d'orientation et de choisir première S au lieu de ES et de contribuer ainsi au fait que je serais docteur en chimie physique. Cher Mouez, merci pour ton soutien, ta compréhension, ta gentillesse et pour toutes les fois que tu as pris soin de moi. Tu es un frère génial et j'aimerais également te dédier ma réussite.

Finally, my heartfelt thanks go to the man of my life Ilija. After obtaining my Master, you convinced me that I had the potential and the ability to do a PhD and I wouldn't have done it without you. I succeeded because of you, your support, your kindness and your love. I also dedicate my accomplishment to you! Now it's time for a new page in our book, you have a new job, I will have a new job so very exciting days are coming. Volim te!

About the author

Sonia Mellouli was born on the 31st of May in La Ciotat, France. She attended Louis et Auguste Lumières high school where she discovered her love for physics and chemistry and received her BAC certificate in 2003. Then, she studied chemistry at the Provence University in Marseille and received her Bachelor degree in 2006. Driven by her will to broaden her knowledge in the field of science with subjects such as project management, computer science, social sciences and communication, she studied at the ENSCPB graduate school of Bordeaux. During the two years of her master, she conducted two internships in the Netherlands at Schering-Plough (Oss). During the first internship, she worked on optimizing a system for the assessment of a powder mixture containing excipient and active compounds using NIR imaging. The second internship was performed in the polymeric department specialized in the development of contraceptive polymeric rings (Nuvaring). Her task was to solve a problem concerning the deviated release of the active compound from rings with high concentrations and managed to find robust explanations. She was graduated with a Master in physics and chemistry in 2009 and decided to do a PhD to expend her skills and because she was captivated with the work in an R&D environment from her experience. In January 2010, she started her PhD research at the Radboud University Nijmegen under the supervision of Prof. Wilhelm T.S Huck. The results of this research are described in this thesis.